



# **Electroweak Corrections to Double Higgs Production**

Master's Thesis of

Philipp Randler

at the Department of Physics  
Institute for Theoretical Physics (ITP)

Reviewer: Prof. Gudrun Heinrich  
Second reviewer: Prof. Matthias Steinhauser  
Advisor: Dr. Marco Bonetti

11. December 2023 – 28. October 2024



---

I declare that I have developed and written the enclosed thesis completely by myself, and have not used sources or means without declaration in the text.

**Karlsruhe, 28.10.2024**

.....  
(Philipp Rendler)



# Abstract

In this thesis I present the amplitude for the leading order quark-initiated double Higgs production up to the order  $\varepsilon^2$  for diagrams that involve a top quark and generate the Higgs boson through electroweak bosons. I calculated the appearing Feynman integrals with the method of differential equations, employing a large mass expansion to generate boundary functions. The resulting expressions agree with pySecDec and the amplitude is free from poles in  $\varepsilon$ . In addition, I present the first step in the calculation of the next-to-leading order electroweak corrections for the gluon- and quark-initiated double Higgs production with a fully symbolic dependence on master integrals by providing the amplitude for diagrams that contain a top quark and generate the Higgs boson through  $W$  bosons.



# Contents

<b>Abstract</b>	<b>i</b>
<b>0. Introduction</b>	<b>1</b>
<b>1. The Standard Model of Particle Physics</b>	<b>3</b>
1.1. The Electroweak Sector . . . . .	3
1.1.1. Massless Gauge Bosons . . . . .	3
1.1.2. Electroweak Symmetry Breaking . . . . .	4
1.1.3. Mass Terms for the Gauge Bosons . . . . .	5
1.1.4. Unphysical Degrees of Freedom . . . . .	6
1.2. Perturbation Theory . . . . .	8
1.2.1. Divergences . . . . .	9
<b>2. Feynman Integrals</b>	<b>13</b>
2.1. Feynman Integrals . . . . .	13
2.1.1. Transformation Properties . . . . .	13
2.1.2. Representations of Feynman Integrals . . . . .	15
2.2. Relations between Feynman Integrals . . . . .	19
2.2.1. Integral Families . . . . .	20
2.2.2. Relations between Feynman Integrals . . . . .	23
2.2.3. Laporta's Algorithm . . . . .	28
<b>3. Differential Equations for Feynman Integrals</b>	<b>31</b>
3.1. Derivation . . . . .	31
3.1.1. Differential Equations for Internal Masses . . . . .	31
3.1.2. Differential Equations for External Kinematics . . . . .	32
3.1.3. Rescaling the Equations . . . . .	32
3.1.4. Combining all Equations . . . . .	33
3.2. Transformation of Differential Equations . . . . .	34
3.2.1. Canonical System . . . . .	35
3.2.2. Fibre Transformation . . . . .	36
3.2.3. Base Transformation . . . . .	38
3.3. Iterated Integrals . . . . .	39
3.3.1. Solution of the Differential Equation . . . . .	39
3.3.2. Shuffle Relations . . . . .	41
3.4. Boundary Conditions . . . . .	44
3.4.1. Direct computation . . . . .	44

3.4.2.	Uniform Transcendental Boundary Conditions . . . . .	48
3.4.3.	Large Mass Expansion . . . . .	49
3.5.	Numerical Evaluation of Feynman Integrals . . . . .	51
3.5.1.	Multiple Polylogarithms . . . . .	51
3.5.2.	Mapping Iterated Integrals on GPLs . . . . .	54
3.5.3.	Analytic Continuation . . . . .	57
<b>4.</b>	<b>EW Corrections for Quark-initiated Double Higgs Production</b>	<b>59</b>
4.1.	The Contributing Diagrams . . . . .	59
4.1.1.	The One-Loop Case . . . . .	60
4.1.2.	The Two-Loop Case . . . . .	60
4.2.	The Tensor Structure . . . . .	60
4.2.1.	The Form Factors . . . . .	60
4.2.2.	The Chiral Projection Operators . . . . .	61
4.2.3.	The Projectors . . . . .	62
4.3.	Reduction to Master Integrals . . . . .	62
4.3.1.	Integral Families . . . . .	62
4.3.2.	Master Integrals . . . . .	63
4.4.	Differential Equations . . . . .	65
4.4.1.	Derivation of the Canonical Form . . . . .	65
4.4.2.	The dLog form . . . . .	66
4.4.3.	Iterated Integrals . . . . .	69
4.4.4.	Boundary Conditions . . . . .	71
4.5.	GPLs . . . . .	72
4.6.	Crosschecks . . . . .	75
4.6.1.	Crosschecks on the Amplitude . . . . .	75
4.6.2.	Crosschecks on the Master Integrals . . . . .	75
<b>5.</b>	<b>NLO EW Corrections for Gluon-initiated Double Higgs Production</b>	<b>77</b>
5.1.	The Contributing Diagrams . . . . .	77
5.2.	The Tensor structure . . . . .	77
5.2.1.	The Form Factors . . . . .	77
5.2.2.	The Projectors . . . . .	79
5.3.	Reduction to Master Integrals . . . . .	79
5.3.1.	Integral Families . . . . .	79
5.3.2.	Master Integrals . . . . .	80
<b>6.</b>	<b>Conclusion and Outlook</b>	<b>81</b>
<b>A.</b>	<b>Appendix</b>	<b>83</b>
	<b>Bibliography</b>	<b>95</b>

# List of Figures

2.1.	Graphical representation of integral relations . . . . .	20
2.2.	Box diagram of electroweak quark initiated double Higgs production. . .	21
2.3.	Illustration of IBPs . . . . .	26
3.1.	Illustration of the integral reparametrization to obtain shuffle relations. .	41
3.2.	Integration path for the Wick rotation . . . . .	45
4.1.	Contributing diagrams for the quark initiated one-loop case . . . . .	60
4.2.	Master integrals for the one-loop case . . . . .	64
A.1.	Contributing diagrams for the quark initiated two-loop case . . . . .	85
A.2.	Contributing planar diagrams for the gluon initiated two-loop case . . .	93
A.3.	Contributing non-planar diagrams for the gluon initiated two-loop case .	94



# List of Tables

2.1. Integral family of the box diagram. . . . .	22
2.2. Scalar products expressed in terms of the inverse propagators and kinematic invariants. . . . .	22
4.1. Integral families for the quark initiated double Higgs production at two-loop level. . . . .	63
5.1. Integral families for the gluon initiated double Higgs production at two-loop level. . . . .	80



# 0. Introduction

The discovery of the Higgs Boson in 2012 by the CMS and ATLAS collaborations at the Large Hadron Collider (LHC) [1, 2] marks one of the greatest milestones in particle physics. Since this groundbreaking discovery, investigating the detailed properties of the Higgs boson has become a major focus of research at the LHC [3, 4]. While parameters like the Higgs mass have been measured with high precision [5], the investigation of Higgs pair production remains a key area of interest [5–10], as it provides the only direct probe of the trilinear coupling  $\lambda_{HHH}$ , which is crucial for reconstructing the Higgs potential.

The Standard Model of particle physics (SM) predicts that the dominant contribution to Higgs pair production comes from gluon-initiated processes. However, due to the destructive interference between the box-like and triangle-like contributions, the cross section for double Higgs production is expected to be three orders of magnitude smaller than that of single Higgs production, making the experimental measurement challenging. The strongest constraints on the ratio between the observed and predicted trilinear coupling are currently given by

$$-1.2 < \frac{\lambda_{HHH}}{\lambda_{HHH}^{\text{SM}}} < 7.2, \quad (0.1)$$

at a 95 % confidence limit [11]. However, the High-Luminosity LHC run presents the opportunity for more precise measurements [12–14].

To match the expected experimental precision, accurate theoretical predictions for double Higgs production at proton-proton colliders are essential. These predictions include both quark- and gluon-initiated processes. Although the LO calculation of the gluon-initiated double Higgs production was performed over two decades ago, [15, 16], the next-to-leading-order (NLO) predictions are significantly more complex, involving two loop-diagrams. Numerical NLO quantum chromodynamic (QCD) corrections were published only a few years ago [17–25], with numerical NLO electroweak (EW) corrections recently computed [26–31].

In comparison to a fully numerical evaluation, an analytic approach offers two key advantages. First, it is more flexible allowing for a precise and faster numerical evaluation across a wide range of external kinematics. Second, it makes physical features of the amplitude, such as threshold behavior, manifest - often expressed as arguments of polylogarithms.

In this thesis, I focus on Feynman diagrams that contain at least one massive and one massless quark line and produce the Higgs boson via  $W$  bosons. I present the analytic results for the quark-initiated LO diagrams with full dependence over all scales. The

calculation is performed using the method of differential equations [32–35] employing a large mass expansion to fix the integration constants. At the two-loop level, I take an initial step toward calculating the EW corrections for both gluon- and quark-initiated double-Higgs production by expressing the diagrams in terms of master integrals with full symbolic dependence on all relevant scales.

The thesis is organized as following. In Chapter 1, I provide a brief overview of the SM and the perturbative techniques relevant to the calculations. Chapter 2 introduces Feynman integrals and discusses their properties, focussing on how to generate and exploit relations among them. The theoretical foundation for solving Feynman integrals using differential equations is discussed in Chapter 3. Chapters 4 and 5 are devoted to the calculations for the quark- and gluon-initiated amplitudes, respectively. To conclude, Chapter 6 summarizes my findings and offers an outlook for future work.

# 1. The Standard Model of Particle Physics

The SM is a quantum field theory that arises from the combination of special relativity and quantum mechanics. It describes all confirmed fundamental particles and three of the four known fundamental forces: the weak force, strong force and electromagnetic force. These particles and forces are embedded in a spontaneously broken gauge theory with the gauge group

$$SU(3)_C \times SU(2)_L \times U(1)_Y, \quad (1.1)$$

which describes the symmetries of QCD and the EW sector.

## 1.1. The Electroweak Sector

The electroweak sector unifies the electromagnetic and weak forces under the gauge group  $SU(2)_L \times U(1)_Y$ , describing the electroweak interactions between fermions via the exchange of gauge bosons: The photon for electromagnetic interactions, and the  $W^\pm$  and  $Z$  bosons for weak interactions. The Higgs mechanism breaks the  $SU(2)_L \times U(1)_Y$  symmetry down to the electromagnetic  $U(1)_{\text{em}}$  symmetry, giving mass to the weak bosons while leaving the photon massless. This section examines the structure of the EW Lagrangian.

### 1.1.1. Massless Gauge Bosons

Massless fermions are described by the Lagrangian

$$\mathcal{L} = \bar{\Psi} i \not{\partial} \Psi, \quad (1.2)$$

where  $\not{\partial} = \gamma^\mu \partial_\mu$ . This Lagrangian is invariant under global transformations of the electroweak symmetry group  $SU(2)_L \times U(1)_Y$ . Fermions transform under this group according to

$$\Psi_L \rightarrow e^{i\tau^a \alpha^a} e^{\frac{i}{2}\beta Y} \Psi_L \quad \text{and} \quad \Psi_R \rightarrow e^{\frac{i}{2}\beta Y} \Psi_R, \quad (1.3)$$

where  $\tau^a$ ,  $a \in \{1, 2, 3\}$ , represent the  $SU(2)$  group generators, and  $Y$  is the hyper charge. To extend this global symmetry to a local one, where  $\alpha = \alpha(x)$  and  $\beta = \beta(x)$ , a gauge field is required for each group generator. These fields, denoted as  $W_\mu^a$  and  $B_\mu$  transform

under a gauge transformation as

$$\begin{aligned} W_\mu^a(x) &\rightarrow W_\mu^a(x) + \frac{1}{g} \partial_\mu \alpha^a(x) - \varepsilon^{abc} \alpha^b(x) W_\mu^c \\ B_\mu(x) &\rightarrow B_\mu(x) + \frac{1}{g'} \partial_\mu \beta(x), \end{aligned} \quad (1.4)$$

The Lagrangian becomes locally invariant under the electroweak symmetry group by minimally coupling these gauge fields to fermions through the modified Lagrangian

$$\mathcal{L} = \bar{\Psi} i \not{D} \Psi, \quad (1.5)$$

where the covariant derivative is defined as

$$D_\mu = \partial_\mu - ig \tau^a W_\mu^a(x) P_L - ig' \frac{Y}{2} B_\mu(x), \quad (1.6)$$

The left-handed projection operator,

$$P_L = \frac{1}{2}(1 - \gamma_5), \quad (1.7)$$

is used to project out the left-handed component of the fermion fields, ensuring that the  $W^\pm$  bosons couple only to left-handed fermions, as required by the weak interaction.

Next, the kinematic and mass terms for the gauge bosons need to be introduced to construct the full EW Lagrangian. The kinematic terms can be formulated in a gauge-invariant manner by generalizing the electromagnetic field strength tensor. However, a straightforward mass term, such as

$$\mathcal{L}_{\text{mass}} = \frac{1}{2} m_W^2 W_\mu W^\mu, \quad (1.8)$$

is not invariant under local  $SU(2)_L$  transformations. This issue necessitates an alternative approach, leading to the introduction of the Higgs mechanism.

### 1.1.2. Electroweak Symmetry Breaking

The mass terms for the gauge fields can be generated through the introduction of the Higgs field. The Higgs field,  $\Phi$ , is a scalar field that transforms as a doublet under  $SU(2)_L$  and carries a hypercharge of  $Y = 1$ . Its Lagrangian is given by

$$\mathcal{L}_{\text{Higgs}} = (D_\mu \Phi)^\dagger (D^\mu \Phi) - V(\Phi), \quad (1.9)$$

where  $V(\Phi)$  denotes the Higgs potential, which is given by

$$V(\Phi) = \mu^2 \Phi^\dagger \Phi + \lambda (\Phi^\dagger \Phi)^2, \quad (1.10)$$

with  $\mu^2 < 0$  and  $\lambda > 0$ . Neglecting quantum corrections, the ground state of  $\Phi$  is determined by minimizing the Higgs potential,

$$\Phi^\dagger \Phi = -\frac{\mu^2}{2\lambda}, \quad (1.11)$$

resulting in a non-zero vacuum expectation value (VEV).

This equation has infinite solutions, but a suitable gauge transformation of the Higgs field allows to select any of these as a ground state. Conventionally, it is chosen as

$$\langle \Phi \rangle = \frac{1}{\sqrt{2}} \begin{pmatrix} 0 \\ v \end{pmatrix}, \quad (1.12)$$

with the real parameter  $v$ .

The choice of the VEV breaks the electroweak symmetry group, as it is not invariant under arbitrary  $SU(2)_L \times U(1)_Y$  transformations. Choosing the Pauli matrices  $\sigma^a$  as  $SU(2)$  generators,

$$\tau^a = \frac{\sigma^a}{2}, \quad (1.13)$$

results in the following condition for the invariance of the ground state:

$$\langle \Phi \rangle \stackrel{!}{=} e^{i\frac{\sigma^a}{2}\alpha^a} e^{i\frac{Y}{2}\beta} \langle \Phi \rangle, \quad (1.14)$$

which implies  $\alpha^1 = \alpha^2 = 0$  and  $\alpha^3 = \beta$ .

As a consequence, the remaining gauge symmetry that leaves the ground state invariant reads

$$\exp \left[ i\beta \left( \tau^3 + \frac{Y}{2} \right) \right], \quad (1.15)$$

which corresponds to the unbroken electromagnetic  $U(1)_{\text{em}}$  symmetry with

$$Q = \tau^3 + \frac{Y}{2}, \quad (1.16)$$

being the conserved electric charge.

### 1.1.3. Mass Terms for the Gauge Bosons

The gauge bosons acquire mass through the kinetic term of the Higgs Lagrangian. By expanding the Higgs field  $\Phi$  around its VEV,

$$\Phi = \frac{1}{\sqrt{2}} \begin{pmatrix} \varphi_1 + i\varphi_2 \\ v + h + i\varphi_3 \end{pmatrix}, \quad (1.17)$$

the resulting Lagrangian contains quadratic terms in the gauge fields,

$$\mathcal{L}_{\text{mass}} = \frac{1}{2} \frac{v^2}{4} \begin{pmatrix} W_\mu^1 \\ W_\mu^2 \\ W_\mu^3 \\ B_\mu \end{pmatrix}^T \begin{pmatrix} g^2 & 0 & 0 & 0 \\ 0 & g^2 & 0 & 0 \\ 0 & 0 & g^2 & -gg' \\ 0 & 0 & -gg' & g^2 \end{pmatrix} \begin{pmatrix} W_\mu^1 \\ W_\mu^2 \\ W_\mu^3 \\ B_\mu \end{pmatrix}. \quad (1.18)$$

Diagonalizing this mass matrix yields three massive gauge bosons,

$$W_\mu^\pm = \frac{1}{\sqrt{2}} (W_\mu^1 \mp iW_\mu^2) \quad \text{with} \quad m_W = \frac{g}{2}v \quad (1.19)$$

$$Z_\mu^\pm = \frac{g'W_\mu^3 - gB_\mu}{\sqrt{g^2 + g'^2}} \quad \text{with} \quad m_Z = \frac{\sqrt{g^2 + g'^2}}{2}v, \quad (1.20)$$

as well as one massless gauge boson,

$$A_\mu = \frac{g'W_\mu^3 + gB_\mu}{\sqrt{g^2 + g'^2}}, \quad (1.21)$$

which is identified as the photon field.

#### 1.1.4. Unphysical Degrees of Freedom

In addition to the physical gauge bosons, the EW sector also contains unphysical degrees of freedom, specifically Goldstone bosons and ghost fields.

##### Ghosts

Ghost fields arise from the gauge freedom of gauge fields. In the path integration formalism of quantum field theory, the quantization process involves integrating over all distinct field configurations. However, for gauge fields  $V_\mu$ , this includes integration over an infinite number of physically equivalent states due to the gauge symmetry.

To eliminate this redundancy a gauge-fixing condition  $G(V)$  must be imposed. The Faddeev-Popov method provides a systematic way to incorporate gauge-fixing into the formalism by inserting the identity

$$1 = \int \mathcal{D}\alpha(x) \delta(G(V^\alpha) - \omega(x)) \det\left(\frac{\delta G(V^\alpha)}{\delta \alpha}\right), \quad (1.22)$$

where  $V^\alpha$  denotes the gauge-transformed field,

$$(V^\alpha)_\mu^a = V_\mu^a + \frac{1}{g} \partial_\mu \alpha^a(x) - f^{abc} \alpha^b(x) V_\mu^c, \quad (1.23)$$

and  $\alpha^a(x)$  is the gauge transformation parameter. The delta distribution ensures that the integration does not include physically equivalent configurations, with  $\omega(x)$  being an arbitrary function.

To simplify calculations, integrating over  $\omega(x)$  with a Gaussian weight allows the delta function to be replaced with an additional term in the Lagrangian,

$$\begin{aligned} \int \mathcal{D}\omega(x) \mathcal{D}\alpha(x) \delta(G(V^\alpha) - \omega(x)) \det\left(\frac{\delta G(V)}{\delta\alpha}\right) e^{-\frac{\omega(x)^2}{2}} \\ = \int \mathcal{D}\alpha(x) \det\left(\frac{\delta G(V^\alpha)}{\delta\alpha}\right) e^{-\frac{G(V)^2}{2}} \end{aligned} \quad (1.24)$$

resulting in what is known as the *gauge-fixing term*.

The determinant can be expressed as a part of the Lagrangian by introducing Grassmann fields, called ghost fields,

$$\det\left(\frac{\delta G(V^\alpha)}{\delta\alpha}\right) = \int \left( \prod_a \mathcal{D}\bar{c}_a \mathcal{D}c_a \right) \exp\left(-\bar{c}_a \left(\frac{\delta G(V^\alpha)}{\delta\alpha}\right)_{ab} c_b\right). \quad (1.25)$$

These fields  $c$  and  $\bar{c}$  are unphysical because, despite being scalar, they anticommute, violating the spin-statistics theorem. However, their presence is necessary to properly account for the gauge-fixing procedure, and their Feynman rules must be considered when calculating amplitudes.

### Goldstone Bosons

The kinetic part of the Lagrangian not only generates mass terms for the gauge bosons but also produces kinetic terms for the Goldstone fields  $\varphi_i$ , bilinear mixing terms between the Goldstone and gauge fields, as well as trilinear and quartic interaction terms, denoted as  $\mathcal{L}_3$  and  $\mathcal{L}_4$ , respectively. This can be written as

$$\begin{aligned} (D_\mu\Phi)(D^\mu\Phi) = \frac{1}{2}V_\mu^a \mathcal{M}_{ab} V^{\mu b} + \frac{1}{2}(\partial_\mu h(x))(\partial^\mu h(x)) + \frac{1}{2}(\partial_\mu \varphi_i(x))(\partial^\mu \varphi_i(x)) \\ + V_\mu^a F_i^a \partial^\mu \varphi_i + \mathcal{L}_3 + \mathcal{L}_4, \end{aligned} \quad (1.26)$$

where  $V_\mu^a$  for  $a \in \{1, 2, 3, 4\}$  denotes the four gauge fields, and  $F_i^a$  represents their bilinear couplings to the Goldstone fields.

Choosing a specific gauge-fixing condition allows to get rid of the bilinear mixing terms between the gauge and Goldstone fields. The  $R_\xi$ -gauge is defined by the gauge-fixing condition,

$$G^a(x) = \frac{1}{\sqrt{\xi}}(\partial^\mu V_\mu^a - \xi F_i^a \varphi_i), \quad (1.27)$$

leading to the gauge-fixing term

$$-\frac{1}{2}G^2 = -\frac{1}{2\xi}(\partial^\mu V_\mu^a - \xi F_i^a \varphi_i)^2. \quad (1.28)$$

Expanding the square and partially integrating the mixing term results in

$$-\frac{1}{2}G^2 = \frac{1}{2\xi}V_\mu^a(\partial^\mu\partial^\nu)V_\nu^a - \frac{1}{2}\xi(F_i^a\varphi_i)^2 - V_\mu^a F_i^a\partial^\mu\varphi_i. \quad (1.29)$$

The mixing term between the gauge fields and the Goldstone bosons cancels the corresponding term in the kinetic part. The quadratic terms in  $\varphi^i$  result in masses for the Goldstone bosons. Diagonalizing the mass matrix  $\xi(F^a F^a)_{ij}$  gives three massive Goldstone bosons

$$\varphi^\pm \quad \text{with} \quad m_{\varphi^\pm}^2 = \xi m_W^2 \quad (1.30)$$

$$\varphi_Z \quad \text{with} \quad m_{\varphi_Z} = \xi m_Z^2, \quad (1.31)$$

as well as one massless Goldstone boson  $\varphi_A$ .

The dependence of the Goldstone boson masses on the gauge parameter  $\xi$  indicates that these fields are unphysical.

### The Unitary Gauge

The gauge-fixing condition in Eq. (1.27) not only introduces mass terms for the Goldstone bosons, but also affects the Feynman rules for ghost fields, as described by Eq. (1.25). In fact, the masses of the ghost fields are equal to those of the corresponding Goldstone bosons.

The *unitary gauge* is defined as the limit  $\xi \rightarrow \infty$ , which causes the masses of the Goldstone bosons and ghosts to become infinitely large. As a result, they decouple entirely from the theory, meaning they no longer contribute to physical processes.

As a consequence, this gauge choice can simplify calculations by significantly reducing the number of required Feynman diagrams.

## 1.2. Perturbation Theory

High energy colliders, like the Large Hadron Collider (LHC), are crucial for testing the SM. By colliding particles at very high energies, these experiments enable precise measurements of observables such as cross sections and decay widths. To compare these experimental results with theoretical predictions, scattering amplitudes  $\mathcal{A}$  must be calculated with high precision.

However, exact calculations of the amplitude are generally not feasible. Instead, the amplitude is typically expressed as an expansion in terms of the coupling constants,

$$\mathcal{A} = \mathcal{A}_0 + \mathcal{A}_1 + \mathcal{A}_2 + \dots \quad (1.32)$$

The lowest non-zero order  $\mathcal{A}_0$  is referred to as the LO of the scattering amplitude, while  $\mathcal{A}_1$  corresponds to the NLO, and higher terms follow accordingly.

The LO amplitude does not always correspond to tree-level Feynman diagrams. Consider for instance the gluon initiated Higgs production. Being massless particles, gluons do not couple directly to the Higgs boson. Consequently, the LO amplitude already requires one-loop diagrams.

Observables depend on the squared magnitude of the amplitude,  $|\mathcal{A}|^2$ . Expanding the amplitude and squaring it yields

$$\begin{aligned} |\mathcal{A}|^2 &= (\mathcal{A}_0 + \mathcal{A}_1 + \mathcal{A}_2 + \dots)(\bar{\mathcal{A}}_0 + \bar{\mathcal{A}}_1 + \bar{\mathcal{A}}_2 + \dots) \\ &= \underbrace{|\mathcal{A}_0|^2}_{\text{Leading order}} + \underbrace{2\text{Re}(\mathcal{A}_0\bar{\mathcal{A}}_1)}_{\text{Next-to-leading order}} + \underbrace{|\mathcal{A}_1|^2 + 2\text{Re}(\mathcal{A}_0\bar{\mathcal{A}}_2)}_{\text{Next-to-next-to-leading order}} + \dots, \end{aligned} \quad (1.33)$$

where  $\bar{\mathcal{A}}_i$  denotes the complex conjugate of  $\mathcal{A}_i$ . Thus, the NLO term in the squared amplitude arises from the interference between the LO and NLO amplitudes, rather than simply from the squared NLO amplitude.

### 1.2.1. Divergences

The calculation of scattering amplitudes requires summing over all possible intermediate states, which leads to intermediate particles with momenta that are not uniquely determined by momentum conservation, referred to as loop momenta. This necessitates integrating over these loop momenta, which can lead to divergent results. Divergences may arise when loop momenta approach infinity or when massless propagators become singular as their momenta approach zero, denoted as ultraviolet (UV) or infrared (IR) divergences, respectively. Properly addressing these divergences is essential for obtaining physically meaningful results.

#### Ultraviolet Divergences

Ultraviolet divergences arise from the behavior of integrals at large momenta. Consider for example the equal mass bubble integral,

$$I_{\nu_1\nu_2} = \int \frac{d^4k}{(2\pi)^4} \frac{1}{[k^2 - m^2 + i\delta]^{\nu_1} [(k+p)^2 - m^2 + i\delta]^{\nu_2}}, \quad (1.34)$$

where  $\nu_1, \nu_2 \in \mathbb{Z}$  are integers. For large momenta  $|k| > \Omega_{\text{UV}}$ , this integral scales as

$$I_{\nu_1\nu_2} \propto \int_{\Omega_{\text{UV}}}^{\infty} dk k^{3-2(\nu_1+\nu_2)}, \quad (1.35)$$

which diverges if  $\nu_1 + \nu_2 \leq 2$ .

For loop-induced LO amplitudes, UV divergences cancel when adding all Feynman diagrams together. At higher orders, in renormalizable theories, they can be eliminated by renormalization of the fields and parameters.

### Infrared Divergences

Infrared divergences arise when massless denominators approach zero. For example for low momenta  $|k| < \Omega_{\text{IR}}$  and  $m = 0$ , the equal mass bubble integral scales as

$$I_{\nu_1, \nu_2} \propto \int_0^{\Omega_{\text{IR}}} dk k^{3-2\nu_1}, \quad (1.36)$$

which diverges if  $\nu_1 > 2$ .

These divergences can be addressed by considering that every detector has a finite resolution, therefore, an  $n$ -particle final state is indistinguishable from an  $(n + 1)$ -particle final state when two particles are sufficiently close together or when an additional particle has energy below the detection threshold. The phase space integrations over these regions of the  $(n + 1)$ -particle squared amplitude produces a divergence with the opposite sign, which cancels the IR divergence of the  $n$ -particle process when summed over all degenerate final states.

To match the powers of coupling constants in the  $n$  and  $(n + 1)$ -particle process, the  $(n + 1)$ -particle process must involve one fewer loop and one additional leg. Consequently, any LO amplitude is protected from IR divergences.

### Dimensional Regularization

Divergences must be made quantifiable to achieve their cancellation. This requires deriving expressions that depend on a regulator and become divergent in a specific limit of such regulator. The behavior of these expressions in that limit reveals the type of singularity the integral produces.

Among the various ways to handle these divergences (see for example [36]), *dimensional regularization* has become the standard approach. Its core idea is to promote the dimension of the integral to a complex parameter  $D$ . After calculating the integration in a converging regime of  $D$ , the result can be continued. The divergences in four dimensions then appear as poles in  $\varepsilon = \frac{D-4}{2}$ .

Dimensional regularization can be seen as an analytic continuation of the Lebesgue integral in positive integer dimensions. As the integration is performed over the full  $D$ -dimensional space it remains translation invariant,

$$\int d^D k f(k) = \int d^D k f(k + p). \quad (1.37)$$

In addition, to be consistent with the Lebesgue integral properties in integer dimensions, it must follow the scaling relation,

$$\int d^D k f(\alpha k) = \frac{1}{\alpha^D} \int d^D k f(k). \quad (1.38)$$

The  $D$ -dimensional measure is continued such that the surface of the  $D$ -dimensional ball reads

$$S_{D-1} = \frac{2\pi^{\frac{D}{2}}}{\Gamma(\frac{D}{2})}. \quad (1.39)$$

Thus, rotationally invariant integrals in  $D$ -dimensional Euclidean space can be computed by changing to spherical coordinates.

$$\int d^D k f(k^2) = \int d^{D-1} \Omega \int_0^\infty dr r^{D-1} f(r^2) \quad (1.40)$$

$$= \frac{2\pi^{\frac{D}{2}}}{\Gamma(\frac{D}{2})} \int_0^\infty dr r^{D-1} f(r^2). \quad (1.41)$$

Due to the factor  $\pi^{\frac{D}{2}}$  it is convenient to rescale the integral measure by  $\pi^{-\frac{D}{2}}$ .



## 2. Feynman Integrals

The evaluation of loop integrals and the handling of the associated divergences can become the main bottleneck in calculating scattering amplitudes. This chapter explores the properties and relations between these integrals, culminating in a method for reducing them to a minimal independent set.

### 2.1. Feynman Integrals

In general, a Feynman integral is a dimensionally regularized integral over a product of inverse propagators

$$P_i = p_i^2 - m_i^2 + i\delta, \quad (2.1)$$

where  $p_i$  is a linear combination of external momenta  $\mathcal{E}$  and loop momenta  $\mathcal{L}$ ,  $m_i$  is the mass of the propagating particle and  $\delta$  is an infinitesimal positive real number that shifts the roots in  $p_i^0$  from the real axis to be consistent with Feynman's causality prescription of Green's functions.

Consider the inverse propagators  $P_1, \dots, P_n$  and the indices  $\nu_1, \dots, \nu_n \in \mathbb{Z}$ . A *Feynman integral* is defined as a dimensionally regularized integral of the form

$$\mu^{l(4-D)} \int \left( \prod_{k \in \mathcal{L}} \frac{d^D k}{i\pi^{\frac{D}{2}}} \right) \prod_{j=1}^n \frac{1}{P_j^{\nu_j}}, \quad (2.2)$$

where  $\mu$  is an energy scaled which is introduced to fix the mass dimension of the integral and  $l = |\mathcal{L}|$  denotes the number of loops. Note, that  $\nu_j$  can be negative, indicating that the inverse propagator occurs in the numerator with the power  $|\nu_j|$ .

#### 2.1.1. Transformation Properties

##### Invariance under Lorentz transformations

Consider an  $l$ -loop Feynman integral depending on a set of external momenta  $\mathcal{E}$  and a set of internal masses  $\mathcal{M}$ ,

$$I(\mathcal{E}, \mathcal{M}) = \mu^{l(4-D)} \int \left( \prod_{k \in \mathcal{L}} \frac{d^D k}{i\pi^{\frac{D}{2}}} \right) j(\mathcal{E}, \mathcal{M}). \quad (2.3)$$

The integrand  $j(\mathcal{E}, \mathcal{M})$  is composed out of propagators, which consist of external momenta  $p^\mu \in \langle \mathcal{E} \rangle$ , internal momenta  $q^\mu \in \langle \mathcal{L} \rangle$ , and masses  $m \in \mathcal{M}$ ,

$$P = (p + q)^2 - m^2 + i\delta. \quad (2.4)$$

If all external momenta are transformed by a Lorentz transformation  $\Lambda^\mu{}_\nu$  this yields

$$P' = (\Lambda^\mu{}_\nu p^\nu + q^\mu)^2 - m^2 + i\delta. \quad (2.5)$$

The substitution  $k^\mu \rightarrow \Lambda^\mu{}_\nu k^\nu$  for all loop momenta  $k \in \mathcal{L}$  gives

$$\begin{aligned} P'' &= (\Lambda^\mu{}_\nu p^\nu + \Lambda^\mu{}_\nu q^\mu)^2 - m^2 + i\delta \\ &= (p + q)^2 - m^2 + i\delta \\ &= P. \end{aligned} \quad (2.6)$$

Since the substitution does not change the integral measure, scalar Feynman integrals are invariant under Lorentz transformations,

$$I(\Lambda \mathcal{E}, \mathcal{M}) = I(\mathcal{E}, \mathcal{M}). \quad (2.7)$$

This means that they do not depend on the components of the external momenta individually, but only through scalar products.

### Scaling Behavior

Consider the Feynman integral from Eq. (2.3). Rescaling the masses and external momenta by a factor  $\lambda$  affects the propagators as

$$P' = (\lambda p + q)^2 - \lambda^2 m^2 + i\delta. \quad (2.8)$$

Substituting  $k \rightarrow \lambda k$  for all loop momenta  $k \in \mathcal{L}$  yields the original propagator scaled by a factor  $\lambda^2$ ,

$$P'' = \lambda^2 P. \quad (2.9)$$

The transformation also affects the measure by a factor of  $\lambda^D$ . Therefore, the Feynman integral transforms as

$$I(\lambda \mathcal{E}, \lambda \mathcal{M}) = \lambda^\alpha I(\mathcal{E}, \mathcal{M}), \quad (2.10)$$

where  $\alpha := \dim_m(I)$  denotes the mass dimension of the integral.

### Scaleless integrals

Consider a scaleless Feynman integral, i.e. an integral which does not depend on internal masses or external scales

$$I = \mu^{l(4-D)} \int \frac{d^D k}{i\pi^{\frac{D}{2}}} j(k). \quad (2.11)$$

From dimensional regularization follows that this integral is zero.

To show this, assume that the mass dimension of the integral is non-zero,

$$\alpha = \dim_m(I) \neq 0. \quad (2.12)$$

Applying Eq. (2.10) then gives  $I = \lambda^\alpha I$ . The only finite solution for this equation is setting the integral to zero,  $I = 0$ .

For a more intuitive reasoning, the result of the integral should depend on one or multiple mass scales raised to the power of  $\alpha$ . However, the integrand does neither depend on any external momenta nor on internal masses. Therefore, there is no quantity to provide the necessary mass dimension. As a consequence, the integral must be constant.

For a rigorous derivation of this property, also for integrals with a mass dimension of 0, the integral must first be evaluated in a converging regime of the dimension  $D$ . The result can then be analytically continued, as shown in Ref. [37].

### 2.1.2. Representations of Feynman Integrals

Feynman integrals can be expressed in various forms, each suited to different applications. The notation introduced above is known as the momentum representation, which is the form obtained by applying Feynman rules. Three further representations are commonly used: The Schwinger parameter representation, which has a relatively simple dependence on the dimension  $D$ , the Feynman parameter representation, which can be used to directly evaluate certain integrals and the Baikov representation, which offers a straightforward method to calculate cuts.

#### Schwinger Parameter Representation

The Schwinger parameter representation shifts the integration over the  $D$ -dimensional momentum space to an integration over Schwinger parameters  $\alpha_i$ . It is based on the identity

$$\frac{1}{A^n} = \frac{1}{\Gamma(\nu)} \int_0^\infty d\alpha \alpha^{\nu-1} e^{-\alpha A} \quad \text{for } \nu > 0, A > 0, \quad (2.13)$$

which is known as Schwinger's trick. Applying it to the propagators  $P_j$  of a Feynman integral of the form,

$$I(\mathcal{S}, \mathcal{M}) = \mu^{l(4-D)} \int \left( \prod_{k \in \mathcal{L}} \frac{d^D k}{i\pi^{\frac{D}{2}}} \right) \prod_{j=1}^n \frac{1}{P_j^{\nu_j}}, \quad (2.14)$$

yields<sup>1</sup>

$$I(\mathcal{S}, \mathcal{M}) = \frac{(-1)^\nu \mu^{l(4-D)}}{\prod_{j=1}^n \Gamma(\nu_j)} \int_{\alpha_j \geq 0} \left( \prod_{j=1}^n d\alpha_j \alpha_j^{\nu_j-1} \right) \int \left( \prod_{k \in \mathcal{L}} \frac{d^D k}{i\pi^{\frac{D}{2}}} \right) e^{-\sum_{j=1}^n \alpha_j (-P_j)}, \quad (2.15)$$

<sup>1</sup>The sign of the propagator depends on the external kinematics. It is convenient to choose the so-called Euclidean kinematics, where  $P_j < 0$ , and analytically continue the result to other regions.

## 2. Feynman Integrals

---

with  $\nu = \sum_{j=1}^n \nu_j$  and  $\mathcal{S}$  denoting the set of scalar products between external momenta. With this parametrization, the integrals over the loop momenta become gaussian integrals which can be evaluated. This gives

$$I(\mathcal{S}, \mathcal{M}) = \frac{(-1)^\nu \mu^{l(4-D)}}{\prod_{j=1}^n \Gamma(\nu_j)} \int_{\alpha_j \geq 0} \left( \prod_{j=1}^n d\alpha_j \alpha_j^{\nu_j-1} \right) \mathcal{U}(\alpha)^{-\frac{D}{2}} e^{-\frac{\mathcal{F}(\alpha; \mathcal{S}, \mathcal{M})}{\mathcal{U}(\alpha)}}. \quad (2.16)$$

$\mathcal{U}(\alpha)$  and  $\mathcal{F}(\alpha; \mathcal{S}, \mathcal{M})$  are homogeneous polynomials in  $\alpha$ , denoted as graph polynomials or as first and second Symanzik polynomial, respectively. The first designation stems from their dependence on the trees and two-trees of the associated Feynman graph. Specifically, the first graph polynomial  $\mathcal{U}(\alpha)$  is obtained by summing over all spanning trees of the sector graph and multiplying over all  $\alpha_i$  that correspond to the edges removed to obtain each tree,

$$\mathcal{U}(\alpha_1, \dots, \alpha_N) = \sum_{\text{trees}} \prod_{\text{chords}} \alpha_{\text{chord}}. \quad (2.17)$$

**Application: Dimensional Shift relations** One advantage of the Schwinger parameter representation is its relatively simple dependence on the space-time dimension  $D$ . This allows to find relations between Feynman diagrams of different dimension [38, 39]. Consider a Feynman integral in Schwinger notation as in Eq. (2.16). The dimension of the Integral can be reduced by two by multiplying the integrand with  $\mathcal{U}(\alpha)$ ,

$$I^{(D-2)}(\mathcal{S}, \mathcal{M}) = \frac{(-1)^n \mu^{l(4-D)}}{\prod_{j=1}^N \Gamma(n_j)} \int_{\alpha_j \geq 0} \left( \prod_{j=1}^N d\alpha_j \alpha_j^{n_j-1} \right) \mathcal{U}(\alpha)^{-\frac{D}{2}} \mathcal{U}(\alpha) e^{-\frac{\mathcal{F}(\alpha; \mathcal{S}, \mathcal{M})}{\mathcal{U}(\alpha)}}. \quad (2.18)$$

This integral can be expressed in terms of Feynman integrals of dimension  $D$  with propagators raised to higher powers.

Following Ref. [40], I introduce the operator  $k^+$ , which acts on a Feynman diagram by increasing the power of the  $k$ -th propagator,

$$k^+ I_{\nu_1, \dots, \nu_k, \dots, \nu_n} = \nu_k I_{\nu_1, \dots, \nu_k+1, \dots, \nu_n}. \quad (2.19)$$

In Schwinger representation the right hand side of this equation reads

$$\nu_k I_{\nu_1, \dots, \nu_k+1, \dots, \nu_n} = \frac{(-1)^\nu \mu^{l(4-D)}}{\prod_{j=1}^n \Gamma(\nu_j)} \int_{\alpha_j \geq 0} \left( \prod_{j=1}^n d\alpha_j \alpha_j^{\nu_j-1} \right) \mathcal{U}(\alpha)^{-\frac{D}{2}} \alpha_k e^{-\frac{\mathcal{F}(\alpha; \mathcal{S}, \mathcal{M})}{\mathcal{U}(\alpha)}}, \quad (2.20)$$

introducing an additional factor of  $\alpha_k$  in the integrand.

As a consequence, applying a suitable combination of these operators on a Feynman integral allows to generate the polynomial  $\mathcal{U}(\alpha)$  within the integrand. This leads to dimensional shift relations,

$$I^{(D-2)}(\mathcal{S}, \mathcal{M}) = \mathcal{U}(1^+, \dots, n^+) I^{(D)}(\mathcal{S}, \mathcal{M}), \quad (2.21)$$

which relate Feynman integrals that differ in dimension by two.

### Feynman Parameter Representation

The Feynman Parameter Representation is based on Feynman's observation that

$$\prod_{j=1}^n \frac{1}{P_j^{\nu_j}} = \frac{\Gamma(\nu)}{\prod_{j=1}^n \Gamma(\nu_j)} \int_{\alpha_j \geq 0} \left( \prod_{j=1}^n d\alpha_j \alpha_j^{\nu_j-1} \right) \frac{\delta\left(1 - \sum_{j=1}^n \alpha_j\right)}{\left(\sum_{j=1}^n \alpha_j P_j\right)^\nu}, \quad (2.22)$$

with  $\nu = \sum_{j=1}^n \nu_j$ . Applying this identity on a Feynman integral with inverse propagators  $P_j$  allows to carry out the momentum integration. In Sec. 3.4.1 I will provide an example to demonstrate how to calculate Feynman integrals using this representation.

### Baikov Representation

Consider a one-loop Feynman integral with  $n$  inverse propagators and  $e$  independent external momenta. The linear span of these external momenta forms a subspace  $P_{\parallel}$  of dimension  $e$ . Decomposing the loop momentum into components parallel and orthogonal to this subspace,

$$k = k_{\parallel} + k_{\perp}, \quad (2.23)$$

allows to perform the angular integration over the perpendicular component  $k_{\perp}$ , as the integrand depends only on  $k_{\perp}^2$ . This results in the *Baikov representation* [41] for Feynman integrals.

The Baikov representation for one-loop Feynman integrals is given by

$$I(\mathcal{S}, \mathcal{M}) = \frac{\mu^{4-D}}{i\pi^{\frac{e}{2}} \Gamma\left(\frac{D-e}{2}\right)} \det(G(p_1, \dots, p_e))^{-\frac{D+e+1}{2}} \int_{\mathcal{C}} d^n z B(z)^{\frac{D-e-2}{2}} \prod_{j=1}^n \frac{1}{z_j^{\nu_j}}. \quad (2.24)$$

The representation depends on the Baikov polynomial  $B(z) = G(k, p_1, \dots, p_e)$  with the Gram determinant

$$G(q_1, \dots, q_m) = \begin{vmatrix} q_1 \cdot q_1 & \dots & q_1 \cdot q_m \\ \vdots & \ddots & \vdots \\ q_m \cdot q_1 & \dots & q_m \cdot q_m \end{vmatrix}. \quad (2.25)$$

The polynomial is written in terms of the Baikov variables  $z_1, \dots, z_n$  corresponding to the inverse propagators  $P_1, \dots, P_n$ . The Gram determinant and Baikov polynomial arise from the change of variables in the integral, while the remaining prefactors come from the angular integration over  $k_{\perp}$ , corresponding to the surface of the  $(D - e)$ -dimensional ball. The integration region  $\mathcal{C}$  is determined by the condition

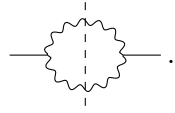
$$0 \geq k_{\perp}^2 = \frac{\det(G(k, p_1, \dots, p_e))}{\det(G(p_1, \dots, p_e))}. \quad (2.26)$$

Due to the complexity of this integration region, the Baikov parametrization is not typically intended for direct evaluation of Feynman integrals. However, its explicit dependence on the inverse propagators  $P_j$  through the Baikov variable  $z_j$  simplifies the analysis of on-shell intermediate particles.

**Application: Thresholds of Feynman Diagrams** Beyond IR and UV divergences, Feynman integrals can also exhibit divergences in specific kinematic configurations. These occur at energy thresholds where intermediate particles are produced on-shell. According to the optical theorem, crossing these thresholds is directly linked to the imaginary part of the amplitude becoming non-zero.

Mathematically, these thresholds manifest as arguments of (poly)logarithms in the  $\varepsilon$ -expansion of one-loop diagrams<sup>2</sup>. The Baikov representation offers a straightforward method to identify such thresholds.

Assume that the intermediate particle associated with the propagator  $P_j$  is produced on-shell. Graphically, this is visualized by cutting the propagator, for example for the bubble integral,



$$(2.27)$$

In the Baikov representation cutting a propagator corresponds to setting the associated Baikov variable to zero. This is achieved by the substitution<sup>3</sup>

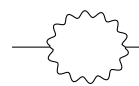
$$\frac{1}{z_j} \rightarrow \delta(z_j). \quad (2.28)$$

Putting all intermediate particles on-shell is referred to as the *maximal cut* of a Feynman integral, which can be calculated with the Baikov representation,

$$\text{MaxCut}(I(\mathcal{S}, \mathcal{M})) = \frac{\mu^{4-D}}{i\pi^{\frac{\varepsilon}{2}} \Gamma(\frac{D-\varepsilon}{2})} \det(G(p_1, \dots, p_e))^{\frac{-D+\varepsilon+1}{2}} B(0)^{\frac{D-\varepsilon-2}{2}}. \quad (2.29)$$

The divergences of the maximal cut correspond directly to the kinematic thresholds, allowing their identification.

**Example: Thresholds of an Equal Mass Bubble Integral** Consider the equal mass bubble integral,



$$= \mu^{4-D} \int \frac{d^D k}{i\pi^{\frac{D}{2}}} \frac{1}{[(k+p)^2 - m^2][k^2 - m^2]}. \quad (2.30)$$

The kinematic thresholds can be determined by computing the divergences of the maximal cut of the bubble, which is straightforward in the Baikov representation. The Baikov

---

<sup>2</sup>From two loops on, the thresholds may appear in more complex structures than polylogarithms such as elliptic functions.

<sup>3</sup>This substitution to obtain the maximal cut is valid for Baikov variables  $z_j$  which occur only with power one. For higher powers, the cut is generalized by expanding the integration region by an additional anticlockwise circle around  $z_j = 0$ . In the case where the propagator appears once, the residue restores the delta distribution.



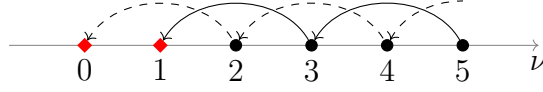


Figure 2.1.: Graphical representation of the relations between the integrals  $I_\nu(\alpha)$

For the cases  $\nu = 0$  and  $\nu = 1$ , the computation is straightforward. In the case  $\nu = 0$ , the formula reduces to the gaussian integral, i.e.

$$I_0(\alpha) = \int_0^\infty e^{-\alpha x^2} dx = \sqrt{\frac{\pi}{2\alpha}}. \quad (2.36)$$

In the case  $\nu = 1$ , the substitution  $y = x^2$  can be used which yields

$$I_1(\alpha) = \int_0^\infty x e^{-\alpha x^2} dx = \frac{1}{2} \int_0^\infty e^{-\alpha y} dy = \frac{1}{2\alpha}. \quad (2.37)$$

To calculate  $I_\nu(\alpha)$  for arbitrary  $\nu$ , a recurrence relation can be constructed by differentiating  $I_\nu$  with respect to  $\alpha$ ,

$$\frac{dI_\nu(\alpha)}{d\alpha} = \int_0^\infty x^\nu \frac{d}{d\alpha} e^{-\alpha x} = \int_0^\infty x^{\nu+2} e^{-\alpha x} = I_{\nu+2}(\alpha). \quad (2.38)$$

Reapplying this identity yields for  $\nu = 2k$

$$I_{2k}(\alpha) = \frac{d^k}{d\alpha^k} I_0(\alpha), \quad (2.39)$$

and for  $\nu = 2k + 1$ ,

$$I_{2k+1}(\alpha) = \frac{d^k}{d\alpha^k} I_1(\alpha). \quad (2.40)$$

Figure 2.1 illustrates the relations among the integrals. The arrows connect the  $(\nu + 2)$ -th integral to the  $\nu$ -th integral. By following the arrows, one can trace the dependence of an integral  $I_\nu(\alpha)$ , which always leads to one of the master integrals,  $I_0$  or  $I_1$ , represented by the red diamonds. Therefore the task of integration is shifted to the algorithmic task of differentiation, insofar the master integrals  $I_0(\alpha)$  and  $I_1(\alpha)$  are known.

Indexing the integrals by the power of  $x$  in the integrand makes it easier to understand the structure of the identities. Therefore it is helpful to introduce a similar systematic notation for Feynman integrals. Integral families fulfill this purpose.

### 2.2.1. Integral Families

An *integral family*  $\mathcal{F}$  is a set of inverse propagators

$$\mathcal{F} = \{P_1, \dots, P_n\} \quad \text{with} \quad P_i = q_i^2 - m_i^2 + i\delta, \quad (2.41)$$

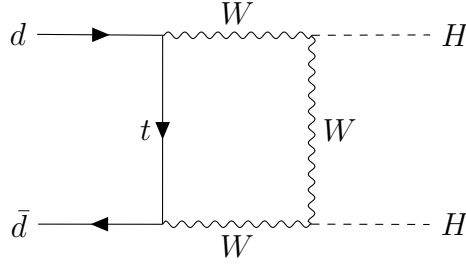


Figure 2.2.: Box diagram of electroweak quark initiated double Higgs production.

where  $q_i$  is a linear combination of external momenta and loop momenta. These propagators are chosen such that every scalar product involving a loop momentum is uniquely expressible in terms of these inverse propagators, external kinematics and internal masses.

For a diagram with  $e$  external momenta and a  $l$  loop momenta, the number of independent scalar products involving at least one loop momentum is

$$N_{\text{sp}} = el + \frac{l(l+1)}{2}. \quad (2.42)$$

The first term of this equation represents the number of scalar products between external momenta and loop momenta. The second term indicates the number of scalar products between two loop momenta.

#### Example: Quark initiated Double Higgs Production at one loop order

Consider the Feynman diagram depicted in Fig. 2.2. The incoming quarks are considered as massless, the top quark has the mass  $m_t$  and the  $W$  and Higgs bosons have masses  $m_W$  and  $m_H$ , respectively. The diagram consists of three independent external momenta  $p_1$ ,  $p_2$  and  $p_3$ , and one loop momentum  $k$ . Using Eq. (2.42) this yields in

$$N_{\text{sp}} = 3 \cdot 1 + \frac{1 \cdot 2}{2} = 4 \quad (2.43)$$

independent scalar products, explicitly given by

$$p_1 \cdot k, \quad p_2 \cdot k, \quad p_3 \cdot k \quad \text{and} \quad k^2. \quad (2.44)$$

Constructing an integral family for this diagram must take two requirements into account:

1. All possible scalar products containing at least one loop momentum must be uniquely expressible using the inverse propagators of the integral family. Since four independent scalar products can occur, the integral family consists of four propagators.
2. All propagators containing a loop momentum occurring in the Feynman integrals must be expressible in terms of the propagators from the integral family. This can involve a redefinition of the loop momentum.

In the case of the one-loop box diagram, the number of propagators in the diagram is the same as the number of independent scalar products. Therefore, in this case, the two requirements already define the integral family up to a redefinition of the loop momentum. The integral family can be chosen as shown in Tab. 2.1. The scalar products can then be expressed in terms of inverse propagators and kinematic invariants as shown in Tab. 2.2, where the Mandelstam variable  $t = (p_1 + p_3)^2$  is used.

Table 2.1.: Integral family of the box diagram.

$\mathcal{F}$	inverse propagator
$P_1$	$k^2 - m_t^2$
$P_2$	$(k + p_1)^2 - m_W^2$
$P_3$	$(k + p_1 + p_3)^2 - m_W^2$
$P_4$	$(k - p_2)^2 - m_W^2$

Table 2.2.: Scalar products expressed in terms of the inverse propagators and kinematic invariants.

scalar product	expressed with inverse propagators
$p_1 \cdot k$	$\frac{1}{2}(P_2 - P_1 + m_W^2 - m_t^2)$
$p_2 \cdot k$	$-\frac{1}{2}(P_4 - P_1 + m_W^2 - m_t^2)$
$p_3 \cdot k$	$\frac{1}{2}(P_3 - P_2 - t + m_H^2)$
$k^2$	$P_1 + m_t^2$

The introduction of the integral family allows a short hand notation for all its integrals. An integral with the propagators  $P_k$  raised to the powers  $\nu_k$  can be written as

$$I_{\nu_1 \nu_2 \nu_3 \nu_4} = \mu^{4-D} \int \frac{d^D k}{i\pi^{\frac{D}{2}}} \prod_{k=1}^4 \frac{1}{P_k^{\nu_k}} \quad (2.45)$$

This short hand notation simplifies the discussion of integral relations.

### Sectors

A *sector*  $\mathcal{S}$  is defined as a subset of an integral family  $\mathcal{I}$ . An integral  $I_{\nu_1, \dots, \nu_n}$  belongs to the sector  $\mathcal{S}$ , if all of the Sector's inverse propagators appear in the denominator of the integrand, meaning  $\nu_k > 0$  for  $P_k \in \mathcal{S}$ . All further inverse propagators are only allowed to appear in the numerator, meaning  $\nu_k \leq 0$  for  $P_k \in \mathcal{I} \setminus \mathcal{S}$ .

$\tilde{\mathcal{S}}$  is called a *subsector* of the sector  $\mathcal{S}$  if it is a proper subset. *Top sectors* are defined as the highest sectors that are necessary for computing a scattering amplitude.

Each sector of an integral family can be uniquely identified by their sector-ID, which is defined as

$$\text{ID} = \sum_{k=1}^n \Theta\left(\nu_k - \frac{1}{2}\right) 2^{k-1}, \quad (2.46)$$

where  $\Theta$  denotes the Heaviside function. This allows sectors to be referenced just by their ID and integral family without listing all of their inverse propagators.

## 2.2.2. Relations between Feynman Integrals

### Integration-by-parts identities

The main source of linear relations among Feynman integrals are integration-by-parts identities (IBPs) [43, 44], which relate integrals from the same integral family. They are a consequence of the translation invariance and scaling behavior of dimensional regularized integrals. Consider a Feynman integral with the set of loop momenta  $\mathcal{L}$  and the set of independent external momenta  $\mathcal{E}$ . Let  $k \in \mathcal{L}$  be a loop momentum and  $q \in \langle \mathcal{E} \cup \mathcal{L} \rangle$  a linear combination of external momenta and loop momenta. Then, the following identities apply,

$$\int \frac{d^D k}{i\pi^{\frac{D}{2}}} \frac{\partial}{\partial k^\mu} (q^\mu f(\mathcal{E} \cup \mathcal{L})) = 0. \quad (2.47)$$

The integral

$$\int \frac{d^D k}{i\pi^{\frac{D}{2}}} f(\mathcal{E} \cup \mathcal{L}), \quad (2.48)$$

is called the seed integral for these identities.

*Proof.* First, let  $q \in \mathcal{Q} := \mathcal{E} \cup \mathcal{L} \setminus \{k\}$  be an external momentum or loop momentum except for  $k$ . The translation invariance of dimensional regularized integrals, Eq. (1.37), yields

$$\int \frac{d^D k}{i\pi^{\frac{D}{2}}} f(k, \mathcal{Q}) = \int \frac{d^D k}{i\pi^{\frac{D}{2}}} f(k + \alpha q, \mathcal{Q}) \quad \text{for } \alpha \in \mathbb{C}. \quad (2.49)$$

Since the left-hand side of Eq. (2.49) does not depend on  $\alpha$ , this must also hold true for the right-hand side. Therefore, the derivative with respect to  $\alpha$  vanishes. Exchanging integration and differentiation gives

$$\begin{aligned} 0 &= \frac{d}{d\alpha} \int \frac{d^D k}{i\pi^{\frac{D}{2}}} f(k + \alpha q, \mathcal{Q}) \Big|_{\alpha=0} \\ &= \int \frac{d^D k}{i\pi^{\frac{D}{2}}} \frac{\partial}{\partial \alpha} f(k + \alpha q, \mathcal{Q}) \Big|_{\alpha=0} \\ &= \int \frac{d^D k}{i\pi^{\frac{D}{2}}} \left( \frac{\partial}{\partial k^\mu} f(q, \mathcal{Q}) \right) q^\mu \\ &= \int \frac{d^D k}{i\pi^{\frac{D}{2}}} \frac{\partial}{\partial k^\mu} (q^\mu f(\mathcal{E} \cup \mathcal{L})). \end{aligned} \quad (2.50)$$

Note that the last equal sign only applies as long as  $q^\mu$  does not depend on  $k^\mu$ . Now consider a translation purely in the direction of  $k$ . Making use of the scaling behavior of dimensional regularized integrals, introduced in Eq. (1.38), gives

$$\begin{aligned} \frac{d}{d\alpha} \int \frac{d^D k}{i\pi^{\frac{D}{2}}} f(k + \alpha k, \mathcal{Q}) \Big|_{\alpha=0} &= \frac{d}{d\alpha} \frac{1}{(\alpha + 1)^D} \int \frac{d^D k}{i\pi^{\frac{D}{2}}} f(\mathcal{E} \cup \mathcal{L}) \Big|_{\alpha=0} \\ &= -D \int \frac{d^D k}{i\pi^{\frac{D}{2}}} f(\mathcal{E} \cup \mathcal{L}) \\ &= - \int \frac{d^D k}{i\pi^{\frac{D}{2}}} \left( \frac{\partial k^\mu}{\partial k^\mu} \right) f(\mathcal{E} \cup \mathcal{L}). \end{aligned} \quad (2.51)$$

On the other hand, exchanging integration and differentiation yields

$$\begin{aligned} \frac{d}{d\alpha} \int \frac{d^D k}{i\pi^{\frac{D}{2}}} f(k + \alpha k, \mathcal{Q}) \Big|_{\alpha=0} &= \int \frac{d^D k}{i\pi^{\frac{D}{2}}} \frac{\partial}{\partial \alpha} f(k + \alpha k, \mathcal{Q}) \Big|_{\alpha=0} \\ &= \int \frac{d^D k}{i\pi^{\frac{D}{2}}} \left( \frac{\partial}{\partial k^\mu} f(\mathcal{E} \cup \mathcal{L}) \right) k^\mu. \end{aligned} \quad (2.52)$$

Combining Eqs. (2.51) and (2.52) gives

$$\begin{aligned} 0 &= \int \frac{d^D k}{i\pi^{\frac{D}{2}}} \left( \frac{\partial k^\mu}{\partial k^\mu} \right) f(\mathcal{E} \cup \mathcal{L}) + \int \frac{d^D k}{i\pi^{\frac{D}{2}}} \left( \frac{\partial}{\partial k^\mu} f(k, \mathcal{Q}) \right) k^\mu \\ &= \int \frac{d^D k}{i\pi^{\frac{D}{2}}} \frac{\partial}{\partial k^\mu} (k^\mu f(\mathcal{E} \cup \mathcal{L})) \end{aligned} \quad (2.53)$$

The full result for  $q \in \langle \mathcal{E} \cup \mathcal{L} \rangle$  follows immediately from the linearity of integration and differentiation.  $\square$

Let  $\mathcal{S}$  be the sector of the seed integral. The integrals related by the corresponding IBPs all belong to the same sector or subsectors of  $\mathcal{S}$ . This can be reasoned by considering the different possibilities the derivative in Eq. (2.47) can act on:

1. When the derivative  $\frac{\partial}{\partial k^\mu}$  acts on an inverse propagator in the numerator, it creates scalar products that can be expressed in terms of inverse propagators, external kinematics and internal masses. This action does not introduce any new inverse propagators in the denominator.
2. When the derivative  $\frac{\partial}{\partial k^\mu}$  acts on an inverse propagator in the denominator, the power of that propagator increases by one, and a scalar product is produced in the numerator. Again, this does not lead to the introduction of new inverse propagators in the denominator.



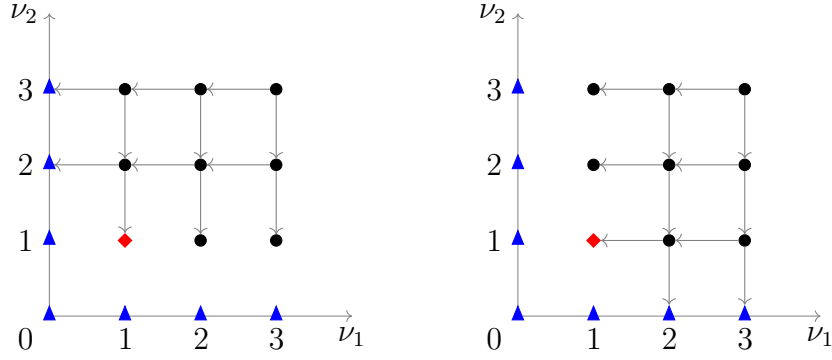


Figure 2.3.: Illustrations of the Eqs. (2.58) (left) and (2.59) (right)

$I_{\nu_1, \nu_2}$  on integrals with the same propagators but raised to lower powers. Combining these two relations it becomes clear, that every integral  $I_{\nu_1, \nu_2}$  can be expressed in terms of the master integral  $I_{1,1}$  of the sector, indicated by the red diamond, as well as integrals of lower sectors, indicated by the blue triangles.

The structure of Feynman integrals related by IBPs can be imagined as vectors within a vector field. Just as any vector in a vector field can be expressed as a linear combination of basis vectors, any Feynman integral can be represented as a linear combination of master integrals. The coefficients for these combinations are determined by the relations obtained through IBPs.

Similar to the basis of a vector field, the choice of master integrals is not unique; only their number is fixed. In the previous example, the equations could have been rearranged to express all the integrals  $I_{\nu_1, \nu_2}$  (including  $I_{1,1}$ ) in terms of integrals from lower sectors and one specific choice for the master integral. The selection of the set of master integrals, often referred to as a basis, is typically based on criteria such as uniform weight, as explained in Sec. 3.4.2, finiteness or numerical stability.

### Lorentz-invariance identities

The idea of Lorentz-invariance (LI) identities, first mentioned in Ref. [33], is based on the fact that Feynman integrals are Lorentz scalars. Therefore, applying a Lorentz transformation onto the external momenta does not change the integral. A general Lorentz transformation  $\Lambda^\mu{}_\nu$  can be written as an expansion,

$$\Lambda^\mu{}_\nu = \delta^\mu{}_\nu + \omega^\mu{}_\nu + \mathcal{O}(\omega^2), \quad (2.60)$$

with the antisymmetric tensor  $\omega^\mu{}_\nu$ . Applying this transformation onto the external momenta  $p_\alpha$  of a Feynman integral yields

$$I(p'_\alpha) = I(p_\alpha) + \frac{\partial I(p_\alpha)}{\partial p_\alpha^\mu} \omega^\mu{}_\nu p_\alpha^\nu + \mathcal{O}(\omega^2). \quad (2.61)$$

Due to the Lorentz invariance of Feynman integrals, the linear term in  $\omega$  must vanish. Using the antisymmetry of  $\omega$  gives

$$0 = \frac{\partial I(p_\alpha)}{\partial p_\alpha^\mu} \omega^\mu{}_\nu p^\nu = \frac{1}{2} \omega^{\mu\nu} \left( p_{\alpha\nu} \frac{\partial}{\partial p_\alpha^\mu} - p_{\alpha\mu} \frac{\partial}{\partial p_\alpha^\nu} \right) I(p_\alpha). \quad (2.62)$$

The term in the brackets can be contracted with an arbitrary combination of independent external momenta  $p_i$  and  $p_j$ , which finally leads to LIs,

$$(p_i^\mu p_j^\nu - p_j^\mu p_i^\nu) \left( p_{\alpha\nu} \frac{\partial}{\partial p_\alpha^\mu} - p_{\alpha\mu} \frac{\partial}{\partial p_\alpha^\nu} \right) I(p_\alpha) = 0. \quad (2.63)$$

It was shown in [45], that LIs are actually not independent to IBPs. However, they can still be useful to accelerate computations since multiple seed integrals might be necessary to write one LI identity in terms of IBPs.

### Equivalent Sectors

When multiple integral families are involved in one calculation, some of their inverse propagators might be the same. As a consequence, the sectors composed out of these propagators are identical, although they belong to different integral families.

Equivalences between sectors can also be less obvious: A substitution of the loop momenta  $\{k_i\}$  of the form

$$k_i \rightarrow k'_i = A_{ij} k_j + b_i \quad \text{with} \quad \det(A) = 1, \quad (2.64)$$

transforms a Feynman integral belonging to a sector  $\mathcal{S}$  as

$$\mu^{4-D} \int \left( \prod_{i=1}^l \frac{d^D k_i}{i\pi^{\frac{D}{2}}} \right) \prod_{j=1}^n \frac{1}{P_j^{\nu_j}} = \mu^{4-D} \int \left( \prod_{i=1}^l \frac{d^D k'_i}{i\pi^{\frac{D}{2}}} \right) \prod_{j=1}^n \frac{1}{P'_j{}^{\nu_j}}, \quad (2.65)$$

where the propagators  $P'_j$  are obtained by substituting  $k_i \rightarrow k'_i$ . If the transformed propagators correspond exactly to those of a different sector  $\mathcal{S}'$ , then the integral can as well be written as an element of  $\mathcal{S}'$ .

More general, transformations as in Eq. (2.64) can map the propagators of one sector  $\mathcal{S}$  to those of another sector  $\mathcal{S}'$ . Sectors related by such a transformation are referred to as *equivalent sectors*. Relations between equivalent sectors can be used in order to remove redundancies for practical purposes.

### Sector Symmetries

A sector symmetry relation is a transformation as in Eq. (2.64) which maps a sector onto itself. Such a symmetry occurs for example for the bubble integral,

$$I_{\nu_1, \nu_2} = \mu^{4-D} \int \frac{d^D k}{i\pi^{\frac{D}{2}}} \frac{1}{[k^2 - m^2 + i\delta]^{\nu_1} [(k+p)^2 - m^2 + i\delta]^{\nu_2}}. \quad (2.66)$$

The transformation  $k \rightarrow -k - p$  maps the sector on itself by changing the powers of the propagators,

$$I_{\nu_1, \nu_2} \rightarrow I_{\nu_2, \nu_1}. \quad (2.67)$$

By applying this relation at the IBPs for massless bubble integrals, Eqs. (2.58) and (2.59), they become equivalent. In general such relations can simplify IBPs significantly.

### Trivial Sectors

It may occur that all integrals within a sector are zero. This happens when the loop momenta can be transformed in such a way that all external kinematic quantities are eliminated and no masses are present. Then, all integrals of the sector are scaleless and therefore set to zero within dimensional regularization. Such a sector is referred to as a *trivial sector* or *zero sector*.

A convenient criterion for identifying trivial sectors was presented in [45]: If the IBPs in the corner point result in the corner integral (i.e. the integral where each propagator of this sector occurs exactly once) being zero, then all integrals in that sector are scaleless and therefore equal to zero. However, this criterion is not sufficient and might miss some zero sectors.

Therefore, a second criterion was presented in Ref. [46]. Consider the function  $\mathcal{G} = \mathcal{U} + \mathcal{F}$  composed of the first and second Symanzik polynomials  $\mathcal{U}$  and  $\mathcal{F}$ , respectively. If the equation

$$\sum_j k_j \alpha_j \frac{\partial \mathcal{G}(\alpha)}{\partial \alpha_j} = G(\alpha) \quad (2.68)$$

yields an  $\alpha$ -independent solution with respect to  $k_j$ , the sector is zero.

Identifying trivial sectors as early as possible increases the efficiency of computations, as many integrals can then be immediately set to zero.

### 2.2.3. Laporta's Algorithm

With all these identities in hand, an algorithm is needed to systematically reduce the integrals to their master integrals. One way of doing this is to combine multiple identities to ladder operators which increase or decrease the power of propagators. This approach allows to reduce whole sectors and therefore an infinite amount of integrals to master integrals. However, a lot of hand work is necessary to get these operators which makes it impractical for more complicated sectors.

Laporta proposed an alternative algorithm which uses a finite set of seed integrals to generate IBPs [47]. Given a Feynman integral, the seed integrals are constrained by the number of dots, which is determined by

$$d = \sum_{\nu_j > 0} (\nu_j - 1). \quad (2.69)$$

Additionally, they are restricted by the number of inverse propagators in the numerator, given by

$$s = \sum_{\nu_j < 0} |\nu_j|. \quad (2.70)$$

The integrals are then reduced to master integrals in a forward elimination algorithm: the IBPs are first generated for the lowest sectors (i.e. the sectors with  $l$  different denominators, with  $l$  being the number of loops, beginning from the seed integrals with  $d = s = 0$ ). Then, the number of dots and scalar products is increased up to a predetermined limit. Each IBP generates a linear equation between integrals of the form

$$\sum_i C_i I_i = 0. \quad (2.71)$$

If the generated identity is linear independent to previous identities, the already reduced integrals can be inserted in the relation resulting in a new linear equation,

$$\sum_i C'_i I'_i = 0. \quad (2.72)$$

This equation can be rearranged with respect to one integral  $I'_k$ , expressing it in terms of the other integrals,

$$I'_k = - \sum \frac{C'_i}{C'_k} I'_i. \quad (2.73)$$

The integral  $I'_k$  is chosen with the following order of priority: First, the highest number of denominators, second the highest number of dots  $d$ , third the highest number of scalar products  $s$  and fourth the lowest sector ID. Once generated all integrals with a certain amount of denominators, their number is increased by one up to a predetermined limit.

Given a set of integrals that need to be reduced, it is not immediately clear how  $s$  and  $d$  should be chosen to ensure that all integrals are fully reduced. However, Laporta proposed an empirical rule for this: Consider the set of integrals

$$G_{d_0 s_0} = \{I \mid d(I) < d_0 \wedge s(I) < s_0\}. \quad (2.74)$$

If all integrals in  $G_{d_0 s_0}$  are used as seed integrals for IBPs, then in most cases, the entire set of the integrals in  $G_{d_0 s_0}$  can be reduced to master integrals. Therefore when using the algorithm, setting the limits for  $s$  and  $d$  to the highest values of  $s$  and  $d$  among the occurring integrals is a good starting point.

Since its publication, numerous implementations of the Laporta algorithm have been developed and published, such as Air[48], Fire[49–51], Reduze[52, 53] or Kira[54, 55]. In this work, Reduze and Kira are employed. They use not just IBPs but also LIs and symmetry relations to accelerate the computation of the reductions.



# 3. Differential Equations for Feynman Integrals

I showed in the previous chapter that a scattering amplitude can be expressed as a combination of master integrals. However, the challenge of analytically solving these integrals remains, especially when they reach a level of complexity where direct calculation methods are no longer feasible.

The method of differential equations (DEs) offers an indirect approach: Instead of calculating the master integrals directly, a system of DEs is derived with respect to their kinematic invariants and internal masses. These DEs can then be solved, usually as a series expansion in  $\varepsilon$ .

## 3.1. Derivation

### 3.1.1. Differential Equations for Internal Masses

Consider a vector of master integrals  $\mathcal{I} = (I_1, \dots, I_{N_{\text{master}}})$  which depends on internal masses  $\mathcal{M}$  and external quantities  $\mathcal{S}$ . Taking the derivative of one of the master integrals  $I_k$  with respect to a squared internal mass  $m_\alpha^2$  gives a sum of Feynman integrals,

$$\frac{\partial I_k}{\partial m_\alpha^2} = \sum_i C_i J_i, \quad (3.1)$$

where  $J_i$  denote the Feynman integrals created by the derivative and  $C_i$  are integer coefficients. The crucial point is, that the Feynman integrals  $J_i$  belong to the same sector as  $I$ . This can be seen by considering two cases:

1. The derivative can act on an inverse propagator with the power  $\nu$  in the denominator. This decreases the power by one and gives a prefactor  $\nu$ , but does not remove any propagators. Therefore, the differentiation does not affect the sector of the integrals.
2. The derivative can act on an inverse propagator with power  $\nu$  in the numerator. this increases the power by one and gives a prefactor  $-\nu$  but does neither annihilate any inverse propagators nor create new ones.

That means, that Laporta's algorithm can be used to express the integrals  $J_i$  as a linear combination of the master integrals  $I_k$  with rational coefficients. The partial derivative

with respect to  $m_\alpha^2$  can therefore be written as

$$\frac{\partial \mathcal{I}}{\partial m_\alpha^2} = A_\alpha(\varepsilon, \mathcal{M}, \mathcal{S}) \mathcal{I}, \quad (3.2)$$

where  $A_\alpha$  is a matrix depending on  $\varepsilon$ , the internal masses  $\mathcal{M}$  and the kinematics  $\mathcal{S}$ .

### 3.1.2. Differential Equations for External Kinematics

The equations for the external kinematics are obtained by applying the chain rule,

$$p_i^\mu \frac{\partial I_k}{\partial p_j^\mu} = \sum_{\alpha=1}^{N_{\text{ext}}} \left( p_i^\mu \frac{\partial s_\alpha}{\partial p_j^\mu} \frac{\partial I_k}{\partial s_\alpha} \right) \quad \text{for } i, j \in \{1, \dots, N\}. \quad (3.3)$$

The obtained system of equations can be solved for  $\frac{\partial I_k}{\partial s_\alpha}$  for all  $s_\alpha$ , yielding

$$\frac{\partial I_k}{\partial s_\alpha} = \sum_{i,j} C_{i,j}(\mathcal{S}) p_i^\mu \frac{\partial I_k}{\partial p_j^\mu}. \quad (3.4)$$

Analogous to the explanation for the IBP relations in Sec. 2.2.2, the integrals occurring in the right-hand side belong to the same sector as  $I_k$ . Therefore, they can be expressed in terms of master integrals of the same or lower sectors as the sector of  $I_k$ . This allows the DE to be written as

$$\frac{\partial \mathcal{I}}{\partial s_\alpha} = A_\alpha(\varepsilon, \mathcal{M}, \mathcal{S}) \mathcal{I}, \quad (3.5)$$

with the matrices  $A_\alpha$ .

### 3.1.3. Rescaling the Equations

Having derived all the DEs in the internal masses and external kinematics  $\{\tilde{x}_1, \dots, \tilde{x}_N\}$  one can immediately decouple one DE. Using Eq. (2.10), the variables can be rescaled by one of them, say  $\tilde{x}_N$ , yielding

$$I_k(\tilde{x}_1, \dots, \tilde{x}_N) = \tilde{x}_N^{\dim_k}, I_k \left( \frac{\tilde{x}_1}{\tilde{x}_N}, \dots, \frac{\tilde{x}_{N-1}}{\tilde{x}_N}, 1 \right), \quad (3.6)$$

with

$$\dim_k = \frac{\dim_m(I_k)}{\dim_m(\tilde{x}_N)}. \quad (3.7)$$

That means that the DEs with respect to the variable  $\tilde{x}_N$  become decoupled, as the associated matrix becomes diagonal with the entries

$$A_{kk} = \dim_k. \quad (3.8)$$

The DEs for the new variables  $\{x_1, \dots, x_{N_{\text{kin}}}\}$  with  $N_{\text{kin}} = N - 1$  can be derived by making use of the chain rule,

$$\frac{\partial \mathcal{I}}{\partial x_\alpha} = \left( \frac{\partial x_\alpha}{\partial x'_\alpha} \right)^{-1} A_\alpha(\varepsilon, \mathcal{M}, \mathcal{S}) = \frac{1}{x_N} A_\alpha(\varepsilon, \mathcal{M}, \mathcal{S}). \quad (3.9)$$

This allows to immediately decrease the number of equations by one.

### 3.1.4. Combining all Equations

For a more compact notation, the system of partial DEs can be combined in one equation,

$$d\mathcal{I} = A\mathcal{I}, \quad (3.10)$$

by introducing the usual notation for the total derivative,

$$d\mathcal{I} = \sum_{x_i \in x} \frac{\partial \mathcal{I}}{\partial x_i} dx_i, \quad (3.11)$$

and defining the one-form  $A$  as,

$$A = \sum_{x_i \in x} A_{x_i} dx_i. \quad (3.12)$$

Assume that the integrals are sorted by their sector, with integrals belonging to subsectors appearing first. Since a master integral depends only on integrals of the same or lower sectors, the one-form  $A$  is a lower block-triangular matrix. The size of a block corresponds to the number of master integrals of the sector. In particular,  $A$  is a triangular matrix-valued one-form in the case that there is only one master integral per sector.

The derivation highlights a key advantage of the DEs method: The process is automatable because it involves nothing more than taking derivatives and applying IBPs. Consequently, the only limitation in obtaining these equations is the availability of computational resources.

**Example: Equal Mass Bubble Integral** Consider the equal mass bubble integrals,

$$I_{\nu_1, \nu_2} := \begin{array}{c} \xrightarrow{p} \\ \bullet \\ \text{---} \bullet \end{array} \begin{array}{c} \nu_1 \\ \text{---} \bullet \\ \bullet \\ \nu_2 \end{array} = \mu^{4-D} \int \frac{d^D k}{i\pi^{\frac{D}{2}}} \frac{1}{P_1^{\nu_1} P_2^{\nu_2}}, \quad (3.13)$$

with the inverse propagators  $P_1 = k^2 - m^2 + i\delta$  and  $P_2 = (k+p)^2 - m^2 + i\delta$ . Similar to the massless case, all integrals  $I_{\nu_1, \nu_2}$  with positive integer indices  $\nu_1$  and  $\nu_2$  can be expressed as a linear combination of  $I_{1,1}$  and  $I_{2,0}$ .

To construct a solution for  $I_{1,1}$ , DEs with respect to the external momentum squared  $p^2$  and the internal mass  $m^2$  can be derived. The equation with respect to the external momentum squared is derived using the chain rule,

$$p^\mu \frac{\partial I_{1,1}}{\partial p^\mu} = p^\mu \frac{\partial p^2}{\partial p^\mu} \frac{\partial I_{1,1}}{\partial p^2}. \quad (3.14)$$

By applying IBPs, the left-hand side can be expressed as a linear combination of  $I_{1,1}$  and  $I_2 := I_{2,0}$ ,

$$\frac{\partial I_{1,1}}{\partial p^2} = -\frac{4m^2 - (D-4)p^2}{2p^2(4m^2 - p^2)} I_{1,1} + \frac{2m^2}{p^2(4m^2 - p^2)} I_2. \quad (3.15)$$

Similarly, the DE for  $I_{1,1}$  with respect to the internal mass is given by

$$\frac{\partial I_{1,1}}{\partial m^2} = -\frac{D-3}{4m^2 - p^2} I_{1,1} - \frac{1}{4m^2 - p^2} I_2. \quad (3.16)$$

The tadpole integral  $I_2$  depends only on the mass, yielding

$$\frac{\partial I_{2,0}}{\partial m^2} = \frac{D-4}{m^2} I_{2,0}. \quad (3.17)$$

Rescaling both variables by the mass transforms the DE with respect to the mass into diagonal form which allows for a direct integration,

$$\begin{aligned} I_2(p^2, m^2) &= (m^2)^{\frac{D-4}{2}} I_2(-x, 1) \\ I_{1,1}(p^2, m^2) &= (m^2)^{\frac{D-4}{2}} I_{1,1}(-x, 1), \end{aligned} \quad (3.18)$$

where the rescaled variable  $x$  is defined as

$$x = -\frac{p^2}{m^2}. \quad (3.19)$$

The DEs with respect to  $x$  are then given by

$$\frac{\partial}{\partial x} \begin{pmatrix} I_2 \\ I_{1,1} \end{pmatrix} = \begin{pmatrix} 0 & 0 \\ \frac{2}{x(4+x)} & -\frac{2+\varepsilon x}{x(4+x)} \end{pmatrix} \begin{pmatrix} I_2 \\ I_{1,1} \end{pmatrix}, \quad (3.20)$$

where  $D = 4 - 2\varepsilon$  was inserted.

## 3.2. Transformation of Differential Equations

The system from Eq. (3.20) can be directly solved to a finite order in  $\varepsilon$  by expanding the equation in  $\varepsilon$ . The solution up to the first order in  $\varepsilon$  is given by

$$\begin{aligned} I_2 &= C_2^{(0)} + \varepsilon C_2^{(1)} + \mathcal{O}(\varepsilon^2) \\ I_{11} &= C_2^{(0)} + \frac{C_{11}^{(0)}}{\sqrt{\frac{x}{4+x}}} + \varepsilon \left( 2C_2^{(0)} + C_2^{(1)} \right. \\ &\quad \left. + \frac{C_{11}^{(1)} - C_{11}^{(0)} \log(4+x) - 2C_2^{(0)} \log(\sqrt{x} + \sqrt{4+x})}{\sqrt{\frac{x}{4+x}}} \right) + \mathcal{O}(\varepsilon^2), \end{aligned} \quad (3.21)$$

where the integration constants are denoted as  $C_i^{(k)}$ .

The solution can be simplified significantly by considering the following linear combinations instead of  $I_2$  and  $I_{1,1}$ ,

$$\begin{aligned} g_1 &= \varepsilon I_2 \\ g_2 &= -\sqrt{\frac{x}{4+x}} \varepsilon (I_2 - (1 - 2\varepsilon) I_{1,1}). \end{aligned} \quad (3.22)$$

The DEs for these functions are homogeneous in  $\varepsilon$ ,

$$\frac{\partial}{\partial x} \begin{pmatrix} g_1 \\ g_2 \end{pmatrix} = \varepsilon \begin{pmatrix} 0 & 0 \\ -\frac{1}{\sqrt{x(4+x)}} & -\frac{1}{4+x} \end{pmatrix} \begin{pmatrix} g_1 \\ g_2 \end{pmatrix}. \quad (3.23)$$

Their solutions up to the first order in  $\varepsilon$  are given by

$$\begin{aligned} g_1 &= \tilde{C}_2^{(0)} + \varepsilon \tilde{C}_2^{(1)} + \mathcal{O}(\varepsilon^2) \\ g_2 &= \tilde{C}_{11}^{(0)} + \varepsilon \left( \tilde{C}_{11}^{(1)} - \tilde{C}_{11}^{(0)} \log(4+x) + 2\tilde{C}_2^{(0)} \log(\sqrt{4+x} - \sqrt{x}) \right) + \mathcal{O}(\varepsilon^2), \end{aligned} \quad (3.24)$$

where  $\tilde{C}_i^{(k)}$  are referred to as weight- $k$  integration constants.

This solution exhibits a notable structure. Unlike the expansion of  $I_{11}$ , all coefficients of logarithms and integration constants are rational numbers. Furthermore, the zeroth order in  $\varepsilon$  consists solely of weight-0 integration constants, while the first order contains weight-1 integration constants and products of weight-0 constants with logarithms.

To formalize such structures, the concept of *transcendental weight* is introduced. The transcendental weight is defined as 1 for logarithms and  $n$  for polylogarithms  $\text{Li}_n$ .  $\pi$  is assigned a transcendental weight of one, as  $\pi = -i \log(-1)$ , and zeta-values  $\zeta_n = \text{Li}_n(1)$  have weight  $n$ . The weight of  $\varepsilon$  is defined as  $-1$  and rational numbers have weight 0. The weight of a product is the sum of the weight of its factor. For instance,  $\pi^2$  has weight 2, and  $\pi^3 \zeta_2$  has weight 5. A function is said to have *uniform transcendental (UT) weight* if all terms in its series expansion in  $\varepsilon$  have an equal weight.

By requiring the constants  $\tilde{C}_i^{(k)}$  to have transcendental weight  $k$ , which is equivalent to imposing UT boundary conditions, the expressions for  $g_1$  and  $g_2$  have UT weight zero.

### 3.2.1. Canonical System

A *canonical system* [34] is defined in a way that it yields a solution as in Eq. (3.24). This can be achieved by requiring three properties:

1. The system of DEs is homogeneous in  $\varepsilon$ .
2. All numerical coefficients are rational numbers.
3. The boundary conditions have UT weight zero.

These conditions allow to write the matrix  $A$  from Eq. (3.10) as

$$A = \varepsilon \sum_i C_i \omega_i, \quad (3.25)$$

where  $C_i$  are rational matrices and  $\omega_i$  are one-forms depending algebraically on the kinematic invariants. Section 3.4.2 outlines why imposing UT boundary conditions inevitably leads to a UT solution.

To obtain a canonical system, two types of transformations are possible:

1. The master integrals  $I_1, \dots, I_{N_{\text{master}}}$  can be replaced by independent linear combinations of the existing master integrals. This includes the replacement of the master integrals with new independent integrals that are related to the original ones via IBPs. Mathematically, the master integrals live in a vector bundle of rank  $N$ : For each configuration of kinematic invariants  $x$ , they map  $x$  to a basis  $I_1(x), \dots, I_{N_{\text{master}}}(x)$  of a vector space. Thus, a linear transformation of the master integrals corresponds to a basis change on a fibre (which is in this case a  $N$ -dimensional vector space) and is therefore called a fibre transformation.
2. The kinematic variables can be transformed, which is called a base transformation. Mathematically, this corresponds to a reparametrization of chart in the base space.

Unfortunately, in practice, a canonical form might not be achievable. From two-loop level on, elliptic integrals might appear, making an algebraic transformation into a homogeneous system in  $\varepsilon$  impossible.

#### 3.2.2. Fibre Transformation

##### Transformation Rule

Consider a vector of master integrals  $\mathcal{I}$  and an invertible complex matrix  $U \in \mathbb{C}^{N_{\text{master}} \times N_{\text{master}}}$  which may depend on the kinematic invariants  $x$  and  $\varepsilon$ . The DEs for  $\mathcal{I}' = U\mathcal{I}$  read

$$\begin{aligned} d\mathcal{I}' &= dU \mathcal{I} + U d\mathcal{I} \\ &= dU \mathcal{I} + U A \mathcal{I} \\ &= (dU U^{-1} + U A U^{-1}) \mathcal{I}'. \end{aligned} \quad (3.26)$$

Consequently the system transforms as

$$\begin{aligned} \mathcal{I} &\rightarrow \mathcal{I}' := U \mathcal{I} \\ A &\rightarrow A' := dU U^{-1} + U A U^{-1}. \end{aligned} \quad (3.27)$$

This allows to change the basis of master integrals by applying an arbitrary linear and invertible transformation.

### The Canonical Form at one-loop level

At one-loop level, a closed formula for a canonical basis exists [56]. Consider a sector with  $e$  independent external momenta and therefore  $N = e + 1$  inverse propagators  $P_i$ . Define  $K_N = G(p_1, \dots, p_e)$  with  $K_1 = 1$  and  $G$  being the Gram determinant from Eq. (2.25). If the number of propagators  $N = 2n - 1$  is odd, the canonical integral is given by

$$g_N \Big|_{N=2n-1} = \varepsilon^n \sqrt{K_N} I_{1, \dots, 1}^{(2n-2\varepsilon)}, \quad (3.28)$$

where  $I_{1, \dots, 1}^{(2n-2\varepsilon)}$  denotes the corner integral of the sector in  $(2n - 2\varepsilon)$  space-time dimensions. For a sector with an even number of distinct propagators  $N = 2n$ , the canonical integrals read

$$g_N \Big|_{N=2n} = \varepsilon^n \sqrt{\mathcal{B}(0)} I_{1, \dots, 1}^{(2n-2\varepsilon)}, \quad (3.29)$$

where  $\mathcal{B}$  denotes the corresponding Baikov polynomial.

### Example: Equal Mass Bubble Integral

Consider the DE for the Bubble integral, given by Eq. (3.20). The canonical basis from Eq. (3.22) can be restored by the above procedure.

According to Eq. (3.28), the canonical tadpole integral is given by

$$g_1 = \varepsilon \sqrt{K_1} I_1^{(2-2\varepsilon)}, \quad (3.30)$$

Using the dimensional shift relations from Eq. (2.21) and  $K_1 = 1$ , this corresponds to

$$g_1 = \varepsilon \mathcal{U}(1^+) I_1^{(4-2\varepsilon)}. \quad (3.31)$$

For a tadpole the first graph polynomial is given by  $U(\alpha_1) = \alpha_1$ . Therefore, the operator  $U(1^+)$  increases the power of the propagator by 1 resulting in the canonical integral

$$g_1 = \varepsilon I_2^{(4-2\varepsilon)}. \quad (3.32)$$

The bubble integral has an even number of distinct propagators. Therefore, the associated canonical integral is given by

$$g_2 = \varepsilon \sqrt{\mathcal{B}(0)} I_{1,1}^{(2-2\varepsilon)}. \quad (3.33)$$

The Baikov polynomial expressed in terms of the Baikov variables is given by

$$\mathcal{B}(z_1, z_2) = (z_2 + m^2) p^2 - \left( \frac{z_1 - z_2 - p^2}{2} \right)^2. \quad (3.34)$$

Setting the Baikov variables to zero gives

$$\mathcal{B}(0) = p^2 m^2 - \frac{1}{4} p^4. \quad (3.35)$$

Next, a dimensional shift relation is needed to express  $I_{1,1}^{(2-2\varepsilon)}$  in terms of  $(4 - 2\varepsilon)$  dimensional integrals. In this case, the graph polynomial corresponds to a sum over two spanning trees,  $\mathcal{U}(\alpha_1, \alpha_2) = \alpha_1 + \alpha_2$ , resulting in

$$g_2 = \varepsilon \sqrt{p^2 m^2 - \frac{1}{4} p^2} \left( I_{1,2}^{(4-2\varepsilon)} + I_{2,1}^{(4-2\varepsilon)} \right). \quad (3.36)$$

The integrals occurring on the right hand side can be expressed in terms of master integrals using IBPs. Inserting these relations and using  $x = -\frac{p^2}{m^2}$  gives the canonical integral for the bubble,

$$g_2 = -\sqrt{\frac{x}{4+x}} \varepsilon \left( I_2^{4-2\varepsilon} - (1 - 2\varepsilon) I_{1,1}^{(4-2\varepsilon)} \right). \quad (3.37)$$

The transformation to obtain the canonical basis can be read off from Eqs. (3.32) and (3.37), resulting in

$$U = \begin{pmatrix} \varepsilon & 0 \\ -\sqrt{\frac{x}{4+x}} \varepsilon & \sqrt{\frac{x}{4+x}} \varepsilon (1 - 2\varepsilon) \end{pmatrix}. \quad (3.38)$$

According to Eq. (2.64), the DE for the canonical integrals reads  $d\mathcal{I}' = A'\mathcal{I}'$  with

$$\mathcal{I}' = \begin{pmatrix} g_1 \\ g_2 \end{pmatrix} \quad \text{and} \quad A' = \varepsilon \begin{pmatrix} 0 & 0 \\ -\frac{1}{\sqrt{x(4+x)}} & -\frac{1}{4+x} \end{pmatrix}, \quad (3.39)$$

which corresponds exactly to the system from Eq. (3.23).

The appearing square roots can not be removed by a fibre transformation. Instead, a redefinition of the kinematic invariants is required.

### 3.2.3. Base Transformation

Square roots  $\sqrt{P(x)}$ , as in the previous example, can appear as soon as massive internal particles enter the diagrams. Physically speaking,  $P(x) = 0$  corresponds to the kinematic threshold at which the massive particle becomes on-shell. Consequently, square roots are an unavoidable feature of massive loop integrals.

#### Transformation Rule

If the canonical system only depends on very few distinct roots, they can be removed on the level of the DE by a change of variables. Consider such a change to new variables  $x'(x)$  depending on the former variables  $x$ . The transformation behavior of the matrices  $A_x$  can be derived within the 1-form notation. Using

$$dx_i = \sum_{j=1}^{N_{\text{kin}}} \frac{\partial x_i}{\partial x'_j} dx'_j, \quad (3.40)$$

gives

$$d\mathcal{I} = \sum_{i=1}^{N_{\text{kin}}} A_{x_i} dx_i = \sum_{i=1}^{N_{\text{kin}}} A_{x_i} \sum_{j=1}^{N_{\text{kin}}} \frac{\partial x_i}{\partial x'_j} dx'_j = \sum_{j=1}^{N_{\text{kin}}} \left( \sum_{i=1}^{N_{\text{kin}}} A_{x_i} \frac{\partial x_i}{\partial x'_j} \right) dx'_j. \quad (3.41)$$

The transformed matrices can be read off as the coefficients of  $dx'_j$  yielding

$$A_{x'_j} = \sum_{i=1}^{N_{\text{kin}}} A_{x_i} \frac{\partial x_i}{\partial x'_j}. \quad (3.42)$$

**Example: Equal Mass Bubble Integral** The canonical form for the equal mass bubble integral derived in Eq. (3.39) contains the square root

$$\sqrt{\frac{x}{4+x}} = \frac{x}{\sqrt{x(4+x)}}. \quad (3.43)$$

The parametrization

$$x = \frac{s^2}{1+s} \quad \text{with} \quad \sqrt{x(4+x)} = \frac{s(2+s)}{1+s}, \quad (3.44)$$

allows to remove the square root. Applying this parametrization at the canonical system from Eq. (3.39) gives

$$\begin{aligned} A_s &= A_x \frac{\partial x}{\partial s} = \varepsilon \begin{pmatrix} 0 & 0 \\ -\frac{1}{1+s} & \frac{1}{1+s} - \frac{2}{2+s} \end{pmatrix} \\ &= \varepsilon \begin{pmatrix} 0 & 0 \\ -d \log(1+s) & d \log(1+s) - 2 d \log(2+s) \end{pmatrix}. \end{aligned} \quad (3.45)$$

When multiple internal mass scales appear, such a complete rationalization at the level of DEs might not be achievable. Instead, the roots can be rationalized during the numerical evaluation, when not all of them occur simultaneously.

This does not prohibit writing the DEs in terms of dlogs. The square root appearing in the canonical system from Eq. (3.39) could also have been written as a dlog,

$$-\frac{1}{\sqrt{x(4+x)}} = 2 d \log(-\sqrt{x} + \sqrt{4+x}) \quad \text{if } x > 0, \quad (3.46)$$

without rationalizing it before.

## 3.3. Iterated Integrals

### 3.3.1. Solution of the Differential Equation

Consider a DE of the form

$$d\mathcal{I}(x) = \varepsilon d \log(\mathcal{R}(x)) \mathcal{I}(x), \quad (3.47)$$

### 3. Differential Equations for Feynman Integrals

---

where  $\mathcal{R}(x)$  is a matrix depending algebraically on a set of kinematic invariants  $x$ , but not on  $\varepsilon$ . A solution of this equation can be constructed by expanding  $\mathcal{I}$  in  $\varepsilon$ ,

$$\mathcal{I}(x) = \sum_{k=0}^{\infty} \varepsilon^k \mathcal{I}^{(k)}(x). \quad (3.48)$$

Inserting this expansion in Eq. (3.47) gives,

$$\sum_{k=0}^{\infty} \varepsilon^k d\mathcal{I}^{(k)}(x) = \sum_{k=0}^{\infty} \varepsilon^{k+1} d \log(\mathcal{R}(x)) \mathcal{I}^{(k)}(x). \quad (3.49)$$

Since  $\mathcal{I}^{(k)}$  and  $\mathcal{R}$  do not depend on  $\varepsilon$ , the coefficients of  $\varepsilon^k$  must agree. Setting them equal yields the equations

$$\begin{aligned} d\mathcal{I}^{(k)}(x) &= d \log(\mathcal{R}(x)) \mathcal{I}^{(k-1)}(x) \quad \text{for } k > 0 \\ d\mathcal{I}^{(0)}(x) &= 0. \end{aligned} \quad (3.50)$$

Integrating both sides results in

$$\mathcal{I}^{(k)}(x) = \int_{\gamma[x]} d \log(\mathcal{R}(t)) \mathcal{I}^{(k-1)}(t) + \mathcal{C}^{(k)}(x_0), \quad (3.51)$$

where  $\mathcal{C}^{(k)}$  is a vector of numerical coefficients,  $\mathcal{I}^{(-1)} = 0$  and  $\gamma[x]$  is an arbitrary path that parametrizes the variables from the boundary point  $x_0$  to the point of evaluation  $x$ . The first orders in  $\varepsilon$  read

$$\begin{aligned} \mathcal{I}^{(0)}(x) &= \mathcal{C}^{(0)}(x_0) \\ \mathcal{I}^{(1)}(x) &= \int_{\gamma[x]} d \log(\mathcal{R}(t_1)) \mathcal{C}^{(0)}(x_0) + \mathcal{C}^{(1)}(x_0) \\ \mathcal{I}^{(2)}(x) &= \int_{\gamma[x]} d \log(\mathcal{R}(t_1)) \int_{\gamma[t_1]} d \log(\mathcal{R}(t_2)) \mathcal{C}^{(0)}(x_0) \\ &\quad + \int_{\gamma[x]} d \log(\mathcal{R}(t_1)) \mathcal{C}^{(1)}(x_0) + \mathcal{C}^{(2)}(x_0) \\ &\quad \vdots \end{aligned} \quad (3.52)$$

where the inner integration is performed along the path  $\gamma$  up to the current point of the outer integration. The vector-valued constants  $\mathcal{C}^{(k)}$  can be determined using the boundary conditions at the point  $x_0$ .

Multiplying out the products of matrices and the vector valued coefficients gives a sum over iterated integrals of scalar quantities  $R_i$ . To express these more compactly, the following notation is introduced,

$$\mathcal{I}(R_1, \dots, R_w; x) = \int_{\gamma[x]} d \log(R_1(t_1)) \dots \int_{\gamma[t^{(w-1)}]} d \log(R_w(t_w)), \quad (3.53)$$

where the number of integrations  $w$  is denoted as the *weight* or *depth* of the iterated integral. Note that the path  $\gamma$  can be chosen arbitrary for all integrals collectively, but generally not for each iterated integral individually. While it is possible to modify the path for individual integrals, it is essential ensure that the correct analytic continuation is restored by including the appropriate residues.

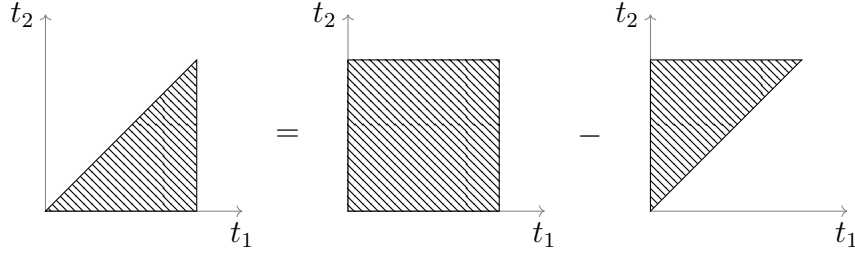


Figure 3.1.: Illustration of the integral reparametrization to obtain shuffle relations.

### 3.3.2. Shuffle Relations

When multiplying the matrices and boundary vectors in Eq. (3.52), each factor increases the number of resulting terms by a factor of  $\mathcal{O}(N_{\text{master}})$ . Starting from  $\mathcal{O}(N_{\text{master}}^2)$  integrals at weight one, this means, that at weight  $w$  the number of scalar iterated integrals is of the order  $\mathcal{O}(N_{\text{master}}^{w+1})$ .

This number can be reduced by making use of relations between iterated integrals. Consider for example an iterated integral of weight two,  $\mathcal{I}(R_1, R_2; x)$ . Parametrizing the path  $\gamma$  with  $t \in [0, 1]$  gives

$$\mathcal{I}(R_1, R_2; x) = \int_0^1 dt_1 \frac{d \log(R_1(\gamma(t_1)))}{dt_1} \int_0^{t_1} dt_2 \frac{d \log(R_2(\gamma(t_2)))}{dt_2}. \quad (3.54)$$

By rearranging the integrals, this can be understood as a two-dimensional integration over a triangle,

$$\mathcal{I}(R_1, R_2; x) = \int_0^1 dt_1 \int_0^{t_1} dt_2 \frac{d \log(R_1(\gamma(t_1)))}{dt_1} \frac{d \log(R_2(\gamma(t_2)))}{dt_2}. \quad (3.55)$$

As depicted in Fig. 3.1, the integral over a triangle can as well be expressed as the integral over a square, minus the integral over the complement triangle, yielding

$$\begin{aligned} \mathcal{I}(R_1, R_2; x) &= \int_0^1 dt_1 \int_0^1 dt_2 \frac{d \log(R_1(\gamma(t_1)))}{dt_1} \frac{d \log(R_2(\gamma(t_2)))}{dt_2} \\ &\quad - \int_0^1 dt_1 \int_{t_1}^1 dt_2 \frac{d \log(R_1(\gamma(t_1)))}{dt_1} \frac{d \log(R_2(\gamma(t_2)))}{dt_2}. \end{aligned} \quad (3.56)$$

The second iterated integral spans the region  $\{0 \leq t_1 \leq t_2 \leq 1\}$ , which can alternatively be handled by first integrating  $t_2$  over the entire interval and then integrating  $t_1$  up to  $t_2$ ,

$$\begin{aligned} \mathcal{I}(R_1, R_2; x) &= \int_0^1 dt_1 \int_0^1 dt_2 \frac{d \log(R_1(\gamma(t_1)))}{dt_1} \frac{d \log(R_2(\gamma(t_2)))}{dt_2} \\ &\quad - \int_0^1 dt_2 \int_0^{t_2} dt_1 \frac{d \log(R_1(\gamma(t_1)))}{dt_1} \frac{d \log(R_2(\gamma(t_2)))}{dt_2} \end{aligned} \quad (3.57)$$

The upper iterated integral can be factorized, since the integration limit of the inner integral does no longer depend on the outer integral. This results in the relation

$$\mathcal{I}(R_1, R_2; x) = \mathcal{I}(R_1; x) \mathcal{I}(R_2; x) - \mathcal{I}(R_2, R_1; x). \quad (3.58)$$

This kind of identities can be generalized to higher dimensions. Just as a square can be decomposed into two triangles, a cube can be decomposed into six tetrahedrons, which gives relations for iterated integrals of weight three. More generally, an  $n$ -dimensional hypercube can be decomposed in  $n$ -simplices yielding relations between iterated integrals of weight  $n$ .

These identities can be expressed by the *shuffle product*: Given two sequences  $A = (a_1, \dots, a_m)$  and  $B = (b_1, \dots, b_n)$ , their shuffle product is the set of all sequences that can be formed by taking the elements of  $A$  and  $B$  and merging them while maintaining the relative order of  $A$  and  $B$ .

The term *shuffle product* can be illustrated with the analogy of a deck of cards. Splitting the deck into two piles and riffle shuffling them together will result in a shuffled deck where the relative order of the cards within each pile is preserved.

As an example, the shuffle product of  $A = (a_1, a_2)$  and  $B = (b_1, b_2)$  is given by the set

$$A \sqcup\sqcup B = \{(a_1, a_2, b_1, b_2), (a_1, b_1, a_2, b_2), (a_1, b_1, b_2, a_2), (b_1, a_1, a_2, b_2), (b_1, a_1, b_2, a_2), (b_1, b_2, a_1, a_2)\}. \quad (3.59)$$

The identity from Eq. (3.58) between weight two integrals can be rewritten in terms of the shuffle product as follows:

$$\mathcal{I}(R_1; x) \mathcal{I}(R_2; x) = \sum_{C \in (R_1) \sqcup\sqcup (R_2)} \mathcal{I}(C; x). \quad (3.60)$$

This relation can be generalized to iterated integrals of arbitrary weights,

$$\mathcal{I}(A; x) \mathcal{I}(B; x) = \sum_{C \in A \sqcup\sqcup B} \mathcal{I}(C; x), \quad (3.61)$$

where  $A$  and  $B$  denote the ordered sets that contain the letters of the first and second iterated integral, respectively.

*Proof.* Consider two sequences  $A$  and  $B$  with  $A = (a_1, \dots, a_m)$  and  $B = (b_{m+1}, \dots, b_n)$  containing at least one element. The proof proceeds by induction over the total number of elements  $n$ . For  $n = 2$ , the relation was already proven.

Consider the case  $n > 2$ . The subsequent equations can be simplified by introducing the notation

$$\tilde{a}_i := \frac{d \log(a_i(\gamma(t_i)))}{dt_i} \quad \text{and} \quad \tilde{b}_i := \frac{d \log(b_i(\gamma(t_i)))}{dt_i}, \quad (3.62)$$

as well as

$$\tilde{\mathcal{I}}(C; t) := \mathcal{I}(C, \gamma(t)). \quad (3.63)$$

Consider the left hand side from Eq. (3.61). Explicitly writing out the integrals gives

$$\mathcal{I}(A; x) \mathcal{I}(B; x) = \int_0^1 dt_1 \tilde{a}_1 \cdots \int_0^{t_{m-1}} dt_m \tilde{a}_m \int_0^1 dt_{m+1} \tilde{b}_{m+1} \cdots \int_0^{t_{n-1}} dt_n \tilde{b}_n. \quad (3.64)$$

The integrals occurring on the right hand side of Eq. (3.61) either start with the first element of  $A$  or  $B$ . The integrals from Eq. (3.64) can be rearranged to represent these two cases by splitting the integration region of  $t_1$  and  $t_{m+1}$  in two subregions:

$$\{0 \leq t_1, t_{m+1} \leq 1\} = \{0 \leq t_{m+1} \leq t_1 \leq 1\} \cup \{0 \leq t_1 < t_{m+1} \leq 1\}. \quad (3.65)$$

The first region corresponds to the case where  $a_1$  is at the first position, while the second region corresponds to the case where  $b_{m+1}$  is at the front. Applying this decomposition gives

$$\begin{aligned} \mathcal{I}(A; x) \mathcal{I}(B; x) &= \int_0^1 dt_1 \tilde{a}_1 \int_0^{t_1} dt_{m+1} \tilde{b}_{m+1} \left( \int_0^{t_1} dt_2 \tilde{a}_2 \cdots \int_0^{t_{m-1}} dt_m \tilde{a}_m \right. \\ &\quad \left. \times \int_0^{t_{m+1}} dt_{m+2} \tilde{b}_{m+2} \cdots \int_0^{t_{n-1}} dt_n \tilde{b}_n \right) \\ &+ \int_0^1 dt_{m+1} \tilde{b}_{m+1} \int_0^{t_{m+1}} dt_1 \tilde{a}_1 \left( \int_0^{t_1} dt_2 \tilde{a}_2 \cdots \int_0^{t_{m-1}} dt_m \tilde{a}_m \right. \\ &\quad \left. \times \int_0^{t_{m+1}} dt_{m+2} \tilde{b}_{m+2} \cdots \int_0^{t_{n-1}} dt_n \tilde{b}_n \right) \\ &= \int_0^1 dt_1 \tilde{a}_1 \tilde{\mathcal{I}}(A \setminus \{a_1\}; t_1) \tilde{\mathcal{I}}(B; t_1) \\ &+ \int_0^1 dt_{m+1} \tilde{b}_{m+1} \tilde{\mathcal{I}}(A; t_{m+1}) \tilde{\mathcal{I}}(B \setminus \{b_{m+1}\}; t_{m+1}). \end{aligned} \quad (3.66)$$

Since the product of iterated integrals in the integrands contains a total of only  $(n - 1)$  arguments, the induction hypotheses can be applied to express them in terms of the shuffle product,

$$\begin{aligned} \mathcal{I}(A; x) \mathcal{I}(B; x) &= \sum_{C \in (A \setminus \{a_1\}) \sqcup B} \int_0^1 dt_1 \tilde{a}_1 \tilde{\mathcal{I}}(C, t_1) \\ &+ \sum_{C \in A \sqcup (B \setminus \{b_{m+1}\})} \int_0^1 dt_{m+1} \tilde{b}_{m+1} \tilde{\mathcal{I}}(C, t_{m+1}) \\ &= \sum_{\substack{C \in A \sqcup B \\ a_1 \text{ in front}}} \mathcal{I}(C; x) + \sum_{\substack{C \in A \sqcup B \\ b_{m+1} \text{ in front}}} \mathcal{I}(C; x) \\ &= \sum_{C \in A \sqcup B} \mathcal{I}(C; x), \end{aligned} \quad (3.67)$$

which concludes the induction.  $\square$

### 3.4. Boundary Conditions

Using the method of DEs, a solution for Feynman integrals can be constructed through iterated integrals as derived in Eq. (3.52). However, this solution still involves unknown integration constants  $\mathcal{C}^{(k)}$ , which correspond to the values of the Feynman integrals at the starting point of the integration path. The starting point can be chosen to simplify the Feynman integrals, for instance by setting a mass to zero or infinity. Nevertheless, these simpler integrals still need to be evaluated by other means. In the following section, some standard methods for calculating Feynman integrals are presented.

#### 3.4.1. Direct computation

##### Wick rotation

For  $\nu \in \mathbb{N}^+$  consider the tadpole integral,

$$I_\nu(m^2) := \text{tadpole diagram} = \mu^{4-D} \int \frac{d^D k}{i\pi^{\frac{D}{2}}} \frac{1}{[k^2 - m^2 + i\delta]^\nu}. \quad (3.68)$$

The integral depends only on the loop momentum squared and does not exhibit any additional angular dependence. It is then natural to change the coordinate system to spherical coordinates. However,  $k^2$  still corresponds to the scalar product in Minkowski space, therefore a transformation to Euclidean space must be applied.

As a first step, the time component  $k^0$  is separated from the spatial components  $\mathbf{k}$ ,

$$I_\nu(m^2) = \mu^{4-D} \int \frac{d^{D-1}\mathbf{k}}{i\pi^{\frac{D}{2}}} \int_{-\infty}^{\infty} dk_0 \frac{1}{[k_0^2 - \mathbf{k}^2 - m^2 + i\delta]^\nu}. \quad (3.69)$$

The integrand has two poles of order  $\nu$  in  $k_0 = \pm\sqrt{\mathbf{k}^2 + m^2} \mp i\delta$ . Closing the integration of  $k_0$  from  $-R$  to  $R$  by extending it to an integral over a closed path  $\gamma_R$  as shown in Fig. 3.2 gives

$$\int_{\gamma_R} dk_0 \frac{1}{[k_0^2 - \mathbf{k}^2 - m^2 + i\delta]^\nu} = 0, \quad (3.70)$$

since the curve does not enclose any poles. For  $R \rightarrow \infty$  the integration over the arcs vanishes due to Jordan's Lemma, yielding

$$\begin{aligned} \int_{-\infty}^{\infty} dk_0 \frac{1}{[k_0^2 - \mathbf{k}^2 - m^2 + i\delta]^\nu} &= \int_{-i\infty}^{i\infty} dk_0 \frac{1}{[k_0^2 - \mathbf{k}^2 - m^2 + i\delta]^\nu} \\ &= (-1)^\nu \int_{-\infty}^{\infty} dq_0 \frac{1}{[q_0^2 + \mathbf{q}^2 - m^2 + i\delta]^\nu}, \end{aligned} \quad (3.71)$$

where the substitution  $k_0 = iq_0$  was used.

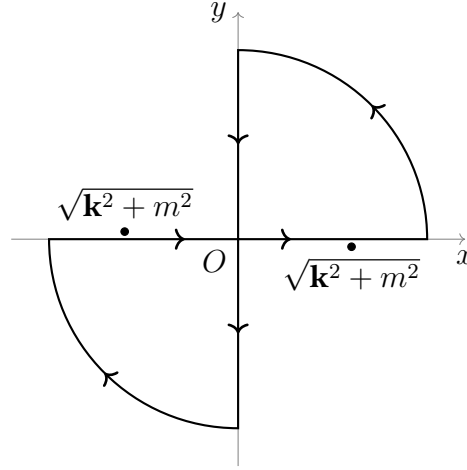


Figure 3.2.: Integration path for the Wick rotation

Inserting Eq. (3.71) into the tadpole integral gives,

$$I_\nu(m^2) = \mu^{4-D} (-1)^\nu \int \frac{d^D q}{i\pi^{\frac{D}{2}}} \frac{1}{[q^2 + m^2 - i\delta]^\nu}, \quad (3.72)$$

where  $q^2$  corresponds to a scalar product in Euclidean metrics, which can be evaluated in spherical coordinates. The explicit evaluation yields

$$I_\nu(m^2) = \frac{(-1)^\nu}{(\nu-1)!} \left( \frac{\mu^2}{m^2 - i\delta} \right)^\varepsilon (m^2)^{2-\nu} \Gamma(\nu - 2 + \varepsilon) \quad (3.73)$$

where  $D = 4 - 2\varepsilon$  was used.

### Feynman Parametrization

The Feynman parameter representation introduced in Sec. 2.1.2 allows a dimensional regularized Feynman integral to be rewritten as an integral over Feynman parameters. In certain special cases, these integrals can be computed analytically.

**Example: Bubble Integral** Consider the bubble integral  $I_{\nu_1, \nu_2}(p^2, m_1^2, m_2^2)$  with the incoming momentum  $p$  and two massive propagators with the masses  $m_1$  and  $m_2$ , raised to the powers  $\nu_1$  and  $\nu_2$ , respectively,

$$\begin{array}{c} \xrightarrow{p} \\ \bullet \\ \text{---} \bullet \text{---} \\ \text{---} \bullet \text{---} \\ \bullet \\ \xrightarrow{m_2} \end{array} = \mu^{4-D} \int \frac{d^D k}{i\pi^{\frac{D}{2}}} \frac{1}{[(k+p)^2 - m_1^2 + i\delta]^{\nu_1} [k^2 - m_2^2 + i\delta]^{\nu_2}} \quad (3.74)$$

The Feynman parameter representation from Eq. (2.22) gives

$$I_{\nu_1, \nu_2} = \mu^{4-D} \frac{\Gamma(\nu_1 + \nu_2)}{\Gamma(\nu_1)\Gamma(\nu_2)} \int_0^1 d\alpha \int \frac{d^D k}{i\pi^{\frac{D}{2}}} \frac{\alpha^{\nu_1-1} (1-\alpha)^{\nu_2-1}}{[(k + \alpha p)^2 - \Omega^2 + i\delta]^{\nu_1 + \nu_2}}, \quad (3.75)$$

### 3. Differential Equations for Feynman Integrals

with  $\Omega^2 = -\alpha(1-\alpha)p^2 + \alpha m_1^2 + (1-\alpha)m_2^2$ . Substituting  $k \rightarrow k + \alpha p$  results in a tadpole integral with the mass  $\Omega$ . Using the expression for the tadpole from Eq. (3.73) gives

$$I_{\nu_1, \nu_2}(p^2, m_1^2, m_2^2) = (-1)^{\nu_1 + \nu_2} \mu^{2\varepsilon} \frac{\Gamma(\nu_1 + \nu_2 - 2 + \varepsilon)}{\Gamma(\nu_1)\Gamma(\nu_2)} \times \int_0^1 d\alpha \alpha^{\nu_1-1} (1-\alpha)^{\nu_2-1} (\Omega^2 - i\delta)^{2-\nu_1-\nu_2-\varepsilon} \quad (3.76)$$

The integral over  $\alpha$  can be evaluated in some special cases:

**Case 1:  $m_1 = m_2 = 0$  and  $p^2 \neq 0$**

$$I_{\nu_1, \nu_2}(p^2, 0, 0) = (-1)^{\nu_1 + \nu_2} \left( \frac{\mu^2}{-p^2 - i\delta} \right)^\varepsilon (-p^2 - i\delta)^{2-\nu_1-\nu_2} \times \frac{\Gamma(\nu_1 + \nu_2 - 2 + \varepsilon)}{\Gamma(\nu_1)\Gamma(\nu_2)} \frac{\Gamma(2 - \nu_1 - \varepsilon)\Gamma(2 - \nu_2 - \varepsilon)}{\Gamma(4 - \nu_1 - \nu_2 - 2\varepsilon)}. \quad (3.77)$$

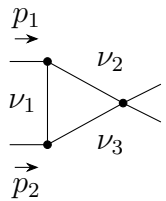
**Case 2:  $m_1 = m, m_2 = 0$  and  $p^2 = 0$**

$$I_{\nu_1, \nu_2}(0, m^2, 0) = (-1)^{\nu_1 + \nu_2} \left( \frac{\mu^2}{m^2 - i\delta} \right)^\varepsilon (m^2 - i\delta)^{2-\nu_1-\nu_2} \times \frac{\Gamma(\nu_1 + \nu_2 - 2 + \varepsilon)}{\Gamma(\nu_1)\Gamma(\nu_2)} \frac{\Gamma(\nu_2)\Gamma(2 - \nu_2 - \varepsilon)}{\Gamma(2 - \varepsilon)}. \quad (3.78)$$

**Case 3:  $m_1 = m_2 = m$  and  $p^2 = 0$**

$$I_{\nu_1, \nu_2}(0, m, m) = (-1)^{\nu_1 + \nu_2} \left( \frac{\mu^2}{m^2 - i\delta} \right)^\varepsilon (m^2 - i\delta)^{2-\nu_1-\nu_2} \times \frac{\Gamma(\nu_1 + \nu_2 - 2 + \varepsilon)}{\Gamma(\nu_1 + \nu_2)}. \quad (3.79)$$

**Example: Massless Triangle Integral** Consider the massless triangle integral  $I_{\nu_1, \nu_2, \nu_3}$  with two massless external legs with momenta  $p_1$  and  $p_2$ ,



$$= \mu^{4-D} \int \frac{d^D k}{i\pi^{\frac{D}{2}}} \frac{1}{[k^2 + i\delta]^{\nu_1} [(k + p_1)^2 + i\delta]^{\nu_2} [(k - p_2)^2 + i\delta]^{\nu_3}}. \quad (3.80)$$

The only non-zero scalar product which can be constructed from the external momenta is  $(p_1 \cdot p_2) = \frac{s}{2}$ . Since no internal masses are present, the integral depends solely on  $s$ . Using the Feynman parametrization for the first two propagators yields

$$I_{\nu_1, \nu_2, \nu_3}(s) = \mu^{4-D} \frac{\Gamma(\nu_1 + \nu_2)}{\Gamma(\nu_1)\Gamma(\nu_2)} \times \int_0^1 d\alpha \int \frac{d^D k}{i\pi^{\frac{D}{2}}} \frac{\alpha^{\nu_1-1} (1-\alpha)^{\nu_2-1}}{[(k + (1-\alpha)p_1)^2 + i\delta]^{\nu_1 + \nu_2} [(k - p_2)^2 + i\delta]^{\nu_3}}. \quad (3.81)$$

The resulting integral over  $k$  equals a massless bubble integral with incoming momentum  $(1 - \alpha)p_1 + p_2$ . Using the result for the massless bubble integral from Eq. (3.77) gives

$$I_{\nu_1, \nu_2, \nu_3}(s) = \frac{\Gamma(\nu_2 + \nu_2 + \nu_3 - 2 + \varepsilon)\Gamma(2 - \nu_1 - \nu_2 - \varepsilon)\Gamma(2 - \nu_3 - \varepsilon)}{\Gamma(\nu_1)\Gamma(\nu_2)\Gamma(\nu_3)\Gamma(4 - \nu_1 - \nu_2 - \nu_3 - 2\varepsilon)} \times \left(\frac{\mu^2}{-s - i\delta}\right)^\varepsilon (-s - i\delta)^{2 - \nu_1 - \nu_2 - \nu_3} \int d\alpha \alpha^{\nu_1 - 1} (1 - \alpha)^{1 - \nu_1 - \nu_3 - \varepsilon}. \quad (3.82)$$

The resulting integral over the Feynman parameter  $\alpha$  can be solved for certain values of  $\nu_1, \nu_2$  and  $\nu_3$ . For example the case  $\nu_1 = \nu_2 = \nu_3 = 1$  gives

$$I_{1,1,1}(s) = \left(\frac{\mu^2}{-s - i\delta}\right)^\varepsilon \frac{1}{-s - i\delta} \frac{1}{\varepsilon} \frac{\Gamma(1 - \varepsilon)\Gamma(1 + \varepsilon)\Gamma(-\varepsilon)}{\Gamma(1 - 2\varepsilon)}. \quad (3.83)$$

### Iterative calculation

Consider the vacuum sunset integral  $I(m^2)$  with one massive line,

$$\begin{array}{c} \overbrace{\text{---}}^{k_1} \\ \text{---} \\ \underbrace{\text{---}}_{k_2} \end{array} = (\mu^{4-D})^2 \int \frac{d^D k_1}{i\pi^{\frac{D}{2}}} \int \frac{d^D k_2}{i\pi^{\frac{D}{2}}} \frac{1}{[k_1^2 + i\delta][(k_1 - k_2)^2 + i\delta][k_2^2 - m^2 + i\delta]}. \quad (3.84)$$

The integration about  $k_1$  corresponds to a massless bubble integral with the incoming momentum  $k_2$ . Using the result for the massive bubble from Eq. (3.77) gives

$$I(m^2) = (-1)^{-\varepsilon} \mu^{4\varepsilon} \frac{\Gamma(1 - \varepsilon)^2 \Gamma(\varepsilon)}{\Gamma(2 - 2\varepsilon)} \int \frac{d^D k_2}{i\pi^{\frac{D}{2}}} \frac{1}{[k_2^2 + i\delta]^\varepsilon [k_2^2 - m^2 + i\delta]}. \quad (3.85)$$

Graphically, this corresponds to combining the two massless lines into a single massless propagator with momentum  $k_2$ , raised to the power  $\varepsilon$ :

$$\begin{array}{c} \text{---} \\ \text{---} \end{array} = \begin{array}{c} \text{---} \\ \text{---} \end{array} \times \begin{array}{c} \text{---} \\ \text{---} \end{array} \quad (3.86)$$

The resulting integral is a bubble integral with one massive line, which can be evaluated using Eq. (3.78), yielding

$$I(m^2) = (-1)^{-\varepsilon} \left(\frac{\mu^2}{m^2}\right)^{2\varepsilon} m^2 \frac{\Gamma(1 - \varepsilon)^2 \Gamma(-1 + 2\varepsilon) \Gamma(\varepsilon) \Gamma(1 + \varepsilon)}{\Gamma(2 - \varepsilon)}. \quad (3.87)$$



**Example: Transcendental Weight of a Tadpole Diagram** Consider the tadpole diagram with one propagator derived in Eq. (3.73). Setting  $\mu^2 = m^2$ , rescaling the integral by  $\exp(\gamma_E \varepsilon)$  in order to remove the otherwise appearing Euler-Mascheroni constant  $\gamma_E$  and expanding the Gamma-function,  $\Gamma(-1 + \varepsilon)$ , in  $\varepsilon$  gives

$$-\frac{\exp(\gamma_E \varepsilon)}{m^2} \text{tadpole}(k) = -\frac{1}{\varepsilon} - 1 + \left(\frac{\pi^2}{12} - 1\right) \varepsilon + \mathcal{O}(\varepsilon^2). \quad (3.94)$$

In the first order in  $\varepsilon$ , the number  $-1$  with weight zero and  $\pi^2$  with weight two occur. Therefore, this expression does not have UT weight. On the other hand, the expression for a general tadpole with the propagator raised to the power  $\nu$  as in Eq. (3.73) contains the factor  $\Gamma(\nu - 2 + \varepsilon)$ . Setting  $\nu = 3$ , the expansion of the gamma function reads

$$\exp(\gamma_E \varepsilon) \Gamma(1 + \varepsilon) = 1 + \frac{\pi^2}{12} \varepsilon^2 + \mathcal{O}(\varepsilon^3), \quad (3.95)$$

which has uniform weight zero. It is therefore natural to use the tadpole with three propagators instead of the tadpole with one propagator as a master integral,

$$-m^2 \exp(\gamma_E \varepsilon) \text{tadpole}_3(k) = \frac{1}{2} \left( 1 + \frac{\pi^2}{12} \varepsilon^2 + \mathcal{O}(\varepsilon^3) \right). \quad (3.96)$$

The transformation is given by the relation,

$$\text{tadpole}_3(k) = \frac{\varepsilon(-1 + \varepsilon)}{m^4} \text{tadpole}(k). \quad (3.97)$$

The tadpole with  $\nu = 3$  exactly corresponds to the first canonical integral from Eq. (3.39).

### 3.4.3. Large Mass Expansion

The difficulty of computing Feynman integrals increases considerably with the number of scales and loops involved. If a propagators of an integral family includes a mass  $m$ , using the boundary condition  $m \rightarrow \infty$  can significantly simplify the dependence on other external scales.

Consider an inverse propagator with mass  $m$ ,

$$P = (k + q)^2 - m^2 + i\delta, \quad (3.98)$$

which depends on the loop momentum  $k$  and on a linear combination of the external momenta  $q$ . Let the energy scale of the external momenta be denoted by  $\Lambda$ . Simply neglecting all momenta relative to the mass when  $m \gg \Lambda$  is not sufficient, since the loop momentum is integrated over the entire  $D$ -dimensional space, which includes both regions where  $k^2 \propto \Lambda^2$  and where  $k^2 \propto m^2$ .

Thus, for the loop momentum, it is necessary to distinguish between the large mass scale  $m$  and the smaller energy scale  $\Lambda$ . The large mass expansion is then given by the sum of both cases [57],

$$\lim_{m^2 \gg \Lambda} \int \frac{d^D k}{i\pi^{\frac{D}{2}}} \prod_{j=1}^n \frac{1}{P_j^{\nu_j}} = \left( \int \frac{d^D k}{i\pi^{\frac{D}{2}}} \prod_{j=1}^n \frac{1}{P_j^{\nu_j}} \Big|_{k^2 \propto \Lambda^2} + \int \frac{d^D k}{i\pi^{\frac{D}{2}}} \prod_{j=1}^n \frac{1}{P_j^{\nu_j}} \Big|_{k^2 \propto m^2} \right). \quad (3.99)$$

Practically, the expansions of the propagators can be calculated by multiplying all small quantities (i.e. all external momenta and masses which are not taken to infinity as well as the loop momentum in the case  $k^2 \ll m^2$ ) by a factor of  $\rho$ . The integrand is then expanded in  $\rho$  around  $\rho = 0$ , corresponding to an expansion in the small quantities. Once the expansion is complete,  $\rho$  is set to 1. Note that all odd orders of the expansion should vanish since they contain factors of  $\rho$  in the numerator, which are zero when  $\rho = 0$ . This can be used as a crosscheck for the expansion.

**Example: Equal Mass Bubble Integral** Consider the equal mass bubble integral  $I_{1,1}$  from Eq. (3.13). In the case where the loop momentum is of the same order as the energy scale of the external momentum,  $\Lambda$ , the external and loop momenta are multiplied with  $\rho$ . The leading order expansion in  $\rho$  around  $\rho = 0$  gives a scaleless integral,

$$I_{1,1}|_{k^2 \propto \Lambda^2} = \mu^{4-D} \int \frac{d^D k}{i\pi^{\frac{D}{2}}} \frac{1}{[-m^2 + i\delta]^2} + \mathcal{O}(\rho^2) = 0. \quad (3.100)$$

For large loop momenta,  $k^2 \propto m^2$ , only the external momentum is multiplied with  $\rho$ . Then, the leading order expansion around  $\rho = 0$  yields

$$I_{1,1}|_{k^2 \propto m^2} = \mu^{4-D} \int \frac{d^D k}{i\pi^{\frac{D}{2}}} \frac{1}{[k^2 - m^2 + i\delta]^2} + \mathcal{O}(\rho^2). \quad (3.101)$$

The resulting integral corresponds to a massive tadpole with its propagator raised to the power two. According to Eq. (3.73) the leading order large mass expansion of the bubble is then given by

$$\lim_{m \gg \Lambda} I_{1,1} = \left( \frac{\mu^2}{m^2 - i\delta} \right)^\varepsilon \Gamma(\varepsilon). \quad (3.102)$$

The above procedure for approximating one-loop Feynman integrals with large masses can be generalized to  $l$ -loop integrals. Then, all possible regions for the loop momenta must be considered.

**Example: Equal Mass Sunset Integral** Consider the equal mass sunset integral with incoming momentum  $p$ ,

$$I_{1,1,1} = \text{Diagram} \quad (3.103)$$

To calculate the large mass expansion, the sum over all kinematic regions of the loop momenta is taken into account. Specifically, this involves the following regions:

- **Both loop momenta are large:** This occurs when  $k_1^2 \propto m^2$  and  $k_2^2 \propto m^2$ . In this case it is important to additionally distinguish whether their difference  $(k_1 - k_2)^2$  is large or small.
- **Both loop momenta are small:** Here,  $k_1 \ll m^2$  and  $k_2 \ll m^2$ .
- **Mixed region:** One loop momentum is large, the other one is small. The difference  $k_1 - k_2$  is considered as large.

Graphically this can be illustrated as

$$\text{Diagram} = \text{Diagram}_1 + \text{Diagram}_2 + \text{Diagram}_3 + \text{Diagram}_4 + \text{Diagram}_5, \quad (3.104)$$

with a dotted line representing a propagator with a small loop momentum.

## 3.5. Numerical Evaluation of Feynman Integrals

To obtain a numerical result, the iterated integrals derived from the DEs must be evaluated. The key challenge in this process is ensuring numerical stability. However, these integrals may have poles near the integration path, which can significantly slow down algorithms for numerical integration. Thus, an efficient method is necessary, which converges sufficiently fast despite the poles.

### 3.5.1. Multiple Polylogarithms

A DE in canonical form can lead to iterated integrals over simple poles which corresponds to the integral representation of *multiple polylogarithms* (GPLs) [58]<sup>1</sup>.

<sup>1</sup>In other literature, multiple polylogarithms might be denoted as generalized polylogarithms or Goncharov polylogarithms.

GPLs are functions that can be computed with high numerical stability. By using their sum representation and further symmetry relations, their convergence can be significantly accelerated, making them efficient for numerical evaluation.

Note that GPLs are not required to examine the analytic properties of the amplitude. Divergencies at specific kinematic configurations can also be investigated using iterated integrals.

### Integral Representation

GPLs of *weight*  $w$  are defined by the recursive relations

$$G(z_1, \dots, z_w; x) = \int_0^x \frac{dt}{t - z_1} G(z_2, \dots, z_w; t), \quad (3.105)$$

with  $G(; t) = 1$  and  $z_1, \dots, z_w \in \mathbb{C}$  with at least one  $z_j \neq 0$ . If all  $z_j$  are zero, the definition reads

$$G(\underbrace{0, \dots, 0}_w; x) = \frac{\log^w(x)}{w!}. \quad (3.106)$$

Iterated integrals with simple poles such as generated from Eq. (3.45), align precisely with this definition.

### Sum Representation

The sum representation of GPLs is useful for their numerical evaluation. Its derivation can be sketched by considering a simple example,

$$G_{m-1}\left(\frac{1}{a}; x\right) = \int_0^x \frac{dt_1}{t_1} \int_0^{t_1} \frac{dt_2}{t_2} \dots \int_0^{t_{m-2}} \frac{dt_{m-1}}{t_{m-1}} \int_0^{t_{m-1}} \frac{dt_m}{t_m - \frac{1}{a}}, \quad (3.107)$$

where the following short hand notation is used,

$$G_{m_1, \dots, m_d}(z_1, \dots, z_d; x) = G(\underbrace{0, \dots, 0}_{m_1-1}, z_1, \dots, z_{d-1}, \underbrace{0, \dots, 0}_{m_d-1}, z_d; x). \quad (3.108)$$

The last integrand can be expressed with the geometric series,

$$\begin{aligned} G_{m-1}\left(\frac{1}{a}; x\right) &= -a \int_0^x \frac{dt_1}{t_1} \int_0^{t_1} \frac{dt_2}{t_2} \dots \int_0^{t_{m-2}} \frac{dt_{m-1}}{t_{m-1}} \int_0^{t_{m-1}} dt_m \sum_{k=0}^{\infty} (at_m)^k \\ &= - \int_0^x \frac{dt_1}{t_1} \int_0^{t_1} \frac{dt_2}{t_2} \dots \int_0^{t_{m-2}} \frac{dt_{m-1}}{t_{m-1}} \sum_{k=0}^{\infty} \frac{(at_{m-1})^{k+1}}{k+1}. \end{aligned} \quad (3.109)$$

Each further integration increases the power of  $(k+1)$  by one, yielding

$$G_{m-1}\left(\frac{1}{a}; x\right) = - \sum_{k>0} \frac{(ax)^k}{k^m}. \quad (3.110)$$

The resulting series converges absolutely for  $|ax| < 1$ , since

$$\sum_{k>0} \left| \frac{(ax)^k}{k^m} \right| < \sum_{k=0}^{\infty} |ax|^k = \frac{1}{1 - |ax|}, \quad (3.111)$$

making it a promising ansatz for numerical evaluation. The next more difficult case is an additional integration over a non-zero pole,

$$\begin{aligned} G_{0,m-1} \left( \frac{1}{a_1}, \frac{1}{a_1, a_2}; x \right) &= - \int_0^x \frac{dt}{t - \frac{1}{a_1}} \sum_{k_2>0} \frac{(a_1 a_2 t)^{k_2}}{k_2^m} \\ &= \sum_{k_2>0} \frac{a_2^{k_2}}{k_2^m} a_1 \int_0^x dt \frac{(a_1 t)^{k_2}}{1 - a_1 t}. \end{aligned} \quad (3.112)$$

This time, the geometric series starting from  $k_1 = k_2$  can be used to carry out the integration,

$$G_{0,m-1} \left( \frac{1}{a_1}, \frac{1}{a_1, a_2}; x \right) = \sum_{k_2>0} \frac{a_2^{k_2}}{k_2^m} a_1 \int_0^x dt \sum_{k_1 \geq k_2} (a_1 t)^{k_1} = \sum_{k_1>k_2>0} \frac{a_1^{k_1} a_2^{k_2}}{k_1^{k_1} k_2^{k_2}}. \quad (3.113)$$

This procedure can be iteratively continued by adding more zeros or non-zero arguments, resulting in the sum representation of GPLs,

$$\begin{aligned} \text{Li}_{m_1, \dots, m_n}(a_1, \dots, a_n) &:= G_{m_1, \dots, m_n} \left( \frac{1}{a_1}, \frac{1}{a_1 a_2}, \dots, \frac{1}{a_1 \dots a_n}; 1 \right) \\ &= \sum_{k_1 > \dots > k_n > 0} \prod_{j=1}^n \frac{a_j^{k_j}}{k_j^{m_j}}, \end{aligned} \quad (3.114)$$

which converges absolutely if  $|a_1 \dots a_j| < 1$  for all  $j \in \{1, \dots, n\}$ .

Two assumptions have been made for the definition of the sum representation. First, the GPL in integral representation is evaluated at  $x = 1$ . This can always be achieved, by making use of the scaling relation,

$$G(\lambda z_1, \dots, \lambda z_w, \lambda x) = G(z_1, \dots, z_w, x), \quad (3.115)$$

which can be derived by substituting  $t_k \rightarrow \lambda t_k$  in the integrals.

Secondly it was assumed, that the GPL does not have a *trailing zero*, meaning that a zero does not appear as the last argument. Trailing zeros can be isolated with shuffle relations, which GPLs inherit from their definition as iterated integrals. Consider a GPL with  $a_j \neq 0$  and  $w - j$  trailing zeros,

$$G(a_1, \dots, a_j, \underbrace{0, \dots, 0}_{w-j}; x). \quad (3.116)$$

The shuffle relation

$$G(0; x) G(a_1, \dots, a_j, \underbrace{0, \dots, 0}_{w-j-1}; x) = (w-j) G(a_1, \dots, a_j, \underbrace{0, \dots, 0}_{w-j}; x) + \sum_{C \in (a_1, \dots, a_{j-1}) \sqcup (0)} G(C, a_j, \underbrace{0, \dots, 0}_{w-j-1}), \quad (3.117)$$

allows to remove a trailing zero by rewriting the GPL with  $w - j$  trailing zeros in terms of GPLs with  $w - j - 1$  trailing zeros and  $G(0; x) = \log(x)$ . By iteratively applying this relation, the trailing zeros can be fully isolated as logarithms.

Therefore, any GPL in the integral notation can be rewritten in terms of GPLs in the sum representation and logarithms.

### Numerical Evaluation

A number of computer codes, such as GiNaC [59], provide fast and automated tools for evaluating GPLs. The principle idea of the computation is to approximate them by calculating their sum representation up to an upper limit  $N$ ,

$$I(N) := \sum_{k_1 > \dots > k_n > 0} \prod_{j=1}^n \frac{a_j^{k_j}}{k_j^{m_j}} \approx \text{Li}_{m_1, \dots, m_n}(a_1, \dots, a_n) + \mathcal{O}(\epsilon). \quad (3.118)$$

The upper limit  $N$  is determined by the desired precision  $\epsilon$  via

$$|I(N) - I(N - 1)| < \epsilon. \quad (3.119)$$

Two aspects need to be highlighted for this approach. First, intermediate particles going on-shell might result in GPLs with poles on the integration path yielding a non-converging sum representation. To solve this, the arguments of the GPLs can be moved to a region of convergence by a suitable transformation as explained in Ref. [40]. Secondly, poles near the integration path can spoil the series convergence. These poles can be moved further away from the path by alternately applying the Hölder convolution [60] and a transformation into a region of convergence.

### 3.5.2. Mapping Iterated Integrals on GPLs

A DE in canonical form does not necessarily yield GPLs as its solution. However, the iterated integrals might still be mapped to GPLs, even when they involve non-rational dependencies on the kinematic invariants. Multiple square roots appearing together in the DEs and avoiding a rationalization may not occur together within the same iterated integral, allowing them to be rationalized independently.

### Rationalizing Square Roots

The square roots appearing in the dlogs contain rational functions, which means that they can be written as

$$y = \sqrt{\frac{g(x_1, \dots, x_{N_{\text{kin}}})}{h(x_1, \dots, x_{N_{\text{kin}}})}} \quad (3.120)$$

with polynomials  $g$  and  $h$ . Following Ref. [61], finding a rational transformation for  $x$  is equivalent to finding a rational parametrization for the hypersurface defined by the equation

$$f(x_1, \dots, x_N, y) := y^2 h(x_1, \dots, x_N) - g(x_1, \dots, x_N) = 0, \quad (3.121)$$

where  $f$  is a polynomial of degree  $n$ .

As a first step to get such a parametrization, the coordinates are shifted to obtain a form where  $f$  can be written as

$$f(x_1, \dots, x_{N_{\text{kin}}}, y) = f_{n-1}(x_1, \dots, x_{N_{\text{kin}}}, y) + f_n(x_1, \dots, x_{N_{\text{kin}}}, y), \quad (3.122)$$

with polynomials  $f_{n-1}$  and  $f_n$  which are homogeneous of degree  $n-1$  and  $n$ , respectively<sup>2</sup>. In general a polynomial of degree  $n$  can just be decomposed in  $(n+1)$  polynomials,

$$f(x_1, \dots, x_{N_{\text{kin}}}, y) = f_0(x_1, \dots, x_{N_{\text{kin}}}, y) + \dots + f_n(x_1, \dots, x_{N_{\text{kin}}}, y), \quad (3.123)$$

where  $f_k$  is homogeneous of degree  $k$ . The assumptions  $f_0 = \dots = f_{n-2} = 0$  and  $f_{n-1} \neq 0$  are equivalent to the vanishing of the first  $(n-2)$  partial derivatives in the origin, with at least one  $(n-1)$ -th partial derivative being non-zero. A point with this property is called to be of *multiplicity*  $(n-2)$ . A point of multiplicity 1 is called *regular*. If any point  $p$  of multiplicity  $(n-2)$  exists, the origin can be shifted to that point by applying the transformation

$$x_k \rightarrow \tilde{x}_k = x_k + p_k. \quad (3.124)$$

Written in these new coordinates,  $f$  can be decomposed as in Eq. (3.122).

In this form, a rational transformation can be found by setting

$$\begin{aligned} \tilde{x}_2 &= t_1 \tilde{x}_1 \\ &\vdots \\ \tilde{x}_{N_{\text{kin}}} &= t_{N_{\text{kin}}-1} \tilde{x}_1 \\ y &= t_{N_{\text{kin}}} \tilde{x}_1, \end{aligned} \quad (3.125)$$

yielding

$$\begin{aligned} f(\tilde{x}_1, t_1 \tilde{x}_1, \dots, t_{N_{\text{kin}}} \tilde{x}_1) &= f_{n-1}(\tilde{x}_1, t_1 \tilde{x}_1, \dots, t_{N_{\text{kin}}} \tilde{x}_1) + f_n(\tilde{x}_1, t_1 \tilde{x}_1, \dots, t_{N_{\text{kin}}} \tilde{x}_1) \\ &= \tilde{x}_1^{n-1} [f_{n-1}(1, t_1, \dots, t_{N_{\text{kin}}}) + \tilde{x}_1 f_n(1, t_1, \dots, t_{N_{\text{kin}}})]. \end{aligned} \quad (3.126)$$

<sup>2</sup>A polynomial  $f$  is homogeneous of degree  $k$  if  $f(\lambda x_1, \dots, \lambda x_{N_{\text{kin}}}) = \lambda^k f(x_1, \dots, x_{N_{\text{kin}}})$ .

The equation vanishes if  $\tilde{x}_1$  is chosen such that the term in the brackets vanishes. This results in the transformation

$$\begin{aligned}\phi_{\tilde{x}_1}(t_1, \dots, t_{N_{\text{kin}}}) &= -\frac{f_{n-1}(1, t_1, \dots, t_{N_{\text{kin}}})}{f_n(1, t_1, \dots, t_{N_{\text{kin}}})} \\ \phi_{\tilde{x}_2}(t_1, \dots, t_{N_{\text{kin}}}) &= -t_1 \frac{f_{n-1}(1, t_1, \dots, t_{N_{\text{kin}}})}{f_n(1, t_1, \dots, t_{N_{\text{kin}}})} \\ &\vdots \\ \phi_{\tilde{x}_N}(t_1, \dots, t_{N_{\text{kin}}}) &= -t_{N-1} \frac{f_{n-1}(1, t_1, \dots, t_{N_{\text{kin}}})}{f_n(1, t_1, \dots, t_{N_{\text{kin}}})}.\end{aligned}\tag{3.127}$$

The rational transformations for the initial coordinates  $x_k$  are obtained by applying the inverse transformation from Eq. (3.124), yielding  $\phi_{x_k}(t_1, \dots, t_{N_{\text{kin}}}) = \phi_{\tilde{x}_k}(t_1, \dots, t_{N_{\text{kin}}}) - p_k$ .

Note that specifically setting the argument  $x_1$  to one in Eq. (3.127) was arbitrary. In general, any of the arguments can be set to one.

**Example: Rationalizing  $\sqrt{\mathbf{x}(4 + \mathbf{x})}$**  The rationalization of the square root  $\sqrt{x(4 + x)}$  from Eq. (3.44) can be derived following the presented method. Rationalizing this square root is equivalent to finding a rational transformation of the hypersurface defined by

$$f(x, y) = y^2 - x(x + 4) = 0.\tag{3.128}$$

Since the origin is a regular point,  $f$  can be decomposed as  $f = f_1 + f_2$  with

$$f_1(x, y) = -4x \quad \text{and} \quad f_2(x, y) = y^2 - x^2.\tag{3.129}$$

Setting  $x = ty$  gives the parametrization

$$\phi_y(t) = \frac{4t}{1 - t^2} \quad \text{and} \quad \phi_x(t) = \frac{4t^2}{1 - t^2},\tag{3.130}$$

which rationalizes the square root. The rationalization can be adjusted by substitutions of the form  $t = g(s)$ . The substitution  $t = -\frac{s}{2+s}$  restores the transformation from Eq. (3.44),

$$\tilde{\phi}_y(s) = -\frac{s(2 + s)}{1 + s} \quad \text{and} \quad \tilde{\phi}_x(s) = \frac{s^2}{1 + s},\tag{3.131}$$

with the properties  $\tilde{\phi}_y(0) = \tilde{\phi}_x(0) = 0$  and  $\tilde{\phi}_y(s), \tilde{\phi}_x(s) > 0$  for  $s > 0$ .

### Logarithmic Properties of Iterated Integrals

To further simplify iterated integrals, their origin from dlogs can be used. This means they behave similar to logarithms with respect to each of their arguments. For instance,

$$\begin{aligned}\mathcal{I}(R_1, \dots, R_k^{(1)} \cdot R_k^{(2)}, \dots, R_w; x) &= \mathcal{I}(R_1, \dots, R_k^{(1)}, \dots, R_w; x) \\ &\quad + \mathcal{I}(R_1, \dots, R_k^{(2)}, \dots, R_w; x).\end{aligned}\tag{3.132}$$

Note that for logarithms an additional phase may be considered, depending on the complex argument of  $R_k^{(1)}$  and  $R_k^{(2)}$ . However, for iterated integrals that are based on dlogs, this phase can be omitted, as it vanishes when taking the derivative.

**Example: A Depth-2 Iterated Integral**

Consider the iterated integral<sup>3</sup>

$$I = \mathcal{I}\left(1 + \frac{\rho}{4}, 1 + \sqrt{\frac{\rho}{4 + \rho}}; x\right) - \mathcal{I}\left(1 + \frac{\rho}{4}, 1 - \sqrt{\frac{\rho}{4 + \rho}}; x\right). \quad (3.133)$$

Applying the rationalization  $\rho = \frac{r^2}{1+r}$  results in

$$I = \mathcal{I}\left(\frac{1}{4} \frac{(2+r)^2}{1+r}, 2 \frac{1+r}{2+r}; \rho_1\right) - \mathcal{I}\left(\frac{1}{4} \frac{(2+r)^2}{1+r}, \frac{2}{2+r}; \rho_1\right), \quad (3.134)$$

with the evaluation point

$$\rho_1 = \frac{1}{2} \left( \sqrt{\rho} + \sqrt{\rho(4 + \rho)} \right). \quad (3.135)$$

The logarithmic properties of dlogs in each argument can be used to obtain simple poles. This allows to write Eq. (3.134) in terms of GPLs,

$$\begin{aligned} I &= 2 \mathcal{I}(r + 2, r + 1; \rho_1) - \mathcal{I}(r + 1, r + 1; \rho_1) \\ &= 2 G(-2, -1; \rho_1) - G(-1, -1; \rho_1). \end{aligned} \quad (3.136)$$

The second weight-2 GPL can be further expressed as two weight-1 GPLs by applying shuffle relations. This yields

$$I = 2 G(-2, -1; \rho_1) - \frac{1}{2} G(-1; \rho_1)^2. \quad (3.137)$$

Combining the presented rationalization algorithm and logarithmic properties allows to express most iterated integrals in terms of polylogarithms.

### 3.5.3. Analytic Continuation

Expressing iterated integrals in terms of GPLs is least complex in the Euclidean region. Here, no intermediate particle is on-shell, ensuring real results. These results then have to be analytically continued to the physical region by selecting the correct analytic continuation.

#### Analytic Continuation to the non-Euclidean Region

Consider the external momenta  $p_i$  yielding the external kinematic invariants  $p_i^2$  and  $s_{ij} = p_i p_j$ . In the Euclidean region where all  $p_i$  are time-like, the kinematic invariants are negative,

$$p_i^2 < 0 \quad \text{and} \quad s_{ij} < 0. \quad (3.138)$$

<sup>3</sup>The example corresponds to the coefficient of  $\varepsilon^2$  of the canonical function  $g_3$  in Eq. (4.13).

In the non-Euclidean region, at least one external kinematic quantity is positive. To carry out the analytic continuation to this region, all positive kinematics must be given a small imaginary part  $i\delta$  to achieve the correct causality [62].

Consider the simple example

$$\psi(x)|_{x>0} = \log(x) \quad \text{with} \quad x = -\frac{p_i^2}{m^2}, \quad (3.139)$$

and therefore  $x > 0$  corresponding to  $p_i^2 < 0$ . To analytically continue  $\psi(x)|_{x>0}$  to the non-Euclidean region,  $p_i^2$  must be given a small imaginary part  $i\delta$  with  $\delta > 0$ ,

$$x \rightarrow \tilde{x} = -\frac{p_i^2 + i\delta}{m^2} = x - i\delta. \quad (3.140)$$

Therefore, the solution for  $x < 0$  is given by

$$\psi(x)|_{x<0} = \lim_{\delta \rightarrow 0^+} \psi(\tilde{x})|_{x>0} = \lim_{\delta \rightarrow 0^+} \log(x - i\delta). \quad (3.141)$$

The complex shift can be removed, by opening the logarithm to obtain a real logarithm and a complex phase,

$$\psi(x)|_{x<0} = \lim_{\delta \rightarrow 0^+} [\log(|x - i\delta|) + i \arg(x - i\delta)] = \log(-x) - i\pi. \quad (3.142)$$

Note that  $\arg$  maps complex numbers to the interval  $(-\pi, \pi]$ , resulting in a discontinuity along the negative real axis. Consequently, changing the sign of  $\delta$  modifies the analytic continuation for  $x < 0$  by  $2\pi i$ .

Algorithms that evaluate (poly)logarithms typically assume a specific sign for  $\delta$  in such cases. Therefore, explicitly rewriting the analytic continuation for the relevant kinematic region, as done in Eq. (3.142), reduces the risk of an incorrect continuation during the numerical evaluation.

However, for polylogarithms of higher weight, calculating an explicit analytic calculation may not always be straightforward. As an alternative, the numerical evaluation can be safeguarded by manually shifting the input values by a small imaginary number. This helps avoid incorrect handling by the algorithm, ensuring a proper continuation.

## 4. EW Corrections for Quark-initiated Double Higgs Production

This chapter focuses on Higgs pair production initiated by two light quarks. I calculate the LO amplitude for diagrams that include at least one top quark propagator, with the Higgs boson coupling exclusively to the  $W$  boson. These diagrams depend on three mass scales: The top quark mass, the Higgs boson mass, and the  $W$  boson mass.

There are no tree-level diagrams for this process since the incoming particles are massless. Thus, the LO amplitude already involves loop contributions. Despite this, the LO must be finite, as explained in Sec. 1.2.1.

To get the finite remainder of the interference between the LO and NLO amplitudes, I calculate the LO amplitude up to the second order in  $\varepsilon$ . Additionally, I derive the NLO amplitude in terms of Master integrals.

The code and results for the LO calculation are available under

[https://git.particle.kit.edu/prendler/lo\\_qq\\_to\\_hh.git](https://git.particle.kit.edu/prendler/lo_qq_to_hh.git)

### 4.1. The Contributing Diagrams

I generated the relevant diagrams using QGRAF 3.6.6 [63] and visualize them with `qgraf-xml-drawer 1.0` [64]. The model file used for the diagram generation, which includes all considered couplings and propagators, is provided in Appendix A.1. By choosing the unitary gauge for the EW bosons, Goldstone bosons and EW ghosts are excluded from consideration.

The LO and NLO diagrams are generated by setting the power of the weak coupling constant to four and the strong coupling constant to zero and two, respectively. All external momenta are defined as incoming. The instruction file used for the generation of the LO diagrams is attached to Appendix A.1.

The incoming quarks are defined to be of the down-type in order to produce a top quark through their interaction with the  $W$  boson. Diagrams with incoming massless up-type quarks and a top quark line only contribute at higher orders of the coupling constants.

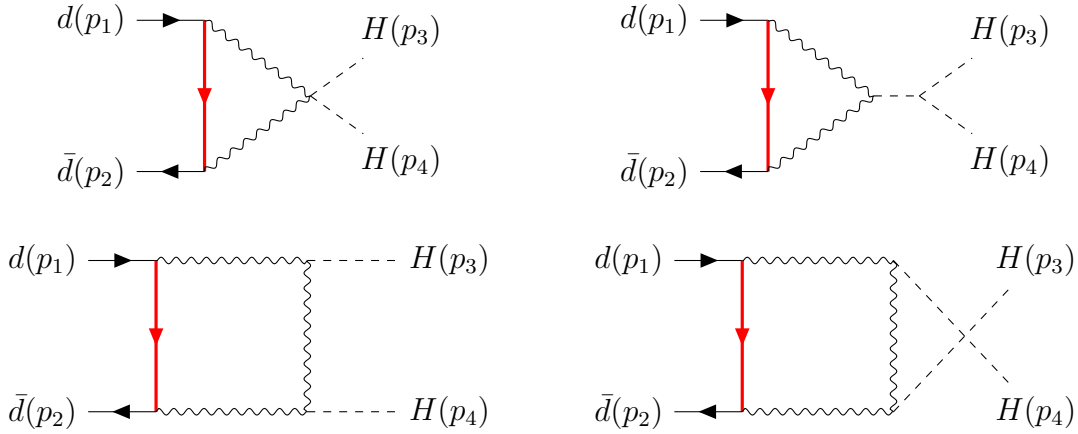


Figure 4.1.: Contributing diagrams for the quark initiated one-loop case

#### 4.1.1. The One-Loop Case

The four diagrams contributing at the one-loop level are depicted in Fig. 4.1. The thick red fermion line represents a top quark.

#### 4.1.2. The Two-Loop Case

There are 24 diagrams contributing at the two-loop level, which are shown in Fig. A.1 in Appendix A.2. Eight of the diagrams contain a gluon in the  $s$ -channel, which carries the color charge of the final state. Given that the considered final state is color-neutral, these diagrams must vanish. However, I retain them as a cross-check during the amplitude calculation.

## 4.2. The Tensor Structure

The diagrams generated by QGRAF are translated into analytic expressions using FORM 4.2 [65, 66] and the Feynman rules provided in Ref. [67], with the choice of  $+$  for all optional signs. These expressions can be projected on form factors by applying appropriate projection operators.

#### 4.2.1. The Form Factors

The amplitude can be expressed as

$$\mathcal{M} = \bar{v}(p_2) \mathcal{M}_{ij}^s \bar{u}(p_1), \quad (4.1)$$

where  $i$  and  $J$  are the color indices and  $\mathcal{M}_{ij}^s$  is matrix-valued in spinor space.

The only structure involving two fundamental color indices is the Kronecker delta. Any combination of the SU(3) generators  $T^a$  will result in deltas. Thus, the color structure of the amplitude is given by  $\mathcal{M}_{ij}^s = \delta_{ij} \mathcal{M}^s$ .

The spinor structure is expressed in terms of gamma matrices. Any spinor structure can be constructed with  $\mathbb{I}$ ,  $\not{\psi}_1$ ,  $\not{\psi}_2$  and  $\not{\psi}_3$ , each combined with the chiral projection operators  $P_L$  and  $P_R$ . This leads to the ansatz

$$\mathcal{M}^s = \left[ F_0^L P_L + F_0^R P_R + \sum_{i=1}^3 \left( F_i^L \not{\psi}_i P_L + F_i^R \not{\psi}_i P_R \right) \right], \quad (4.2)$$

with the form factors  $F_i^{L/R}$ .

Due to the Dirac equations for massless spinors,

$$\not{\psi}_1 u(p_1) = 0 \quad \text{and} \quad \bar{v}(p_2) \not{\psi}_2 = 0, \quad (4.3)$$

terms involving a  $\not{\psi}_1$  or  $\not{\psi}_2$  vanish when multiplied with the spinors. Consequently, the form factors  $F_{1/2}^{L/R}$  do not contribute to the amplitude.

#### 4.2.2. The Chiral Projection Operators

Projecting the scattering amplitude onto the tensor structure requires to take traces over products of  $D$ -dimensional gamma matrices. EW interactions introduce a distinction between left- and right-handed fermions, resulting the presence of  $\gamma_5$  matrices. However, generalizing the  $\gamma_5$  matrix into  $D$  dimensions proves to be quite complex. The four-dimensional definition,

$$\gamma_5 = \frac{i}{4!} \varepsilon_{\mu\nu\rho\sigma} \gamma^\mu \gamma^\nu \gamma^\rho \gamma^\sigma, \quad (4.4)$$

cannot be extended to arbitrary dimension  $D$ , due to the totally antisymmetric tensor  $\varepsilon_{\mu\nu\rho\sigma}$  being uniquely defined in four dimensions.

I use the naive scheme [68] for the dimensional regularization of  $\gamma_5$  matrices, which is defined by two properties: The anticommutativity with gamma matrices is extended to  $D$ -dimensions,

$$\{\gamma_5, \gamma^\mu\} = 0, \quad (4.5)$$

and the normalization condition is

$$\gamma_5^2 = 1. \quad (4.6)$$

This prescription allows to anticommute the chiral projection operators along the massless propagators to the external spinors, which leads to

$$\mathcal{M} = \bar{v}_L(p_1) \delta_{ij} \tilde{\mathcal{M}}^s u_L(p_2), \quad (4.7)$$

with left-handed external spinors. The remaining tensor structure  $\tilde{\mathcal{M}}^s$  does not contain  $\gamma_5$  matrices, allowing for simplification to

$$\tilde{\mathcal{M}}^s = F_0 \mathbb{I} + F_1 \not{p}_1 + F_2 \not{p}_2 + F_3 \not{p}_3. \quad (4.8)$$

The orthogonality of the chiral projectors implies that  $\bar{v}_L(p_1)u_L(p_2) = 0$ . Consequently,  $F_0$  does not contribute to the amplitude. As a result,  $F_3$  is the only relevant form factor.

### 4.2.3. The Projectors

I construct the projector onto  $\not{p}_3$  by calculating the action of the tensor structure components on the overall tensor structure. These actions are given by

$$\text{tr}(\mathbb{I} \tilde{\mathcal{M}}^s) = 4 F_0 \quad (4.9a)$$

$$\text{tr}(\not{p}_1 \tilde{\mathcal{M}}^s) = 4[(p_1 \cdot p_2)F_2 + (p_1 \cdot p_3)F_3] \quad (4.9b)$$

$$\text{tr}(\not{p}_2 \tilde{\mathcal{M}}^s) = 4[(p_1 \cdot p_2)F_1 + (p_2 \cdot p_3)F_3] \quad (4.9c)$$

$$\text{tr}(\not{p}_3 \tilde{\mathcal{M}}^s) = 4[(p_1 \cdot p_3)F_1 + (p_2 \cdot p_3)F_2 + (p_3 \cdot p_3)F_3], \quad (4.9d)$$

Rearranging Eqs. (4.9) with respect to  $F_3$  allows to construct a projector onto  $\not{p}_3$ , given by

$$\mathbb{P}_3 \tilde{\mathcal{M}}^s = \frac{1}{4} \frac{(p_1 \cdot p_2) \text{tr}(\not{p}_3 \tilde{\mathcal{M}}^s) - (p_1 \cdot p_3) \text{tr}(\not{p}_2 \tilde{\mathcal{M}}^s) - (p_2 \cdot p_3) \text{tr}(\not{p}_1 \tilde{\mathcal{M}}^s)}{(p_1 \cdot p_2)(p_3 \cdot p_3) - 2(p_1 \cdot p_3)(p_2 \cdot p_3)}, \quad (4.10)$$

which yields the form factor  $F_3$ .

## 4.3. Reduction to Master Integrals

The analytic expressions for the diagrams contain  $\mathcal{O}(10^2)$  distinct Feynman integrals at the one-loop level and  $\mathcal{O}(10^3)$  integrals at the two-loop level. To reduce them to a more manageable set of master integrals, they are categorized into integral families with `Reduze 2.5` starting from the output generated by `QGRAF`. Subsequently, I use `FORM 4.2` to extract the corresponding Feynman Integrals. These integrals are then reduced to master integrals using `Reduze 2.5` for the one-loop case and `KIRA 2.2` for the two-loop case.

### 4.3.1. Integral Families

#### The One-Loop Case

At the one-loop level, all four diagrams are mapped onto the integral family labeled as P4 and shown in Tab. 2.1, together with its crossed topology P4x12, which is obtained by interchanging the external momenta  $p_1$  and  $p_2$ .

### The Two-Loop Case

The two-loop diagrams are mapped onto three planar integral families and their crossed topologies. The three uncrossed integral families, labeled as P1, P2 and P3, are presented in Tab. 4.1. Although the second integral family, P2, is necessary to map all diagrams onto integral families, it does not occur in the result as all corresponding diagrams vanish due to their color structure.

Table 4.1.: Integral families for the quark initiated double Higgs production at two-loop level.

$\mathcal{F}$	P1	P2	P3
$P_1$	$k_1^2$	$k_1^2 - m_t^2$	$k_1^2$
$P_2$	$(k_1 + p_1)^2$	$(k_1 + p_1)^2 - m_t^2$	$k_2^2 - m_t^2$
$P_3$	$(k_2 + p_1)^2 - m_W^2$	$(k_2 + p_1)^2 - m_W^2$	$(k_2 - k_1)^2 - m_t^2$
$P_4$	$(k_1 - p_2)^2$	$(k_1 - p_2)^2 - m_t^2$	$(k_1 + p_1)^2$
$P_5$	$(k_2 - p_2)^2 - m_W^2$	$(k_2 - p_2)^2 - m_W^2$	$(k_2 + p_1)^2 - m_W^2$
$P_6$	$(k_2 - p_2 - p_3)^2 - m_W^2$	$(k_2 - p_2 - p_3)^2 - m_W^2$	$(k_2 - p_2)^2 - m_W^2$
$P_7$	$(k_2 - k_1)^2 - m_t^2$	$(k_2 - k_1)^2$	$(k_2 - p_2 - p_3)^2 - m_W^2$
$P_8$	$(k_1 - p_2 - p_3)^2$	$k_2^2$	$(k_1 - p_2)^2$
$P_9$	$k_2^2$	$(k_1 - p_2 - p_3)^2$	$(k_1 - p_2 - p_3)^2$

The first seven inverse propagator of the three integral families can be associated with edges of the contributing Feynman diagrams. The last two inverse propagators are required solely to express all scalar products in terms of inverse propagators. As a result, the top sectors do not include these last two propagators.

### 4.3.2. Master Integrals

#### The One-Loop Case

At the one-loop level, the reduction is carried out using Reduze 2.5, which applies IBPs, LIs and sector relations. As a result, the Feynman integrals are reduced to a set of nine master integrals from the topology P4 and three master integrals from the topology P4x12.

The 12 master integrals are illustrated in Fig. 4.2. The depicted graphs are not Feynman diagrams but rather a graphical representation of the Feynman integrals, with each line corresponding to a scalar propagator appearing in the integral. Wavy lines indicate propagators with a  $W$  mass, thick red lines represent top quark masses and dashed lines correspond to the Higgs boson mass. The labels 1, 2, 3 and 4 at the external edges denote the incoming momenta  $p_1, p_2, p_3$  and  $p_4$ , respectively.

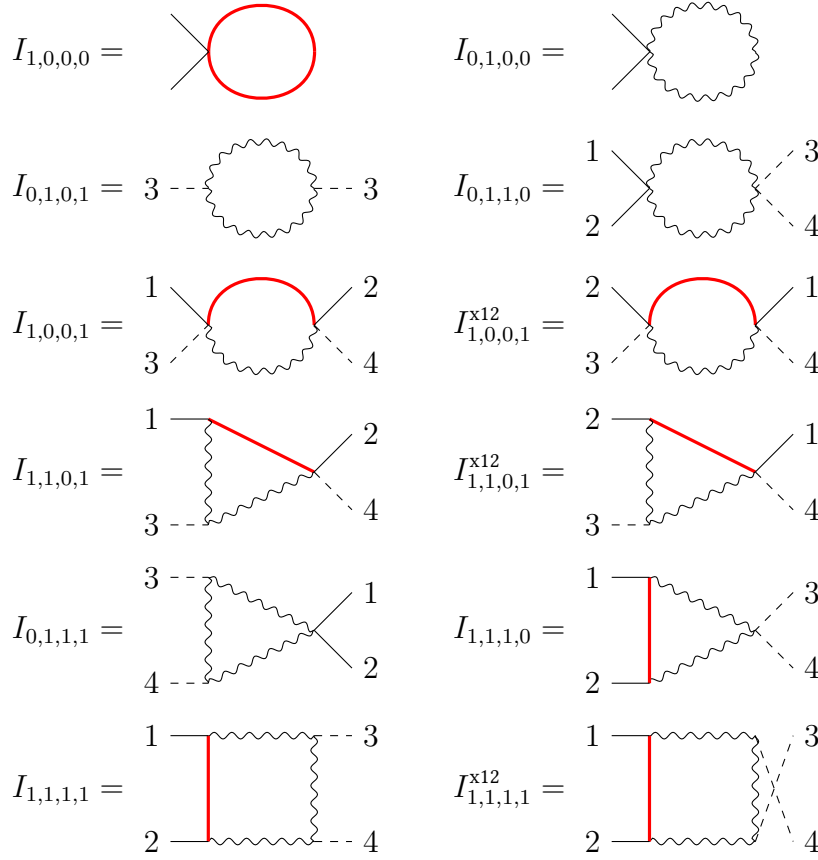


Figure 4.2.: Master integrals for the one-loop case

### The Two-Loop Case

At the two-loop level, sector relations are determined using Reduze 2.5. Applying these sector relations before the reduction can lower the number of integrals, accelerating the reduction process.

The fully symbolic reduction is carried out for each integral family individually using KIRA 2.2. For both P1 and P1x12, 60 master integrals are identified. For P3 and P3x12, 51 master integrals are sufficient for each family.

The master integrals of the different integral families are not independent, but can be mapped onto each other using sector relations. Applying these mappings with KIRA 2.2 reduces the number of master integrals, decreasing them from 222 to 111.

The obtained master integrals correspond to the basis obtained from the Laporta algorithm. Inserting them into the amplitude is not practical before finding a suitable basis, which will be addressed in future work.

## 4.4. Differential Equations

The analytic solution for the master integrals at the one-loop level is obtained using the method of differential equations, as discussed in Chapter 3. The master integrals from the crossed sector P4x12 are omitted, as they can be reconstructed from P4 by interchanging the Mandelstam variables  $t$  and  $u$ .

The evaluation of the two-loop master integrals will be addressed in future work.

### 4.4.1. Derivation of the Canonical Form

I derive the DEs in terms of the internal masses  $m_W^2$  and  $m_t^2$ , and the external quantities  $m_H^2 = p_3^2$ ,  $s = (p_1 + p_2)^2$  and  $t = (p_1 + p_3)^2$  using Reduze. I further process them using Mathematica 13.2 [69].

As a first step, the variables are rescaled by the  $W$ -mass, introducing the new variables

$$\omega = -\frac{m_t^2}{m_W^2}, \quad \rho = -\frac{m_H^2}{m_W^2}, \quad \sigma = -\frac{s}{m_W^2} \quad \text{and} \quad \tau = -\frac{t}{m_W^2}. \quad (4.11)$$

As a result, the partial derivatives with respect to  $m_W$  decouple, making the corresponding matrix diagonal. The dependence on  $m_W^2$  can be resolved immediately, giving

$$I = m_W^{\dim_m(I)} \tilde{I}. \quad (4.12)$$

The functions  $\tilde{I}$  are dimensionless and only depend on the rescaled variables.

The system is then transformed into canonical form by using the closed formula from Eqs. (3.28) and (3.29) and applying transformations as described in Section 3.2. The canon-

ical basis reads,

$$\begin{aligned}
 g_1 &= -\frac{1}{C} \frac{\varepsilon(1-\varepsilon)}{\omega} \tilde{I}_{1000} \\
 g_2 &= \frac{1}{C} \varepsilon(1-\varepsilon) \tilde{I}_{0100} \\
 g_3 &= \frac{1}{C} \varepsilon \sqrt{\frac{\rho}{4+\rho}} \left( (1-2\varepsilon) \tilde{I}_{0101} - (1-\varepsilon) \tilde{I}_{0100} \right) \\
 g_4 &= \frac{1}{C} \varepsilon \sqrt{\frac{\sigma}{4+\sigma}} \left( (1-2\varepsilon) \tilde{I}_{0110} - (1-\varepsilon) \tilde{I}_{0100} \right) \\
 g_5 &= \frac{1}{C} \frac{\varepsilon}{\omega \sqrt{\tau^2 + 2\tau(1-\omega) + (1+\omega)^2}} \left( -2(1-2\varepsilon)\tau\omega \tilde{I}_{1001} \right. \\
 &\quad \left. - (1-\varepsilon)(1-\tau+\omega)\omega \tilde{I}_{0100} - (1-\varepsilon)(1+\tau+\omega) \tilde{I}_{1000} \right) \\
 g_6 &= \frac{1}{C} \varepsilon^2 (\tau - \rho) \tilde{I}_{1101} \\
 g_7 &= -\frac{1}{C} \varepsilon^2 \sqrt{\sigma(4+\sigma)} \tilde{I}_{0111} \\
 g_8 &= -\frac{1}{C} \varepsilon^2 \sigma \tilde{I}_{1110} \\
 g_9 &= \frac{1}{C} \varepsilon^2 \left[ \sigma \left( 4\tau^2 - 4\rho^2\omega + \sigma(\tau^2 - 2\tau(-1+\omega) + (1+\omega)^2) \right. \right. \\
 &\quad \left. \left. - 4\rho(\tau - \tau\omega + (1+\omega)^2) \right) \right]^{\frac{1}{2}} \tilde{I}_{1111},
 \end{aligned} \tag{4.13}$$

where the constant

$$C = \frac{\Gamma(1+\varepsilon)}{2} \mu^{2\varepsilon} \tag{4.14}$$

normalizes all integrals to the second canonical integral, effectively setting its value to 1.

#### 4.4.2. The dLog form

In the canonical form, the four partial differential equations are combined into a lower triangular matrix containing dlogs, denoted as  $A$ , satisfying the equation

$$d\mathbf{g} = \varepsilon A \mathbf{g}, \tag{4.15}$$

where  $\mathbf{g}$  represents the vector of the canonical integrals. The matrix  $A$  can be expressed as

$$A = \sum_{i=1}^{66} A_i d \log(l_i), \tag{4.16}$$

with  $A_i$  being matrices that contain rational coefficients and a sign that depends on the kinematic region. The 66 distinct  $l_i$  are algebraic functions of the external kinematics and invariant masses, referred to as *letters*.

The letters on the diagonal provide insight into the kinematic thresholds of the master integrals. Since these letters appear as arguments of polylogarithms, the integrals become imaginary when the letters turn negative, with a divergence occurring at zero. According to the optical theorem, this behavior indicates that an intermediate particle has gone on-shell.

An alternative way to point out the connection between the diagonal elements and kinematic thresholds is by applying the maximal cut to the canonical functions. When the maximal cut is applied to a Feynman diagram, it effectively eliminates all its subtopologies, setting them to zero. For the differential equations at one loop, this implies that the off-diagonal entries are set to zero, leaving only the diagonal elements. As a result, the remaining homogeneous differential equations describe the behavior of the maximal cut, directly linking these diagonal elements to the kinematic thresholds of the diagram.

The kinematic thresholds computed by the maximal cut can therefore be used as a cross-check for the letters on the diagonal. Starting from the lowest sectors, the two tadpoles do not depend on the external kinematics. However they differ by their mass. This manifests in the first diagonal entry,

$$A_{11} = -d \log(-\omega). \quad (4.17)$$

The second diagonal entry vanishes.

The third and fourth diagonal entries of  $A$  are given by

$$A_{33} = -d \log(4 + \rho) \quad \text{and} \quad A_{44} = -d \log(4 + \sigma), \quad (4.18)$$

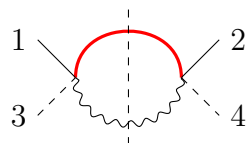
resulting in the thresholds  $m_H^2 = 4 m_W^2$  and  $s = 4 m_W^2$ , respectively. These thresholds correspond to the  $\varepsilon$ -dependent divergence in the maximal cut of the equal mass bubble, Eq. (2.34). The divergences of the maximal cut at  $\rho = 0$  and  $\sigma = 0$  do not appear because the canonical functions are divided by the corresponding pole.

In fact, removing  $\varepsilon$ -independent poles is essential to obtain a  $d \log$  form, as they do not generate logarithms in the  $\varepsilon$ -expansion.

The fifth diagonal entry reads

$$A_{55} = d \log(\tau) - d \log(\tau^2 + 2\tau(1 - \omega) + (1 + \omega)^2). \quad (4.19)$$

The letters are equivalent to the divergences of the maximal cut,



$$\propto \tau^{\frac{2-D}{2}} (\tau^2 + 2\tau(1 - \omega) + (1 + \omega)^2)^{\frac{D-3}{2}}. \quad (4.20)$$

The thresholds in  $\tau$  of the second logarithm are given by  $\tau_{\pm} = -1 \pm 2\sqrt{-\omega} + \omega$ , corresponding to the condition  $t = (m_W \pm m_t)^2$ .

#### 4. EW Corrections for Quark-initiated Double Higgs Production

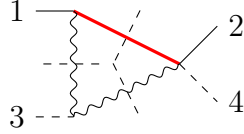
---

The sixth entry on the diagonal is given by

$$A_{66} = \text{d log}(\rho - \tau) - \text{d log}(\tau^2 + \rho\tau(\omega - 1) - \rho - \rho\omega(2 + \rho + \omega)) \quad (4.21)$$

$$-2 \text{d log}(-1 - \omega). \quad (4.22)$$

The corresponding maximal cut has the same divergences,



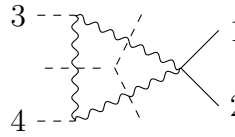
$$\propto ((\rho - \tau)^2)^{\frac{3-D}{2}} (\tau^2 + \rho\tau(\omega - 1) - \rho - \rho\omega(2 + \rho + \omega))^{\frac{D-4}{2}} \quad (4.23)$$

The first threshold corresponds to the energy required to produce an on-shell Higgs boson,  $t = m_H^2$ .

The seventh diagonal entry is equal to

$$A_{77} = \text{d log}(\sigma - 4\rho) - \text{d log}(\sigma - \rho(4 + \rho)). \quad (4.24)$$

The thresholds are equivalent to the divergences of the maximal cut,



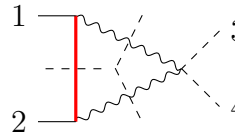
$$\propto \sigma^{-\frac{1}{2}} (\sigma - 4\rho)^{\frac{3-D}{2}} (\sigma - \rho(4 + \rho))^{\frac{D-4}{2}} \quad (4.25)$$

The first dlog represents the necessary center of mass energy required to produce two on-shell Higgs bosons, while the second dlog also accounts for the  $W$ -bosons propagating within the triangle diagram.

The eighth diagonal entry reads

$$A_{88} = \text{d log}(\sigma) - \text{d log}(1 + (2 + \sigma)\omega + \omega^2) - 2 \text{d log}(-1 - \omega), \quad (4.26)$$

which is in accordance to the maximal cut of the corresponding diagram,

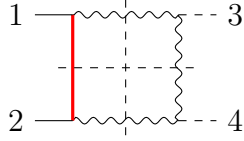


$$\propto \sigma^{\frac{3-D}{2}} (1 + (2 + \sigma)\omega + \omega^2)^{\frac{D-4}{2}}. \quad (4.27)$$

The ninth diagonal entry, which corresponds to the box diagram, is given by

$$A_{99} = \text{d log}((\rho - \tau)^2 + \tau\sigma) + \text{d log}(4\tau^2 - 4\rho^2\omega - 4\rho(\tau - \tau\omega + (\omega + 1)^2) + \sigma(\tau^2 + 2\tau(1 - \omega) + (\omega + 1)^2)) \quad (4.28)$$

The maximal cut of the box has the same divergences,



$$\propto \sigma^{-\frac{1}{2}} \left( (\rho - \tau)^2 + \tau \sigma \right)^{\frac{4-D}{2}} \left[ 4\tau^2 - 4\rho^2\omega - 4\rho(\tau - \tau\omega + (\omega + 1)^2) + \sigma(\tau^2 + 2\tau(1 - \omega) + (\omega + 1)^2) \right]^{\frac{D-5}{2}} \quad (4.29)$$

The non-diagonal entries of the dlog relate the canonical functions to lower sectors. These terms tend to become significantly more complex and are displayed in Appendix A.3.

### 4.4.3. Iterated Integrals

The DEs written in dlog form naturally lead to solutions expressed as iterated integrals. To compute the amplitude up to the second order in  $\varepsilon$ , the tadpole and bubble integrals need to be evaluated up to the third order in  $\varepsilon$ , while the triangle and box diagrams require evaluation up to the fourth order. This is necessary to obtain the finite remainder in the interference with the NLO amplitude. Consequently, this involves iterated integrals of depth three for the tadpoles and bubbles, and depth four for the triangles and boxes.

#### Integration Path

The integration path is chosen from  $x_0 = (0, 0, 0)$  to  $x = (\sigma, \rho, \tau)$  by successively increasing each variable to the desired value,

$$\gamma : [(0, 0, 0), (\sigma, 0, 0)] \circ [(\sigma, 0, 0), (\sigma, \rho, 0)] \circ [(\sigma, \rho, 0), (\sigma, \rho, \tau)], \quad (4.30)$$

where  $[x_1, x_2]$  is the straight path from  $x_1$  to  $x_2$ , and the operator  $\circ$  represents the concatenation of two paths. The three straight paths are denoted as  $\gamma_\sigma$ ,  $\gamma_\rho$  and  $\gamma_\tau$ . An iterated integral of weight one along the path is calculated by performing three integrations, one over each of the straight lines:

$$\begin{aligned} \mathcal{I}(R_1; x) &= \int_{\gamma} d \log(R_1(t_1)) \\ &= \int_{\gamma_\sigma} d \log(R_1(t_1)) + \int_{\gamma_\rho} d \log(R_1(t_1)) + \int_{\gamma_\tau} d \log(R_1(t_1)), \end{aligned} \quad (4.31)$$

where  $t_1$  denotes the position on the integration path. Iterated integrals of arbitrary weight can be split recursively, beginning from the left-most integration,

$$\begin{aligned} \mathcal{I}(R_1, \dots, R_w; x) &= \int_{\gamma_\sigma} d \log(R_1(t_1)) \mathcal{I}(R_2, \dots, R_w; t_1) \\ &+ \int_{\gamma_\rho} d \log(R_1(t_1)) \mathcal{I}(R_2, \dots, R_w; t_1) \\ &+ \int_{\gamma_\tau} d \log(R_1(t_1)) \mathcal{I}(R_2, \dots, R_w; t_1). \end{aligned} \quad (4.32)$$

The second integration should only be carried out up to the current point of the first integration. Therefore, if the first integration is restricted to the path  $\gamma_\sigma$ , the second integrations along  $\gamma_\rho$  and  $\gamma_\tau$  are excluded,

$$\begin{aligned} & \int_{\gamma_\sigma} d \log(R_1(t_1)) \mathcal{I}(R_2, \dots, R_w; t_1) \\ &= \int_{\gamma_\sigma} d \log(R_1(t_1)) \int_{\gamma_\sigma[t_1]} d \log(R_2(t_2)) \mathcal{I}(R_3, \dots, R_w; t_2). \end{aligned} \quad (4.33)$$

The square brackets  $\gamma_\sigma[t_1]$  indicate that the integration is carried out only up to the point  $t_1$ . By recursively splitting the path into three straight lines, this results in  $w$  integrations over  $\gamma_\sigma$ , as the integrations over  $\gamma_\rho$  and  $\gamma_\tau$  are omitted at each step of the recursion.

If the first integration is performed along  $\gamma_\rho$ , the second integration over  $\gamma_\sigma$  needs to be carried out completely, while the integration over  $\rho$  is performed only up to the current point of the first integration. The integration over  $\tau$  is omitted,

$$\begin{aligned} & \int_{\gamma_\rho} d \log(R_1(t_1)) \mathcal{I}(R_2, \dots, R_w; t_1) \\ &= \int_{\gamma_\rho} d \log(R_1(t_1)) \times \int_{\gamma_\sigma} d \log(R_2(t_2)) \mathcal{I}(R_3, \dots, R_w; t_2) \\ &+ \int_{\gamma_\rho} d \log(R_1(t_1)) \int_{\gamma_\rho[t_1]} d \log(R_2(t_2)) \mathcal{I}(R_3, \dots, R_w; t_2). \end{aligned} \quad (4.34)$$

Finally, if the first integration is performed along  $\gamma_\tau$ , the second integral is evaluated fully along  $\gamma_\sigma$  and  $\gamma_\rho$ , and only partially along  $\gamma_\tau$ , up to the current point of the first integration,

$$\begin{aligned} & \int_{\gamma_\tau} d \log(R_1(t_1)) \mathcal{I}(R_2, \dots, R_w; t_1) \\ &= \int_{\gamma_\tau} d \log(R_1(t_1)) \times \int_{\gamma_\sigma} d \log(R_2(t_2)) \mathcal{I}(R_3, \dots, R_w; t_2) \\ &+ \int_{\gamma_\tau} d \log(R_1(t_1)) \times \int_{\gamma_\rho} d \log(R_2(t_2)) \mathcal{I}(R_3, \dots, R_w; t_2) \\ &+ \int_{\gamma_\tau} d \log(R_1(t_1)) \int_{\gamma_\tau[t_1]} d \log(R_2(t_2)) \mathcal{I}(R_3, \dots, R_w; t_2). \end{aligned} \quad (4.35)$$

Using these prescriptions recursively, an iterated integral over weight  $w$  results in one iterated integral along  $\gamma_\tau$ ,  $w$  iterated integrals along  $\gamma_\rho$  and  $\frac{w(w+1)}{2}$  iterated integrals along  $\gamma_\sigma$ .

### Shuffle Relations

Shuffle relations are applied to reduce the number and weight of the appearing iterated integrals. Shuffle relations are particularly effective for this purpose if multiple integrals with different arrangements of the same letters occur. In this case, only a small number

of integrals shares the exact same letters, making shuffle relations relative ineffective for reducing the number of integrals. While the total number of iterated integrals is of the order  $\mathcal{O}(10^4)$ , the number of iterated integrals removed by shuffle relations is just of the order  $\mathcal{O}(10^2)$ .

Shuffle relations play a crucial role in managing potential divergences that arise in iterated integrals when the left-most argument of an integral approaches zero. For example, consider the iterated integral

$$\mathcal{I}(x, x + 2; x_1) = \int_{\gamma} \frac{dx}{x} \log(x + 2). \quad (4.36)$$

As  $x \rightarrow 0$ , the denominator approaches zero, potentially causing the integral to diverge if the path crosses this pole. When a finite result is expected, divergences of this kind might cancel each other. To simplify such an analytic cancellation and make it explicit, shuffle relations can be used to reorganize the terms and isolate the poles. In the previous example, the shuffle relation

$$\mathcal{I}(x, x + 2; x_1) = \mathcal{I}(x; x_1) \mathcal{I}(x + 2; x_1) - \mathcal{I}(x + 2, x; x_1), \quad (4.37)$$

separates the pole in  $x = 0$  into an iterated integral, which only contains the letter causing the divergence.

It's important to note that not all cases where the left-most letter approaches zero lead to an actual divergence. For instance, consider the iterated integral

$$\mathcal{I}(x, x + 1; x_1) = \int_{\gamma} \frac{dx}{x} \log(x + 1). \quad (4.38)$$

Although the denominator  $x$  appears to cause a divergence at  $x = 0$ , the potential singularity is cancelled by the logarithm, which vanishes at  $x = 0$ . Thus, no divergence occurs in this case.

#### 4.4.4. Boundary Conditions

I make use of boundary function to fix the integration constants. An efficient way to generate boundary functions is to consider the case where one of the internal masses is much larger than any other scales in the problem. In this case, I consider the limit where the top and  $W$  masses are large while preserving their ratio. This corresponds to the point  $\rho = \sigma = \tau = 0$ , with  $\omega$  being kept at the desired value.

I compute the LO large mass expansions of the nine master integrals from P1 depicted in Fig. 4.2. The resulting expressions are inserted into the formula for the canonical basis, Eq. (4.13), and the remaining  $W$ -boson and top-quark masses are taken to infinity. Expanding the result in  $\varepsilon$  allows to compare each order of  $\varepsilon$  to the corresponding integration constants.

In the large mass expansion, two kinematic regions for the loop momentum  $k$  must be distinguished: The region where  $k^2 \ll m_W^2$  and the region where  $k^2 \sim m_W^2$ .

For small loop momenta,  $k^2 \ll m_W^2$ , all canonical integrals considered here vanish, as all momenta are negligible compared to the masses. What remains are scaleless Feynman integrals, which are zero in dimensional regularization.

In the case where  $k^2 \sim m_W^2$ , the master integrals reduce to tadpoles involving either the top-quark mass, the  $W$ -boson mass, or both. This results in the non-zero boundary conditions

$$\begin{aligned} g_1(x_0) &= 1 - \varepsilon \log(-\omega) + \frac{\varepsilon^2}{2} \log^2(-\omega) - \frac{\varepsilon^3}{6} \log^3(-\omega) + \frac{\varepsilon^4}{24} \log^4(-\omega) + \mathcal{O}(\varepsilon^5) \\ g_2(x_0) &= 1 \\ g_5(x_0) &= \varepsilon \log(-\omega) - \frac{\varepsilon^2}{2} \log^2(-\omega) + \frac{\varepsilon^3}{6} \log^3(-\omega) - \frac{\varepsilon^4}{24} \log^4(-\omega) + \mathcal{O}(\varepsilon^5). \end{aligned} \quad (4.39)$$

The remaining canonical integrals vanish at the boundary point.

Diverging or zero letters at the boundary point can be a challenge when determining the integration constants. For instance, consider the letters  $\sigma$  and  $\sigma + \sqrt{\sigma(4 + \sigma)}$ . An iterated integral of weight 1 containing these letters diverges for  $\sigma \rightarrow 0^+$  because

$$\lim_{\sigma \rightarrow 0^+} \log(x) = \infty \quad \text{and} \quad \lim_{\sigma \rightarrow 0^+} \log\left(x + \sqrt{x(4 + x)}\right) \rightarrow \infty. \quad (4.40)$$

However, by considering linear combinations of these letters, the divergences may cancel, leaving a finite remainder,

$$\lim_{\sigma \rightarrow 0^+} \left( \frac{1}{2} \log(x) - \log\left(x + \sqrt{x(4 + x)}\right) \right) = \log(2). \quad (4.41)$$

To avoid such implicit cancellations, divergences at the boundary point are extracted by rescaling all composite letters to ensure they remain finite. The only diverging letters are then  $\sigma$ ,  $\rho$  and  $\tau$ . Referring to the above example, the second letter can be rescaled as

$$\log\left(x + \sqrt{x(4 + x)}\right) \rightarrow \frac{1}{2} \log(x) + \log\left(\sqrt{x} + \sqrt{4 + x}\right), \quad (4.42)$$

which makes the cancellation more apparent.

By rescaling the letters, all divergences cancel perfectly. Consequently, all iterated integrals clearly vanish at the boundary point leading to the following expression for the canonical integrals at that point,

$$\mathbf{g}(0) = \mathcal{C}^{(0)} + \varepsilon \mathcal{C}^{(1)} + \varepsilon^2 \mathcal{C}^{(2)} + \varepsilon^3 \mathcal{C}^{(3)} + \varepsilon^4 \mathcal{C}^{(4)} + \mathcal{O}(\varepsilon^5). \quad (4.43)$$

This allows for a simple determination of the constants.

## 4.5. GPLs

For an efficient numerical evaluation, the iterated integrals are rewritten in terms of GPLs whenever possible. For simplicity, the kinematics at the evaluation point are restricted

such that no intermediate particles are produced on-shell. Furthermore, it is assumed that the mass of the top-quark is greater than the mass of the  $W$ -boson, resulting in  $\omega < -1$ . This corresponds to the region defined as

$$\{(\sigma, \rho, \tau, \omega) \in \mathbb{R}^4 \mid \sigma > \rho(4 + \rho) > 0 \wedge \tau > 0 \wedge \omega < -1\}. \quad (4.44)$$

This assumption allows to fix the sign that depends on the kinematic region. In addition, handling square roots becomes simpler, as separating them no longer requires a case-by-case analysis.

The canonical tadpole integrals do not depend on external kinematics. Therefore, their expressions correspond to the boundary conditions,

$$g_1 = 1 - \varepsilon \log(-\omega) + \frac{\varepsilon^2}{2} \log^2(-\omega) - \frac{\varepsilon^3}{6} \log^3(-\omega) + \frac{\varepsilon^4}{24} \log^4(-\omega) + \mathcal{O}(\varepsilon^5) \quad (4.45)$$

$$g_2 = 1. \quad (4.46)$$

The bubble integrals  $g_3$  and  $g_4$  contain the square roots  $r_1$  and  $r_2$ , respectively (see Appendix A.3). They can be rationalized using the transformation from Eq. (3.131).

The expression for  $g_3$  up to the third order in  $\varepsilon$  after applying shuffle relations is given by,

$$\begin{aligned} g_3 = & -G(-1; \rho_1) \varepsilon + \left[ 2G(-2, -1; \rho_1) - \frac{1}{2}G(-1; \rho_1)^2 \right] \varepsilon^2 \\ & + \left[ -2G(-2, -1, -1; \rho_1) - 4G(-2, -2, -1; \rho_1) \right. \\ & \left. + 2G(-1, \rho_1)G(-2, -1; \rho_1) - \frac{1}{6}G(-1, \rho_1)^3 \right] \varepsilon^3 + \mathcal{O}(\varepsilon^4), \end{aligned} \quad (4.47)$$

with the evaluation point

$$\rho_1 = \frac{1}{2} \left( \rho + \sqrt{\rho(4 + \rho)} \right). \quad (4.48)$$

At this stage, the shuffle relations prove highly effective, reducing the number of distinct GPLs of weights 2 and 3 by half.

The expression for  $g_4$  is given by

$$\begin{aligned} g_4 = & -G(-1; \sigma_1) \varepsilon + \left[ 2G(-2, -1; \sigma_1) - \frac{1}{2}G(-1; \sigma_1)^2 \right] \varepsilon^2 \\ & + \left[ -2G(-2, -1, -1; \sigma_1) - 4G(-2, -2, -1; \sigma_1) \right. \\ & \left. + 2G(-1, \sigma_1)G(-2, -1; \sigma_1) - \frac{1}{6}G(-1, \sigma_1)^3 \right] \varepsilon^3 + \mathcal{O}(\varepsilon^4), \end{aligned} \quad (4.49)$$

with

$$\sigma_1 = \frac{1}{2} \left( \sigma + \sqrt{\sigma(4 + \sigma)} \right). \quad (4.50)$$

As the expression for the canonical integrals, Eq. (4.13), and the diagrams in Fig. 4.2 indicate, the third and fourth canonical integrals can be converted into each other by interchanging the variables  $\rho$  and  $\sigma$ .

The triangle integral  $g_5$  contains the square root  $r_4$ . Inserting the parametrization

$$\tau = \frac{2t(1-t(1-\omega)+\omega)}{t^2-1}, \quad (4.51)$$

allows to rationalize it, yielding

$$r_4 = \frac{(t-1)^2 + (t+1)^2\omega}{t^2-1}. \quad (4.52)$$

The resulting expressions are quite lengthy and are available in Eq. (A.14), Appendix A.4. As for the previous canonical functions, the shuffle relations prove their effectiveness. Applying them reduces the number of distinct weight-two GPLs from 42 to 26, and the number of distinct weight-three GPLs from 72 to 50.

The triangle integral  $g_6$  contains two square roots,  $r_1$  and  $r_4$ . Since these square roots contain different integration variables, they can be rationalized simultaneously. The first two orders in  $\varepsilon$  are provided in Eq. (A.15).

In the expression for the triangle integral  $g_7$ , three square roots appear:  $r_1$ ,  $r_2$  and  $r_3$ . Rationalizing all three square roots simultaneously is quite complicated. However, the process can be simplified by noting that the first and second square roots never appear together in the same iterated integral. By changing the integration path to

$$\tilde{\gamma} : [(0, 0, 0), (\sigma, \rho, 0)] \circ [(\sigma, \rho, 0), (\sigma, \rho, \tau)], \quad (4.53)$$

the square root  $r_3$  becomes constant along the path. What remains are iterated integrals containing at most one square root at a time. These square roots can then be rationalized with the transformations

$$\sigma \rightarrow \frac{s^2}{1+s} \quad \text{and} \quad \rho \rightarrow \frac{r^2}{1+r}. \quad (4.54)$$

Due to the absence of poles in the region between the two integration paths, no additional residues are required to change the path. The expressions for  $g_7$  up to the third order in  $\varepsilon$  are given in Eq. (A.16).

The triangle integral  $g_8$  is relatively simple, containing only the square root  $r_2$ . The corresponding expression up to order  $\varepsilon^3$  is provided in Eq. (A.17).

The iterated integrals for the box diagram contain the square roots  $r_1$ ,  $r_2$ ,  $r_4$  and  $r_5$ . These are not simultaneously rationalizable with the method introduced in Sec. 3.5.2. Therefore, it is not obvious how to express the iterated integrals in terms of GPLs. At present these integrals must be numerically integrated by other means.

## 4.6. Crosschecks

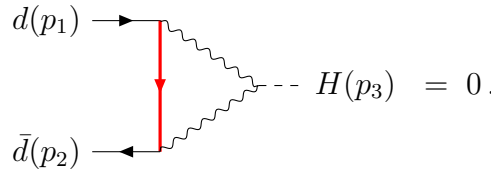
To check the validity of the calculation, I have performed two independent crosschecks. On the one hand, the amplitude must fulfill certain analytic constraints. On the other hand, integrals expressed as GPLs can be numerically evaluated and compared to the results obtained by pySecDec.

### 4.6.1. Crosschecks on the Amplitude

The amplitude must fulfill two analytic properties:

1. The expressions for the triangle diagrams from Fig. 4.1 are zero.
2. The amplitude must be finite.

The first constraint must be fulfilled because a single Higgs boson cannot couple to massless quarks, as the Yukawa coupling is directly proportional to the quark mass. This means that all virtual corrections to the Yukawa coupling should vanish. In particular



$$d(p_1) \rightarrow \text{---} H(p_3) = 0. \quad (4.55)$$

The expressions for the triangle diagrams in Fig. 4.1 are proportional, up to a constant factor, to these corrections. Hence, they must also vanish.

The expressions for the triangle diagrams vanish once the amplitude is written in terms of master integrals.

The second requirement prohibits any poles in  $\varepsilon$  as the computed amplitude corresponds to the LO of a process. This is checked by inserting the explicit expressions for the master integrals into the amplitude and expanding it in  $\varepsilon$ . The master integrals are obtained by inverting the expressions for the canonical functions, Eq. (4.13).

Inserting the master integrals into the amplitude reveals two poles of order 1 with opposite signs originating from the two box-like Feynman diagrams,

$$\pm \frac{1}{\varepsilon} g^4 |V|^2 \frac{s - 3m_H^2 + 18m_W^2}{24m_W^4} \bar{v}_L \not{p}_3 u_L(p_1), \quad (4.56)$$

where  $V$  denotes the appropriate entry of the CKM matrix. As expected, the amplitude is finite in  $\varepsilon$ .

### 4.6.2. Crosschecks on the Master Integrals

The expressions for the master integrals in terms of GPLs are checked up to the order  $\varepsilon^2$  by evaluating the GPLs using PolyLogTools and comparing the results to those obtained

by `pySecDec`. For this crosscheck, points from different kinematic regions are selected, both in the Euclidean and Minkowski domain.

To ensure the correct analytic continuation, a small imaginary part is added to each positive external kinematic variable. This guarantees the correct logarithm branches.

The results show that the values up to the second order in  $\varepsilon$  are consistent within the requested numerical uncertainty of  $\mathcal{O}(10^{-15})$ .

For the Box diagram, which lacks an expression in terms of GPLs, the function `NIntegrate` from `Mathematica` is used to crosscheck the zeroth order in  $\varepsilon$  in the Euclidean region. This already involves the evaluation of weight-2 integrals. For higher weights, `NIntegrate` does not converge, requiring a more sophisticated analysis.

As a further crosscheck, the master integrals are evaluated for small top quark masses,  $\omega \sim 10^{-10}$ . The numerical results agree with those from `pySecDec` for the massless quark case.

# 5. NLO EW Corrections for Gluon-initiated Double Higgs Production

Gluon-initiated diagrams are the dominant contribution to double Higgs production due to the dominance of gluons in the parton distribution functions. A numerical study in Ref. [26] shows that the corresponding NLO EW corrections can significantly impact observables such as the differential cross section with respect to the invariant mass, resulting in changes of up to 15 %.

In this chapter I perform the initial step of an analytic calculation of the gluon initiated double Higgs production, focusing on Feynman diagrams that involve a top quark and generate the Higgs boson via  $W$  bosons. I express the amplitudes for these Feynman diagrams in terms of scalar Feynman integrals and compute the reduction to a Laporta basis of master integrals with full dependence on all scales.

## 5.1. The Contributing Diagrams

The contributing Feynman Diagrams are generated using QGRAF, with slight adaptations made to the code from Appendix A.1: gluons are now incoming instead of quarks. The power of the weak coupling is set to four, and the power of the strong coupling to two. With these parameters, QGRAF generates 32 Feynman diagrams, depicted in Appendix A.5. The thick red fermion lines indicate propagating top quarks. Eight of the planar diagrams contain a gluon in the  $s$ -channel. The corresponding expressions are expected to be zero due to the color structure. The explicit check will serve as a validation of the setup.

## 5.2. The Tensor structure

### 5.2.1. The Form Factors

The incoming gluons depend on adjoint color indices  $a$  and  $b$ , and Lorentz indices  $\mu$  and  $\nu$ . The amplitude takes the form

$$\mathcal{M}_{ab} = \epsilon_\mu(p_1) \epsilon_\nu(p_2) \mathcal{M}_{ab}^{\mu\nu}. \quad (5.1)$$

The color structure of the amplitude must contain exactly two color indices  $a$  and  $b$ . The only tensor structures that fulfill this requirement is the Kronecker delta<sup>1</sup>  $\delta^{ab}$ . As a result,

---

<sup>1</sup>Traces over products of SU(3) generators  $T_{ij}^a$  also result in Kronecker deltas.

the color structure is proportional to the Kronecker delta,

$$\mathcal{M}_{ab}^{\mu\nu} = \delta_{ab} \mathcal{M}^{\mu\nu}. \quad (5.2)$$

The dependence over Lorentz indices can be constructed by considering all possible structures containing two Lorentz indices:

$$\begin{aligned} \mathcal{M}^{\mu\nu} = & F_{00} g_{\mu\nu} + F_{11} p_1^\mu p_1^\nu + F_{22} p_2^\mu p_2^\nu + F_{33} p_3^\mu p_3^\nu \\ & + F_{12} p_1^\mu p_2^\nu + F_{21} p_2^\mu p_1^\nu + F_{13} p_1^\mu p_3^\nu + F_{31} p_3^\mu p_1^\nu \\ & + F_{23} p_2^\mu p_3^\nu + F_{32} p_3^\mu p_2^\nu + \mathcal{M}_5^{\mu\nu}, \end{aligned} \quad (5.3)$$

where  $\mathcal{M}_5^{\mu\nu}$  depends on the totally antisymmetric tensor  $\varepsilon^{\mu\nu\rho\sigma}$ .

For the computation of the NLO EW corrections, the NLO amplitude must be interfered with the LO amplitude. The only structures with Lorentz indices in the LO amplitude are the three momenta  $p_1^\mu$ ,  $p_2^\mu$  and  $p_3^\mu$  as well as the metric tensor  $g_{\mu\nu}$ . Consequently, in the interference of the two amplitudes, the totally antisymmetric tensor from the NLO amplitude is contracted with any combination of the three momenta and the metric tensor, which in either case yields zero. Therefore, for the calculation of the NLO EW corrections  $\mathcal{M}_5^{\mu\nu}$  can be dropped.

Terms proportional to  $p_1^\mu$  and  $p_2^\nu$  also do not contribute to the amplitude, as they vanish once polarization vectors are applied.

Current conservation allows to further simplify  $\mathcal{M}$ ,

$$p_{1\mu} \mathcal{M}^{\mu\nu} = p_{2\nu} \mathcal{M}^{\mu\nu} = 0. \quad (5.4)$$

Applying these relations on Eq. (5.3) and omitting the terms proportional to  $p_1^\mu$  and  $p_2^\nu$  results in two independent tensor structures  $T_1^{\mu\nu}$  and  $T_2^{\mu\nu}$ . A convenient choice for  $T_1$  and  $T_2$  is [15]

$$\begin{aligned} T_1^{\mu\nu} &= g^{\mu\nu} - \frac{p_1^\nu p_2^\mu}{p_1 \cdot p_2} \\ T_2^{\mu\nu} &= g^{\mu\nu} + \frac{1}{p_T^2 (p_1 \cdot p_2)} \left[ m_H^2 p_1^\nu p_2^\mu - 2(p_1 \cdot p_3) p_3^\nu p_2^\mu \right. \\ &\quad \left. - 2(p_2 \cdot p_3) p_3^\mu p_1^\nu + 2(p_1 \cdot p_2) p_3^\nu p_3^\mu \right], \end{aligned} \quad (5.5)$$

where the transverse momentum  $p_T$  is defined as,

$$p_T^2 = \frac{ut - m_H^4}{s}. \quad (5.6)$$

The tensor structure of the matrix element reduces to

$$\mathcal{M}^{\mu\nu} = F_1 T_1^{\mu\nu} + F_2 T_2^{\mu\nu} + \mathcal{M}_0^{\mu\nu} + \mathcal{M}_5^{\mu\nu}, \quad (5.7)$$

where  $\mathcal{M}_0$  contains all terms proportional to  $p_1^\mu$  and  $p_2^\nu$ . Note that  $\mathcal{M}_0$  and  $\mathcal{M}_5$  do not contribute to the amplitude.

### 5.2.2. The Projectors

The projection operators are constructed by applying  $T_1$  and  $T_2$  onto  $\mathcal{M}^{\mu\nu}$  itself. Applying  $T_1^{\mu\nu}$  onto Eq. (5.7) gives

$$T_{1\mu\nu}\mathcal{M}^{\mu\nu} = (D-2)F_1 + (D-4)F_2 + T_{1\mu\nu}\mathcal{M}_0^{\mu\nu} + T_{1\mu\nu}\mathcal{M}_5^{\mu\nu}. \quad (5.8)$$

The contraction of  $T_{1\mu\nu}$  with  $\mathcal{M}_0^{\mu\nu}$  is zero because  $T_{1\mu\nu}p_1^\mu = 0$  and  $T_{1\mu\nu}p_2^\nu = 0$ . The contraction of  $T_{1\mu\nu}$  with  $\mathcal{M}_5^{\mu\nu}$  is zero, since  $\varepsilon^{\mu\nu\rho\sigma}$  is either contracted with the metric tensor or with any combination of only three independent momenta  $p_1$ ,  $p_2$  and  $p_3$ .

A similar result holds for  $T_2$ , giving

$$\begin{aligned} T_{1\mu\nu}\mathcal{M}^{\mu\nu} &= (D-2)F_1 + (D-4)F_2 \\ T_{2\mu\nu}\mathcal{M}^{\mu\nu} &= (D-4)F_1 + (D-2)F_2, \end{aligned} \quad (5.9)$$

which yields

$$\begin{aligned} \mathbb{P}_1^{\mu\nu} &= \frac{1}{4} \frac{D-2}{D-3} T_1^{\mu\nu} - \frac{1}{4} \frac{D-4}{D-3} T_2^{\mu\nu} \\ \mathbb{P}_2^{\mu\nu} &= -\frac{1}{4} \frac{D-4}{D-3} T_1^{\mu\nu} + \frac{1}{4} \frac{D-2}{D-3} T_2^{\mu\nu}, \end{aligned} \quad (5.10)$$

such that

$$\begin{aligned} \mathbb{P}_1\mathcal{M} &= F_1 \\ \mathbb{P}_2\mathcal{M} &= F_2. \end{aligned} \quad (5.11)$$

Consequently,  $\mathbb{P}_1$  and  $\mathbb{P}_2$  project out  $F_1$  and  $F_2$ , respectively.

## 5.3. Reduction to Master Integrals

The form factors depend on  $\mathcal{O}(10^3)$  distinct Feynman integrals. As seen for the quark-initiated case, most of these integrals are related by IBPs. I use `Reduze 2.5` to map them on integral families, and `Kira 2.2` to reduce them to a Laporta basis of master integrals.

### 5.3.1. Integral Families

Two planar and one non-planar integral families as well as their crossed topologies are needed to describe the Feynman integrals appearing in the amplitude and are listed in Tab. 5.1. The last two inverse propagators of each family are not associated with edges of Feynman diagrams, but are required to express all appearing scalar products in terms of inverse propagators.

Table 5.1.: Integral families for the gluon initiated double Higgs production at two-loop level.

$\mathcal{F}$	inverse propagator of P1	inverse propagator of P2	inverse propagator of NP
$P_1$	$k_1^2$	$k_1^2 - m_t^2$	$k_1^2 - m_t^2$
$P_2$	$(k_1 + p_1)^2$	$(k_1 + p_1)^2 - m_t^2$	$k_2^2$
$P_3$	$(k_2 + p_1)^2 - m_W^2$	$(k_2 + p_1)^2 - m_W^2$	$(k_1 + p_1)^2 - m_t^2$
$P_4$	$(k_1 - p_2)^2$	$(k_1 - p_2)^2 - m_t^2$	$(k_2 + p_2)^2$
$P_5$	$(k_2 - p_2)^2 - m_W^2$	$(k_2 - p_2)^2 - m_W^2$	$(k_2 + -k_1 + p_2)^2 - m_W^2$
$P_6$	$(k_2 - p_2 - p_3)^2 - m_W^2$	$(k_2 - p_2 - p_3)^2 - m_W^2$	$(k_2 - k_1 + p_2 + p_3)^2 - m_W^2$
$P_7$	$(k_2 - k_1)^2 - m_t^2$	$(k_2 - k_1)^2$	$(k_1 - k_2 + p_1)^2 - m_W^2$
$P_8$	$(k_1 - p_2 - p_3)^2$	$k_2^2$	$(k_1 + p_3)^2$
$P_9$	$k_2^2$	$(k_1 - p_2 - p_3)^2$	$(k_1 - k_2)^2$

### 5.3.2. Master Integrals

The Feynman integrals are first reduced for each integral family separately. To minimize the set of required seed integrals, the sectors are reduced iteratively, starting from sectors with fewer propagators. This results in 64 master integrals for NP and NPx12, 32 master integrals for P1, and 79 master integrals for P2 and P2x12.

Some of the master integrals from different sectors are still related by sector relations. I use KIRA 2.2 to identify such relations, which decreases the total number of independent master integrals to 165.

As for the NLO amplitude of the quark initiated case, I calculated the amplitude in terms of Feynman integrals and computed the fully symbolic reduction. Inserting these results into the amplitude is not practical, until a suitable basis for the amplitude is found. This is a highly non-trivial task, which will be addressed in future work.

## 6. Conclusion and Outlook

This thesis presents the calculation of the leading order amplitude for double Higgs production initiated by two light quarks, focusing on diagrams that include at least one top quark propagator and generate the Higgs Bosons through  $W$  bosons.

The diagrams were generated using QGRAF and translated into analytic expressions with FORM. Through the application of IBPs, LIs and sector symmetries, available in Reduze, I reduced the amplitude to twelve master integrals, with three of them being related to the other nine by the interchange of two momenta. I calculated these integrals analytically using the method of differential equations and large mass expansion to fix the integration constants. The solution is provided in terms of iterated integrals up to weight 4, with ten of these twelve master integrals expressed in terms of GPLs.

Inserting the iterated integrals into the amplitude results in the analytic cancellation of all poles in  $\varepsilon$ . In addition, all numerical crosschecks of the master integrals with pySecDec were successfully completed.

Future work will extend this result to the full LO amplitude by including diagrams with massless internal quarks and Yukawa couplings.

The NLO EW corrections for both quark- and gluon-initiated cases were calculated in terms of master integrals, with the analysis again restricted to diagrams containing at least one top quark propagator and generating the Higgs through  $W$  bosons. The generation of diagrams was performed with QGRAF, and transformed into analytic expressions with FORM. The reduction of the Feynman integrals to master integrals was achieved using KIRA and Reduze.

Further work will require a detailed analysis to determine a convenient basis of master integrals. Additionally, the master integrals must be evaluated either numerically or analytically to provide expressions for phenomenological applications.



# A. Appendix

## A.1. QGRAF Code

The QGRAF model file shown in Listing A.1 defines all the propagators and vertices relevant to the process under consideration. In this case, I include the propagators of the Higgs boson, gluon, top quark, down quark and  $W$ -boson. Additionally, the model incorporates the couplings between gluons and quarks, trilinear and quartic self-coupling of gluons, the couplings between Higgs bosons and  $W$  bosons, as well as the trilinear Higgs self-coupling. The arguments  $gpow$  and  $spow$  track the powers of the weak and strong coupling constants, respectively.

```
1 % propagators
2
3 [higgs, higgs, +; mass=mH]
4 [gluon, gluon, +; mass = 0]
5 [tQuark, tbarQuark, -; mass = mt]
6 [dQuark, dbarQuark, -; mass = 0]
7 [Wp, Wm, +; mass = mW]
8
9 % vertices
10
11 [tbarQuark, tQuark, gluon; gpow = 0, spow = 1]
12 [dbarQuark, dQuark, gluon; gpow = 0, spow = 1]
13 [gluon, gluon, gluon; gpow = 0, spow = 1]
14 [gluon, gluon, gluon, gluon; gpow = 0, spow = 2]
15 [tbarQuark, dQuark, Wp; gpow = 1, spow = 0]
16 [dbarQuark, tQuark, Wm; gpow = 1, spow = 0]
17 [Wp, Wm, higgs; gpow = 1, spow = 0]
18 [Wp, Wm, higgs, higgs; gpow = 2, spow = 0]
19 [higgs, higgs, higgs; gpow = 1, spow = 0]
```

Listing A.1: QGRAF model file

Listing A.2 provides the instructions for executing QGRAF in the case of the quark-initiated one-loop diagrams. After specifying the three export formats and importing the model file from Listing A.1, all momenta are defined as incoming and on-shell. We apply several restrictions: tadpole diagrams are excluded, diagrams must include at least one top quark propagator, and the weak coupling constant must be raised to the fourth power. The strong coupling constant is not allowed to appear in the one-loop case.

For the two-loop cases, the restrictions differ only in the number of loops and the powers of the strong coupling constant, which is set to two instead of zero. In the gluon-initiated case, gluons replace quarks as the incoming particles.

```
1  % Export for FORM
2  output = 'FORM/dd_to_HH_1loop.frm' ;
3  style = 'styles/form_CORRECT.sty' ;
4
5  % Export for REDUZE
6  output = 'REDUZE/dd_to_HH_1loop.yml' ;
7  style = 'styles/reduze_CORRECT.sty' ;
8
9  % Export for xml-drawer
10 output = 'graphics/grafs' ;
11 style = 'styles/xmldraw.sty' ;
12
13 % define model file
14 model = 'model' ;
15
16 % define external particles
17 in = dQuark[p1], dbarQuark[p2], higgs[p3], higgs[p4];
18 out = ;
19
20 options = onshell, notadpole;
21
22 % restrict diagrams
23 loops = 1;
24 loop_momentum = k ;
25
26 true = iprop[tQuark, 1, 10];
27 true = vsum[gpow, 4, 4];
28 true = vsum[spow, 0, 0];
```

Listing A.2: QGRAF instruction file

## A.2. Feynman Diagrams for the Quark-Initiated Two-Loop Case

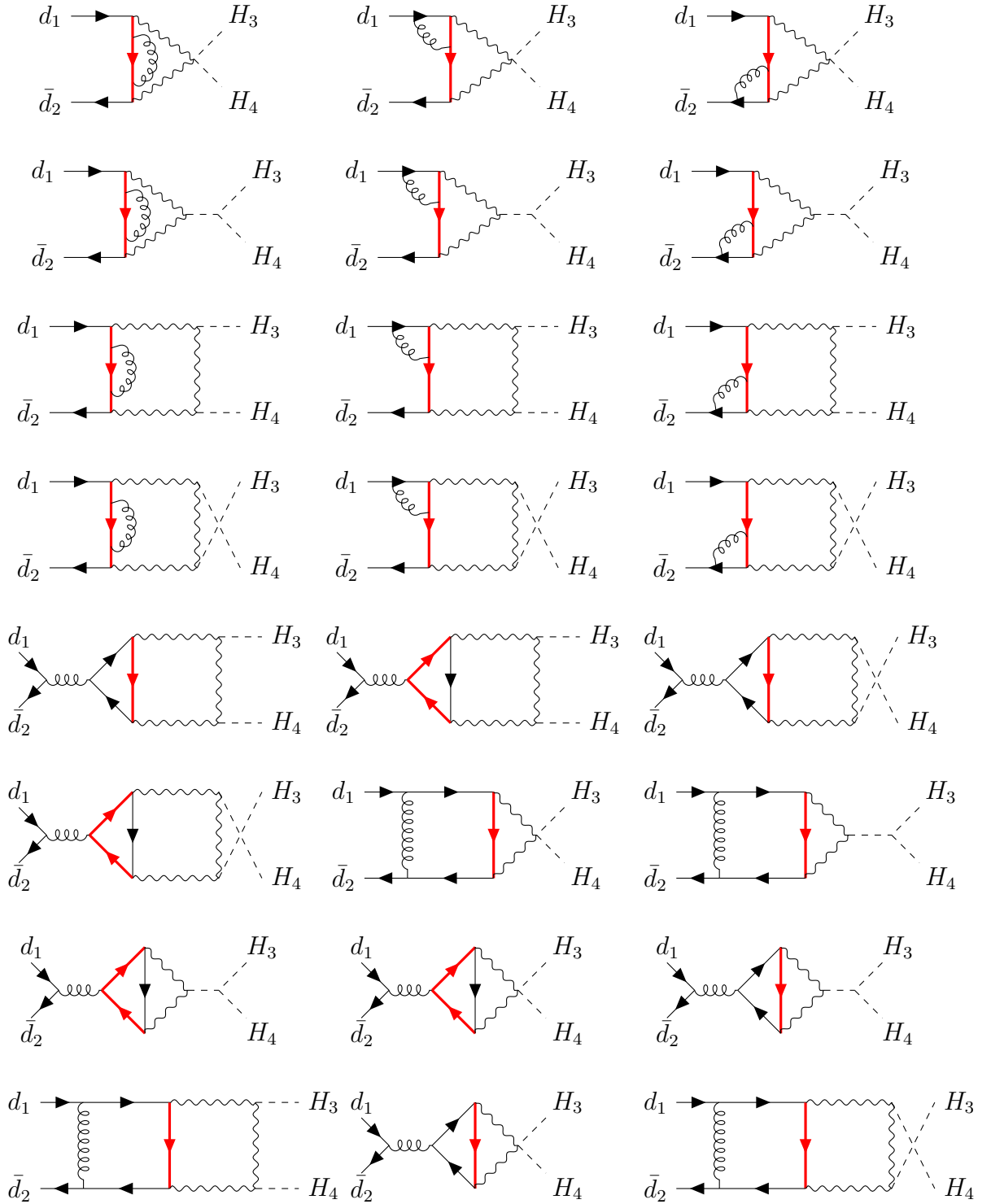


Figure A.1.: Contributing diagrams for the quark initiated two-loop case

### A.3. The dlog Form

In this section, the non-zero entries of the dlog form for the one-loop case are presented. For simplicity, certain entries are expressed in terms of inverse hyperbolic tangents. These can be converted to logarithmic forms using the identity

$$\operatorname{arctanh}(x) = \frac{1}{2} \log(1+x) - \frac{1}{2} \log(1-x). \quad (\text{A.1})$$

In addition the following sign is introduced, which depends solely on the kinematic region,

$$\operatorname{sgn} := \sqrt{\frac{\rho}{4+\rho}} \sqrt{\frac{4+\rho}{\rho}}, \quad (\text{A.2})$$

as well as the following square roots,

$$\begin{aligned} r_1 &= \sqrt{\frac{4+\rho}{\rho}} \\ r_2 &= \sqrt{\frac{4+\sigma}{\sigma}} \\ r_3 &= \sqrt{1 - \frac{4\rho}{\sigma}} \\ r_4 &= \sqrt{\tau^2 + 2\tau(1-\omega) + (1+\omega)^2} \\ r_5 &= \sqrt{\frac{4\tau^2 - 4\rho^2\omega + 4\rho(\tau(\omega-1) - (\omega+1)^2) + \sigma(\tau^2 - 2\tau(\omega-1) + (\omega+1)^2)}{\sigma}}. \end{aligned} \quad (\text{A.3})$$

Finally, the dlog form  $A$  is defined as  $A = d\tilde{A}$ , with the entries of  $\tilde{A}$  listed sequentially, starting from the lowest sector.

#### First Line

$$\tilde{A}_{11} = -\log(-\omega) \quad (\text{A.4})$$

#### Third Line

$$\begin{aligned} \tilde{A}_{32} &= -2 \operatorname{arctanh}(r_1) \\ \tilde{A}_{33} &= -\log(4+\rho) \end{aligned} \quad (\text{A.5})$$

#### Fourth Line

$$\begin{aligned} \tilde{A}_{42} &= -2 \operatorname{arctanh}(r_2) \\ \tilde{A}_{44} &= -\log(4+\sigma) \end{aligned} \quad (\text{A.6})$$

**Fifth Line**

$$\begin{aligned}
 \tilde{A}_{51} &= -\log(\tau) + \log(1 + \omega + \tau + r_4) + 2 \operatorname{arctanh}(\omega - \tau + r_4) \\
 \tilde{A}_{52} &= \log(\tau) - 2 \log(1 - \omega + \tau - r_4) \\
 \tilde{A}_{55} &= \log(\tau) - \log(\tau^2 + 2\tau(1 - \omega) + (1 + \omega)^2)
 \end{aligned} \tag{A.7}$$

**Sixth Line**

$$\begin{aligned}
 \tilde{A}_{61} &= -\frac{1}{2} \log(\tau) + \frac{1}{2} \log(\tau^2 - \rho^2 \omega - \rho(\tau - \tau \omega + (1 + \omega)^2)) - \log(-1 - \omega) \\
 \tilde{A}_{62} &= \frac{1}{2} \log(\tau) - \frac{1}{2} \log(\tau^2 - \rho^2 \omega - \rho(\tau - \tau \omega + (1 + \omega)^2)) + \log(-1 - \omega) \\
 \tilde{A}_{63} &= -2 \operatorname{arctanh}\left(\frac{r_1(\rho - \tau)}{2(2 + \omega) + \rho - \tau}\right) \\
 \tilde{A}_{65} &= \frac{1}{2} \log(\tau) - \frac{1}{2} \log(1 + \omega + \tau + r_4) - \operatorname{arctanh}(\omega - \tau + r_4) \\
 &\quad + \operatorname{arctanh}\left(\frac{\tau + 2\rho\omega - \tau\omega + (1 + \omega)^2}{r_4(\omega + 1)}\right) \\
 \tilde{A}_{66} &= 2 \log(\rho - \tau) - \log(\tau^2 - \rho^2 \omega - \rho(\tau - \tau \omega + (1 + \omega)^2))
 \end{aligned} \tag{A.8}$$

**Seventh Line**

$$\begin{aligned}
 \tilde{A}_{73} &= 4 \operatorname{arctanh}(r_1 r_3) \\
 \tilde{A}_{74} &= 2 \operatorname{arctanh}\left(\frac{r_3}{r_2}\right) - 2 \operatorname{arctanh}\left(\frac{(2 + \rho)r_3}{r_2 \rho}\right) \\
 \tilde{A}_{77} &= \log(\sigma - 4\rho) - \log(\sigma - \rho(4 + \rho))
 \end{aligned} \tag{A.9}$$

**Eights Line**

$$\begin{aligned}
 \tilde{A}_{81} &= \log(\sigma \omega + (1 + \omega)^2) - 2 \log(-1 - \omega) \\
 \tilde{A}_{82} &= -\log(\sigma \omega + (1 + \omega)^2) + 2 \log(-1 - \omega) \\
 \tilde{A}_{84} &= 2 \operatorname{arctanh}\left(\frac{(4 + \sigma)}{r_2(2 + \sigma + 2\omega)}\right) \\
 \tilde{A}_{88} &= \log(\sigma) - \log(\sigma \omega + (1 + \omega)^2)
 \end{aligned} \tag{A.10}$$

**Ninth Line**

$$\begin{aligned}
\tilde{A}_{91} &= -2 \operatorname{arctanh} \left( \frac{\tau + 2\rho\omega - \tau\omega + (1 + \omega)^2}{r_4(1 + \omega)} \right) \\
&\quad + \operatorname{arctanh} \left( \frac{(1 + \omega)(\tau + 2\rho\omega - \tau\omega + (1 + \omega)^2)}{r_4(\sigma\omega + (1 + \omega)^2) + r_5\sigma\omega(\tau^2 + 2\tau(1 - \omega) + (1 + \omega)^2)} \right) \\
\tilde{A}_{92} &= 2 \operatorname{arctanh} \left( \frac{\tau + 2\rho\omega - \tau\omega + (1 + \omega)^2}{r_4(\omega + 1)} \right) \\
&\quad - \operatorname{arctanh} \left( \frac{(1 + \omega)(\tau + 2\rho\omega - \tau\omega + (1 + \omega)^2)}{r_4(\sigma\omega + (1 + \omega)^2) + r_5\sigma\omega(\tau^2 + 2\tau(1 - \omega) + (1 + \omega)^2)} \right) \\
\tilde{A}_{93} &= 4 \operatorname{arctanh} \left( \frac{\rho(1 + \tau - \omega) + 2\tau + \sqrt{\sigma}(r_5 - r_4)}{r_1 r_4 \rho} \right) \\
&\quad + 4 \operatorname{arctanh} \left( \frac{\rho(1 + \tau - \omega) + 2\tau - \sqrt{\sigma}(r_5 - r_4)}{r_1 r_4 \rho} \right) \\
&\quad - 4 \operatorname{arctanh} \left( \frac{1 + r_4 + \rho - \tau + \omega}{r_1 \rho} \right) \\
&\quad - 4 \operatorname{arctanh} \left( \frac{1 - r_4 + \tau + \rho(1 + \omega)}{r_1 \rho \omega} \right) \\
&\quad - 8 \operatorname{sgn} \log(r_1 - 1) - 4 \operatorname{sgn} \log(\rho) \\
\tilde{A}_{94} &= -2 \operatorname{arctanh} \left( \frac{r_2(\tau + 2\rho\omega - \tau\omega + (1 + \omega)^2)}{r_5(1 - \omega)} \right) \\
&\quad - 2 \operatorname{arctanh} \left( \frac{r_2(2\tau + \rho(1 + \tau - \omega))}{r_5(2 + \rho)} \right) \\
\tilde{A}_{95} &= 2 \log(r_4 + r_5) + \log(\sigma) - \log(\tau^2 - \rho^2\omega - \rho(\tau - \tau\omega + (\omega + 1)^2)) \\
\tilde{A}_{96} &= -2 \log(\tau^2 - 2\tau\omega + (1 + \omega)^2 - \rho(1 + \tau - \omega) + r_4(1 + \omega - \tau + \rho)) \\
&\quad + 2 \log(\tau^2 + \rho\omega(1 - \omega) + (1 + \omega)^2 + 2\tau + \tau\rho\omega - r_4(1 + \omega + \tau + \rho\omega)) \\
&\quad - 2 \log(1 - r_4 + \tau - \omega) + 4 \operatorname{arctanh} \left( \frac{r_4 - \tau}{1 + \omega} \right) \\
&\quad - 4 \operatorname{arctanh} \left( \frac{(\rho - \tau)(\tau(1 + \omega - \tau) + \rho(1 + \omega + \tau))}{r_4(((\rho - \tau)^2 + \sigma\tau) - r_5\sigma\tau)} \right) \\
\tilde{A}_{97} &= 2 \operatorname{arctanh} \left( \frac{(\rho + 2\tau + \rho\tau - \rho\omega)r_3}{r_5\rho} \right) \\
&\quad - \operatorname{arctanh} \left( \frac{(\tau(1 + \omega - \tau) + \rho(1 + \omega + \tau)r_3)}{r_5(\rho + \tau)} \right) \\
\tilde{A}_{98} &= 2 \operatorname{arctanh} \left( \frac{\tau + 2\rho\omega - \tau\omega + (1 + \omega)^2}{r_5(\omega + 1)} \right) \\
&\quad + 2 \operatorname{arctanh} \left( \frac{\tau(1 + \omega - \tau) + \rho(1 + \omega + \tau)}{r_5(\rho - \tau)} \right) \\
\tilde{A}_{99} &= \log((\rho - \tau)^2 + \tau\sigma) + \log(4\tau^2 - 4\rho^2\omega - 4\rho(\tau - \tau\omega + (\omega + 1)^2) \\
&\quad + \sigma(\tau^2 + 2\tau(1 - \omega) + (\omega + 1)^2))
\end{aligned} \tag{A.11}$$

## A.4. Expressions for Canonical Integrals

To simplify the expressions for the GPLs, we introduce short hand notations for terms that appear repeatedly in the canonical integral expressions. The typical evaluation points are

$$\begin{aligned}
\sigma_1 &:= \frac{1}{2} \left( \sigma + \sqrt{\sigma(4 + \sigma)} \right) \\
\rho_1 &:= \frac{1}{2} \left( \rho + \sqrt{\rho(4 + \rho)} \right) \\
\tau_1 &:= \frac{\sqrt{\tau^2 - 2\tau(\omega - 1) + (\omega + 1)^2} + \omega + 1}{\tau - 2\omega + 2}.
\end{aligned} \tag{A.12}$$

In addition, we introduce the following abbreviations,

$$\begin{aligned}
\omega_{\pm} &:= \frac{-\omega \pm 2\sqrt{-\omega} + 1}{\omega + 1} \\
\omega_1 &:= -(1 + \omega) \\
\omega_2 &:= -\frac{1 + \omega}{\omega} \\
\omega_3 &:= \frac{1 + \omega}{1 - \omega} \\
\rho_1 &:= \sqrt{\frac{\rho}{4 + \rho}} \\
a_{\pm} &:= \frac{1 - \omega^2 \pm \sqrt{\rho(4 + \rho)} \omega^2}{1 - (2 + \rho)\omega + \omega^2} \\
b_{\pm\pm} &:= \left[ \left( \rho \pm_1 \sqrt{\rho(4 + \rho)} \right) (1 + \omega) \right. \\
&\quad \left. \pm_2 \sqrt{2\rho \left( (2 + \rho)(\rho(4 + \rho) + (1 + \omega)^2) + \sqrt{\rho(4 + \rho)} \left( (2 + \rho)^2 - (1 - \omega)^2 \right) \right)} \right] \\
&\quad \times \left[ \rho(4 + \rho) \pm_1 \sqrt{\rho(4 + \rho)} (2 + \rho - 2\omega) \right]^{-1} \\
c_{\pm} &:= -\frac{2}{1 \pm \sqrt{1 - \frac{4\rho}{\sigma}}} \\
d_{\pm} &:= \pm \sqrt{1 - \frac{4\rho}{\sigma}} c_{\pm} \\
e_{\pm\pm} &:= -\frac{\rho \pm_1 \sigma \sqrt{1 - \frac{4\rho}{\sigma}} \pm_2 (\sigma - 3\rho)}{\rho \left( 1 \pm_1 \sqrt{1 - \frac{4\rho}{\sigma}} \right)} \\
f_{\pm} &:= \frac{-4\rho + \sigma \pm \sqrt{1 - \frac{4\rho}{\sigma}} \sigma}{2\rho} \\
g_{\pm} &:= \frac{\sigma \left( \sigma - 4\rho \pm \sqrt{1 - \frac{4\rho}{\sigma}} (\sigma - 2\rho) \right)}{2\rho^2}.
\end{aligned} \tag{A.13}$$

**Fifth Canonical Integral** The first two orders in  $\varepsilon$  of the fifth canonical integral  $g_5$  are given by

$$\begin{aligned}
g_5 = & \left[ 2G(-1; \tau_1) - 2G(1; \tau_1) + \log(-\omega) \right] \varepsilon \\
& + \left[ G(-1; \tau_1)^2 - G(1; \tau_1)^2 \right. \\
& \quad + 2G(0; \tau_1)G(-1; \tau_1) + 2G(1; \tau_1)G(-1; \tau_1) \\
& \quad - 2G(-1, 0; \tau_1) - 4G(-1, 1; \tau_1) - 2G(0, 1; \tau_1) \\
& \quad - 2G(1; \tau_1)G(\omega_3; \tau_1) + 2G(1-; \tau_1)G(\omega_3; \tau_1) \\
& \quad - 4G(-1; \tau_1)G(\omega_+; \tau_1) - 4G(-1; \tau_1)G(\omega_-; \tau_1) \\
& \quad + 4G(1; \tau_1)G(\omega_+; \tau_1) + 4G(1; \tau_1)G(\omega_-; \tau_1) \\
& \quad - 2G(-1, \omega_3; \tau_1) + 2G(1, \omega_3; \tau_1) \\
& \quad + 4G(-1, \omega_-; \tau_1) + 4G(-1, \omega_+; \tau_1) \\
& \quad - 4G(1, \omega_+; \tau_1) - 4G(1, \omega_-; \tau_1) \\
& \quad + 2\log(-\omega)G(1; \tau_1) + 2\log(-\omega)G(\omega_3; \tau_1) \\
& \quad - 2\log(-\omega)G(\omega_+; \tau_1) - 2\log(-\omega)G(\omega_-; \tau_1) \\
& \quad \left. - \frac{1}{2}\log^2(-\omega) \right] \varepsilon^2 \\
& + \mathcal{O}(\varepsilon^3).
\end{aligned} \tag{A.14}$$

**Sixth Canonical Integral** The first two orders in  $\varepsilon$  of the sixth canonical integral  $g_6$  read

$$\begin{aligned}
g_6 = & \left[ \frac{1}{2}G(-1; \rho_1)^2 - \frac{1}{2}G(1; \tau_1)^2 - \frac{1}{2}G(-1; \tau_1)^2 \right. \\
& \quad - G(-1; \tau_1)G(0; \tau_1) + G(-1; \tau_1)G(1; \tau_1) \\
& \quad - G(1; \tau_1)G(\omega_3; \tau_1) + G(-1; \tau_1)G(\omega_3; \tau_1) \\
& \quad + G(-1; \rho_1)G(b_{++}; \tau_1) + G(-1; \rho_1)G(b_{+-}; \tau_1) \\
& \quad - G(-1; \rho_1)G(b_{-+}; \tau_1) - G(-1; \rho_1)G(b_{--}; \tau_1) \\
& \quad + G(-1, 0; \tau_1) + G(0, 1; \tau_1) \\
& \quad - G(-1, \omega_3; \tau_1) + G(1, \omega_3; \tau_1) \\
& \quad + G(-\rho_1, -1; \tau_1) - G(-\rho_1, 1; \tau_1) \\
& \quad + G(\rho_1, -1; \tau_1) - G(\rho_1, 1; \tau_1) \\
& \quad + G(\omega_1, -1; \rho_1) - G(\omega_2, -1; \rho_1) \\
& \quad - G(a_-, -1; \tau_1) + G(a_-, 1; \tau_1) \\
& \quad - G(a_+, -1; \tau_1) + G(a_+, 1; \tau_1) + \log(-\omega)G(-1; \rho_1) \\
& \quad + \log(-\omega)G(1; \tau_1) - \log(-\omega)G(\omega_1; \rho_1) \\
& \quad + \log(-\omega)G(\omega_3; \tau_1) - \log(-\omega)G(\omega_2; \rho_1) \\
& \quad \left. - \log(-\omega)G(a_-; \tau_1) - \log(-\omega)G(a_+; \tau_1) \right] \varepsilon^2 \\
& + \mathcal{O}(\varepsilon^3).
\end{aligned} \tag{A.15}$$

**Seventh Canonical Integral** The expression for  $g_7$  up to the third order in  $\varepsilon$  is given by

$$\begin{aligned}
g_7 = & \left[ -2G(d_+, -1; \rho_1) + 2G(d_-, -1; \rho_1) \right. \\
& + G(c_+, -1; \sigma_1) - G(c_-, -1; \sigma_1) \\
& + G(e_{++}, -1; \sigma_1) + G(e_{+-}, -1; \sigma_1) \\
& \left. - G(e_{-+}, -1; \sigma_1) - G(e_{--}, -1; \sigma_1) \right] \varepsilon^2 \\
& \left[ -2G(c_+, -2, -1, \sigma_1) + 2G(c_-, -2, -1, \sigma_1) \right. \\
& + G(c_+, -1; \sigma_1)G(-1; \sigma_1) - G(c_+, -1; \sigma_1)G(-1; \sigma_1) \\
& + G(c_+, -1, -1, \sigma_1) - G(c_-, -1, -1, \sigma_1) \\
& - 2G(e_{++}, -2, -1; \sigma_1) - 2G(e_{+-}, -2, -1; \sigma_1) \\
& + 2G(e_{-+}, -2, -1; \sigma_1) + 2G(e_{--}, -2, -1; \sigma_1) \\
& - G(e_{++}, -1, -1; \sigma_1) - G(e_{+-}, -1, -1; \sigma_1) \\
& + G(e_{-+}, -1, -1; \sigma_1) + G(e_{--}, -1, -1; \sigma_1) \\
& + G(e_{++}, -1; \sigma_1)G(-1; \sigma_1) + G(e_{+-}, -1; \sigma_1)G(-1; \sigma_1) \\
& - G(e_{-+}, -1; \sigma_1)G(-1; \sigma_1) - G(e_{--}, -1; \sigma_1)G(-1; \sigma_1) \\
& - G(g_+, c_+, -1; \sigma_1) - G(g_-, c_+, -1; \sigma_1) \\
& + G(g_+, c_-, -1; \sigma_1) + G(g_-, c_-, -1; \sigma_1) \\
& - G(g_+, e_{++}, -1; \sigma_1) - G(g_-, e_{++}, -1; \sigma_1) \\
& - G(g_+, e_{+-}, -1; \sigma_1) - G(g_-, e_{+-}, -1; \sigma_1) \\
& + G(g_+, e_{-+}, -1; \sigma_1) + G(g_-, e_{-+}, -1; \sigma_1) \\
& + G(g_+, e_{--}, -1; \sigma_1) + G(g_-, e_{--}, -1; \sigma_1) \\
& + 4G(d_+, -2, -1; \rho_1) - 4G(d_-, -2, -1; \rho_1) \\
& + 2G(d_+, -1, -1; \rho_1) - 2G(d_-, -1, -1; \rho_1) \\
& + 2G(f_+, d_+, -1; \rho_1) + 2G(f_-, d_+, -1; \rho_1) \\
& - 2G(f_+, d_-, -1; \rho_1) - 2G(f_-, d_-, -1; \rho_1) \\
& \left. - 2G(d_+, -1; \rho_1)G(-1; \rho_1) + 2G(d_-, -1; \rho_1)G(-1; \rho_1) \right] \varepsilon^3 \\
& + \mathcal{O}(\varepsilon^4).
\end{aligned} \tag{A.16}$$

**Eights Canonical Integral** The eights canonical integral  $g_8$  is given by

$$\begin{aligned}
 g_8 = & \left[ G(-1; \sigma_1) G(\omega_1; \sigma_1) - G(-1; \sigma_1) G(\omega_2; \sigma_1) \right. \\
 & - G(-1, \omega_1; \sigma_1) + G(-1, \omega_2; \sigma_1) \\
 & + \log(-\omega) G(-1; \sigma_1) - \log(-\omega) G(\omega_1; \sigma_1) \\
 & \left. - \log(-\omega) G(\omega_2; \sigma_1) + \frac{1}{2} G(-1; \sigma_1)^2 \right] \varepsilon^2 \\
 & \left[ -2 G(-1, -2, -1; \sigma_1) + G(-1, -1, -1; \sigma_1) + 2 G(0, -1, -1; \sigma_1) \right. \\
 & + 2 G(0, \omega_1, -1; \sigma_1) - 2 G(0, \omega_2, -1; \sigma_1) \\
 & - 2 G(\omega_2, -1, -1; \sigma_1) - 2 G(\omega_1, -2, -1; \sigma_1) \\
 & + 2 G(\omega_2, -2, -1; \sigma_1) - G(\omega_1, \omega_1, -1; \sigma_1) \\
 & + G(\omega_1, \omega_2, -1; \sigma_1) - G(\omega_2, \omega_1, -1; \sigma_1) \\
 & + G(\omega_2, \omega_2, -1; \sigma_1) + 2 \log(-\omega) G(0, -1; \sigma_1) \\
 & - 2 \log(-\omega) G(0, \omega_1; \sigma_1) - 2 \log(-\omega) G(0, \omega_2; \sigma_1) \\
 & - \log(-\omega) G(\omega_1, -1; \sigma_1) - \log(-\omega) G(\omega_2, -1; \sigma_1) \\
 & + \log(-\omega) G(\omega_1, \omega_1; \sigma_1) + \log(-\omega) G(\omega_1, \omega_2; \sigma_1) \\
 & + \log(-\omega) G(\omega_2, \omega_1; \sigma_1) + \log(-\omega) G(\omega_2, \omega_2; \sigma_1) \\
 & - \frac{1}{2} \log^2(-\omega) G(-1; \sigma_1) + \frac{1}{2} \log^2(-\omega) G(\omega_1; \sigma_1) \\
 & \left. + \frac{1}{2} \log^2(-\omega) G(\omega_2; \sigma_1) \right] \varepsilon^3 \\
 & + \mathcal{O}(\varepsilon^4).
 \end{aligned} \tag{A.17}$$

### A.5. Feynman Diagrams for the Gluon-Initiated Two-Loop Case

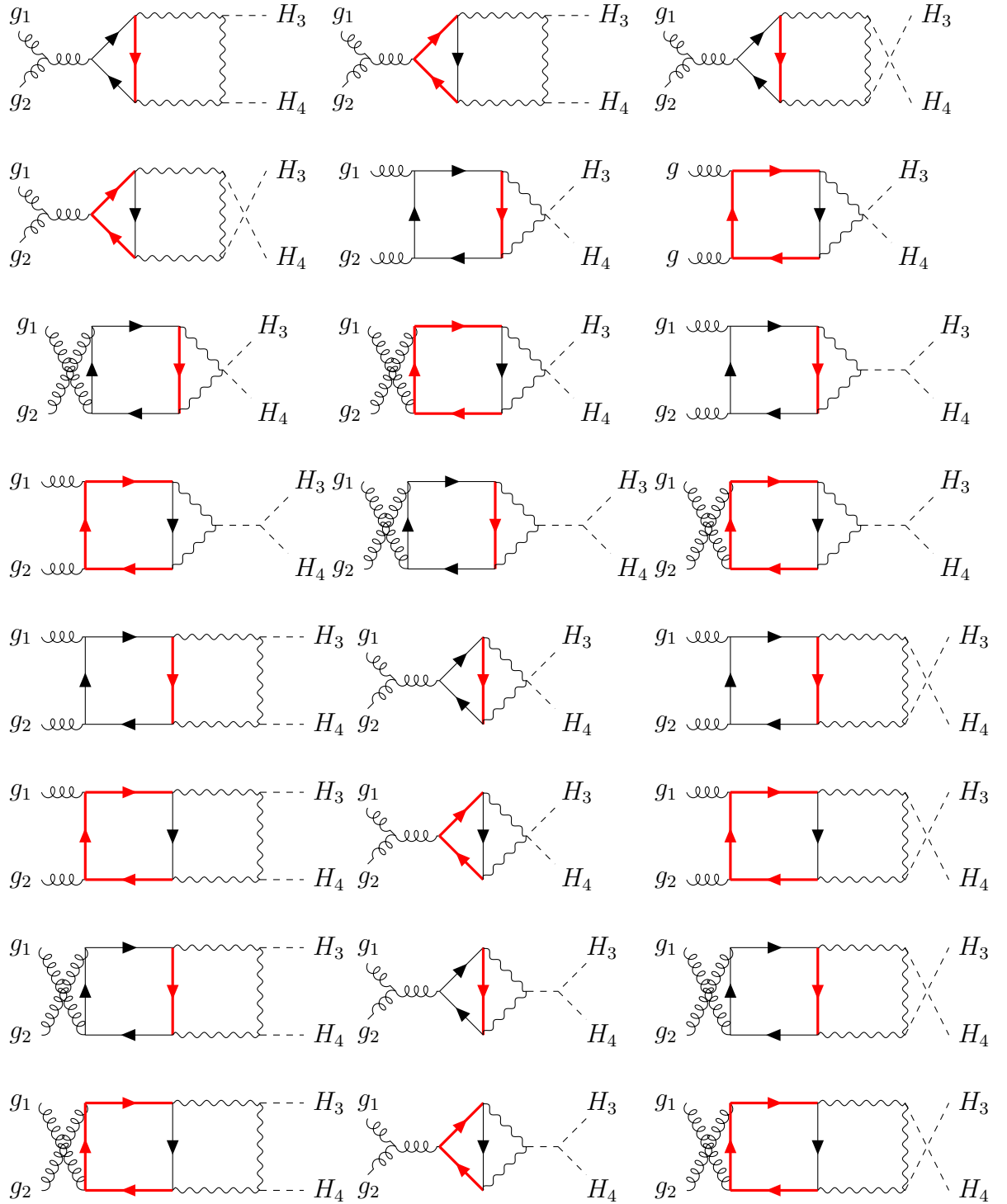


Figure A.2.: Contributing planar diagrams for the gluon initiated two-loop case

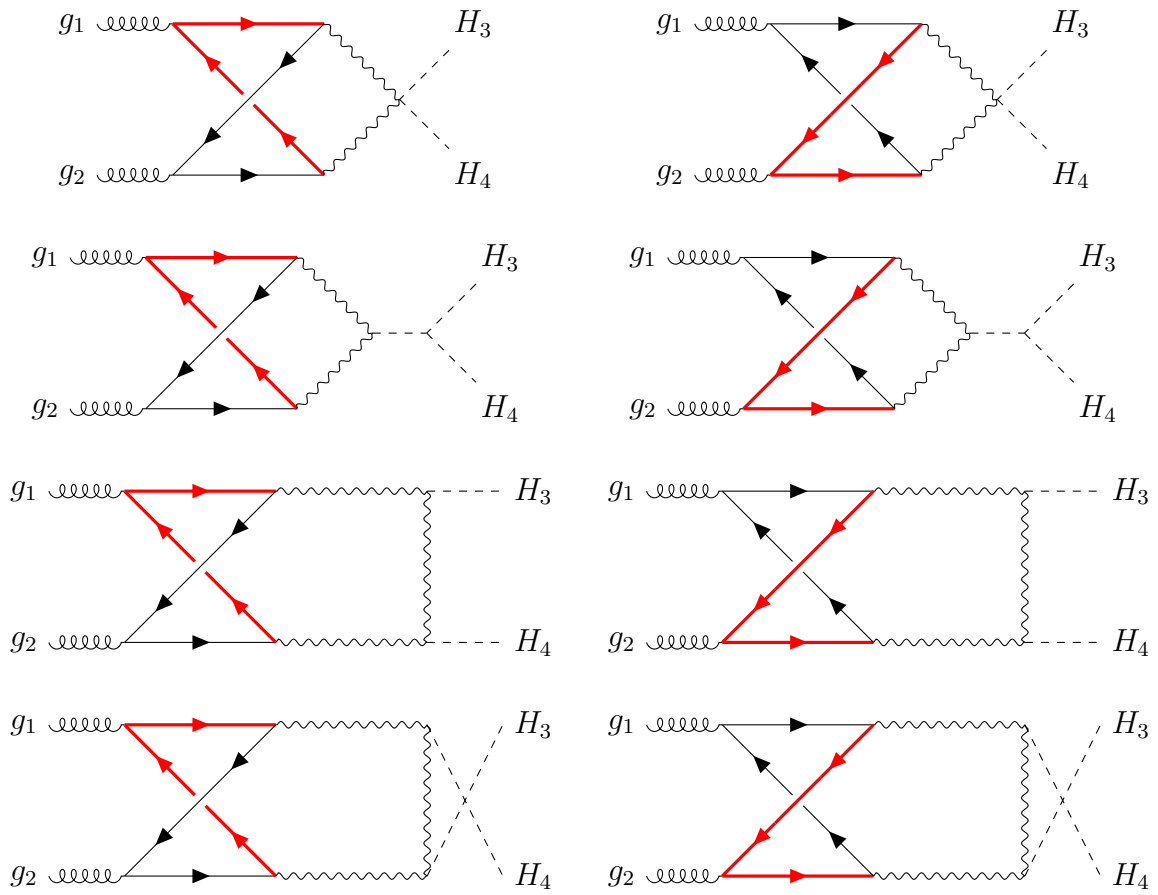


Figure A.3.: Contributing non-planar diagrams for the gluon initiated two-loop case

## Bibliography

- [1] Serguei Chatrchyan et al. “Observation of a New Boson at a Mass of 125 GeV with the CMS Experiment at the LHC”. In: *Phys. Lett. B* 716 (2012), pp. 30–61. DOI: 10.1016/j.physletb.2012.08.021. arXiv: 1207.7235 [hep-ex].
- [2] Georges Aad et al. “Observation of a new particle in the search for the Standard Model Higgs boson with the ATLAS detector at the LHC”. In: *Phys. Lett. B* 716 (2012), pp. 1–29. DOI: 10.1016/j.physletb.2012.08.020. arXiv: 1207.7214 [hep-ex].
- [3] Armen Tumasyan et al. “A portrait of the Higgs boson by the CMS experiment ten years after the discovery.” In: *Nature* 607.7917 (2022). [Erratum: *Nature* 623, (2023)], pp. 60–68. DOI: 10.1038/s41586-022-04892-x. arXiv: 2207.00043 [hep-ex].
- [4] Georges Aad et al. “A detailed map of Higgs boson interactions by the ATLAS experiment ten years after the discovery”. In: *Nature* 607.7917 (2022). [Erratum: *Nature* 612, E24 (2022)], pp. 52–59. DOI: 10.1038/s41586-022-04893-w. arXiv: 2207.00092 [hep-ex].
- [5] Georges Aad et al. “Combined Measurement of the Higgs Boson Mass in  $pp$  Collisions at  $\sqrt{s} = 7$  and 8 TeV with the ATLAS and CMS Experiments”. In: *Phys. Rev. Lett.* 114 (2015), p. 191803. DOI: 10.1103/PhysRevLett.114.191803. arXiv: 1503.07589 [hep-ex].
- [6] Albert M Sirunyan et al. “Combination of searches for Higgs boson pair production in proton-proton collisions at  $\sqrt{s} = 13$  TeV”. In: *Phys. Rev. Lett.* 122.12 (2019), p. 121803. DOI: 10.1103/PhysRevLett.122.121803. arXiv: 1811.09689 [hep-ex].
- [7] Armen Tumasyan et al. “Search for nonresonant Higgs boson pair production in final state with two bottom quarks and two tau leptons in proton-proton collisions at  $s=13$  TeV”. In: *Phys. Lett. B* 842 (2023), p. 137531. DOI: 10.1016/j.physletb.2022.137531. arXiv: 2206.09401 [hep-ex].
- [8] M. Aaboud et al. “Search for Higgs boson pair production in the  $\gamma\gamma b\bar{b}$  final state with 13 TeV  $pp$  collision data collected by the ATLAS experiment”. In: *JHEP* 11 (2018), p. 040. DOI: 10.1007/JHEP11(2018)040. arXiv: 1807.04873 [hep-ex].
- [9] Georges Aad et al. “Combination of searches for Higgs boson pairs in  $pp$  collisions at  $\sqrt{s} = 13$  TeV with the ATLAS detector”. In: *Phys. Lett. B* 800 (2020), p. 135103. DOI: 10.1016/j.physletb.2019.135103. arXiv: 1906.02025 [hep-ex].
- [10] Georges Aad et al. “Search for Higgs boson pair production in the two bottom quarks plus two photons final state in  $pp$  collisions at  $\sqrt{s} = 13$  TeV with the ATLAS detector”. In: *Phys. Rev. D* 106.5 (2022), p. 052001. DOI: 10.1103/PhysRevD.106.052001. arXiv: 2112.11876 [hep-ex].

- [11] Georges Aad et al. “Combination of Searches for Higgs Boson Pair Production in pp Collisions at  $s=13$  TeV with the ATLAS Detector”. In: *Phys. Rev. Lett.* 133.10 (2024), p. 101801. DOI: 10.1103/PhysRevLett.133.101801. arXiv: 2406.09971 [hep-ex].
- [12] Danilo Enoque Ferreira de Lima, Andreas Papaefstathiou, and Michael Spannowsky. “Standard model Higgs boson pair production in the  $(b\bar{b})(b\bar{b})$  final state”. In: *JHEP* 08 (2014), p. 030. DOI: 10.1007/JHEP08(2014)030. arXiv: 1404.7139 [hep-ph].
- [13] “Higgs Pair Production in the  $H(\rightarrow \tau\tau)H(\rightarrow b\bar{b})$  channel at the High-Luminosity LHC”. In: (2015).
- [14] “Prospects for measuring Higgs pair production in the channel  $H(\rightarrow \gamma\gamma)H(\rightarrow b\bar{b})$  using the ATLAS detector at the HL-LHC”. In: (Oct. 2014).
- [15] T. Plehn, M. Spira, and P. M. Zerwas. “Pair production of neutral Higgs particles in gluon-gluon collisions”. In: *Nucl. Phys. B* 479 (1996). [Erratum: *Nucl.Phys.B* 531, 655–655 (1998)], pp. 46–64. DOI: 10.1016/0550-3213(96)00418-X. arXiv: hep-ph/9603205.
- [16] E. W. Nigel Glover and J. J. van der Bij. “HIGGS BOSON PAIR PRODUCTION VIA GLUON FUSION”. In: *Nucl. Phys. B* 309 (1988), pp. 282–294. DOI: 10.1016/0550-3213(88)90083-1.
- [17] Joshua Davies et al. “Double Higgs boson production at NLO in the high-energy limit: complete analytic results”. In: *JHEP* 01 (2019), p. 176. DOI: 10.1007/JHEP01(2019)176. arXiv: 1811.05489 [hep-ph].
- [18] S. Borowka et al. “Full top quark mass dependence in Higgs boson pair production at NLO”. In: *JHEP* 10 (2016), p. 107. DOI: 10.1007/JHEP10(2016)107. arXiv: 1608.04798 [hep-ph].
- [19] S. Borowka et al. “Higgs Boson Pair Production in Gluon Fusion at Next-to-Leading Order with Full Top-Quark Mass Dependence”. In: *Phys. Rev. Lett.* 117.1 (2016). [Erratum: *Phys.Rev.Lett.* 117, 079901 (2016)], p. 012001. DOI: 10.1103/PhysRevLett.117.079901. arXiv: 1604.06447 [hep-ph].
- [20] Julien Baglio et al. “Gluon fusion into Higgs pairs at NLO QCD and the top mass scheme”. In: *Eur. Phys. J. C* 79.6 (2019), p. 459. DOI: 10.1140/epjc/s10052-019-6973-3. arXiv: 1811.05692 [hep-ph].
- [21] Joshua Davies et al. “Double Higgs boson production at NLO: combining the exact numerical result and high-energy expansion”. In: *JHEP* 11 (2019), p. 024. DOI: 10.1007/JHEP11(2019)024. arXiv: 1907.06408 [hep-ph].
- [22] Giancarlo Ferrera and Joao Pires. “Transverse-momentum resummation for Higgs boson pair production at the LHC with top-quark mass effects”. In: *JHEP* 02 (2017), p. 139. DOI: 10.1007/JHEP02(2017)139. arXiv: 1609.01691 [hep-ph].
- [23] G. Heinrich et al. “NLO predictions for Higgs boson pair production with full top quark mass dependence matched to parton showers”. In: *JHEP* 08 (2017), p. 088. DOI: 10.1007/JHEP08(2017)088. arXiv: 1703.09252 [hep-ph].

- 
- [24] Stephen Jones and Silvan Kuttimalai. “Parton Shower and NLO-Matching uncertainties in Higgs Boson Pair Production”. In: *JHEP* 02 (2018), p. 176. DOI: 10.1007/JHEP02(2018)176. arXiv: 1711.03319 [hep-ph].
- [25] G. Heinrich et al. “Probing the trilinear Higgs boson coupling in di-Higgs production at NLO QCD including parton shower effects”. In: *JHEP* 06 (2019), p. 066. DOI: 10.1007/JHEP06(2019)066. arXiv: 1903.08137 [hep-ph].
- [26] Huan-Yu Bi et al. “Electroweak Corrections to Double Higgs Production at the LHC”. In: *Phys. Rev. Lett.* 132.23 (2024), p. 231802. DOI: 10.1103/PhysRevLett.132.231802. arXiv: 2311.16963 [hep-ph].
- [27] Gudrun Heinrich et al. “Electroweak corrections to Higgs boson pair production: the top-Yukawa and self-coupling contributions”. In: *JHEP* 11 (2024), p. 040. DOI: 10.1007/JHEP11(2024)040. arXiv: 2407.04653 [hep-ph].
- [28] Sophia Borowka et al. “Probing the scalar potential via double Higgs boson production at hadron colliders”. In: *JHEP* 04 (2019), p. 016. DOI: 10.1007/JHEP04(2019)016. arXiv: 1811.12366 [hep-ph].
- [29] Margarete Mühlleitner, Johannes Schlenk, and Michael Spira. “Top-Yukawa-induced corrections to Higgs pair production”. In: *JHEP* 10 (2022), p. 185. DOI: 10.1007/JHEP10(2022)185. arXiv: 2207.02524 [hep-ph].
- [30] Joshua Davies et al. “Higgs boson contribution to the leading two-loop Yukawa corrections to  $gg \rightarrow HH$ ”. In: *JHEP* 08 (2022), p. 259. DOI: 10.1007/JHEP08(2022)259. arXiv: 2207.02587 [hep-ph].
- [31] Joshua Davies et al. “Next-to-leading order electroweak corrections to  $gg \rightarrow HH$  and  $gg \rightarrow gH$  in the large- $m_t$  limit”. In: *JHEP* 10 (2023), p. 033. DOI: 10.1007/JHEP10(2023)033. arXiv: 2308.01355 [hep-ph].
- [32] A. V. Kotikov. “Differential equations method: New technique for massive Feynman diagrams calculation”. In: *Phys. Lett. B* 254 (1991), pp. 158–164. DOI: 10.1016/0370-2693(91)90413-K.
- [33] T. Gehrmann and E. Remiddi. “Differential equations for two-loop four-point functions”. In: *Nucl. Phys. B* 580 (2000), pp. 485–518. DOI: 10.1016/S0550-3213(00)00223-6. arXiv: hep-ph/9912329.
- [34] Johannes M. Henn. “Multiloop integrals in dimensional regularization made simple”. In: *Phys. Rev. Lett.* 110 (2013), p. 251601. DOI: 10.1103/PhysRevLett.110.251601. arXiv: 1304.1806 [hep-th].
- [35] Roman N. Lee. “Reducing differential equations for multiloop master integrals”. In: *JHEP* 04 (2015), p. 108. DOI: 10.1007/JHEP04(2015)108. arXiv: 1411.0911 [hep-ph].
- [36] Michael E. Peskin and Daniel V. Schroeder. *An Introduction to quantum field theory*. Reading, USA: Addison-Wesley, 1995. ISBN: 978-0-201-50397-5, 978-0-429-50355-9, 978-0-429-49417-8. DOI: 10.1201/9780429503559.

- [37] John C. Collins. *Renormalization*. Vol. 26. Cambridge Monographs on Mathematical Physics. Cambridge: Cambridge University Press, July 2023. ISBN: 978-0-521-31177-9, 978-0-511-86739-2, 978-1-009-40180-7, 978-1-009-40176-0, 978-1-009-40179-1. DOI: 10.1017/9781009401807.
- [38] O. V. Tarasov. “Connection between Feynman integrals having different values of the space-time dimension”. In: *Phys. Rev. D* 54 (1996), pp. 6479–6490. DOI: 10.1103/PhysRevD.54.6479. arXiv: hep-th/9606018.
- [39] O. V. Tarasov. “Generalized recurrence relations for two loop propagator integrals with arbitrary masses”. In: *Nucl. Phys. B* 502 (1997), pp. 455–482. DOI: 10.1016/S0550-3213(97)00376-3. arXiv: hep-ph/9703319.
- [40] Stefan Weinzierl. *Feynman Integrals. A Comprehensive Treatment for Students and Researchers*. UNITEXT for Physics. Springer, 2022. ISBN: 978-3-030-99557-7, 978-3-030-99560-7, 978-3-030-99558-4. DOI: 10.1007/978-3-030-99558-4. arXiv: 2201.03593 [hep-th].
- [41] P. A. Baikov. “Explicit solutions of the multiloop integral recurrence relations and its application”. In: *Nucl. Instrum. Meth. A* 389 (1997). Ed. by M. Werlen and D. Perret-Gallix, pp. 347–349. DOI: 10.1016/S0168-9002(97)00126-5. arXiv: hep-ph/9611449.
- [42] Mario Argeri and Pierpaolo Mastrolia. “Feynman Diagrams and Differential Equations”. In: *Int. J. Mod. Phys. A* 22 (2007), pp. 4375–4436. DOI: 10.1142/S0217751X07037147. arXiv: 0707.4037 [hep-ph].
- [43] F. V. Tkachov. “A theorem on analytical calculability of 4-loop renormalization group functions”. In: *Phys. Lett. B* 100 (1981), pp. 65–68. DOI: 10.1016/0370-2693(81)90288-4.
- [44] K. G. Chetyrkin and F. V. Tkachov. “Integration by parts: The algorithm to calculate  $\beta$ -functions in 4 loops”. In: *Nucl. Phys. B* 192 (1981), pp. 159–204. DOI: 10.1016/0550-3213(81)90199-1.
- [45] R. N. Lee. “Group structure of the integration-by-part identities and its application to the reduction of multiloop integrals”. In: *JHEP* 07 (2008), p. 031. DOI: 10.1088/1126-6708/2008/07/031. arXiv: 0804.3008 [hep-ph].
- [46] Roman N. Lee. “LiteRed 1.4: a powerful tool for reduction of multiloop integrals”. In: *J. Phys. Conf. Ser.* 523 (2014). Ed. by Jianxiong Wang, p. 012059. DOI: 10.1088/1742-6596/523/1/012059. arXiv: 1310.1145 [hep-ph].
- [47] S. Laporta. “High-precision calculation of multiloop Feynman integrals by difference equations”. In: *Int. J. Mod. Phys. A* 15 (2000), pp. 5087–5159. DOI: 10.1142/S0217751X00002159. arXiv: hep-ph/0102033.
- [48] Charalampos Anastasiou and Achilleas Lazopoulos. “Automatic integral reduction for higher order perturbative calculations”. In: *JHEP* 07 (2004), p. 046. DOI: 10.1088/1126-6708/2004/07/046. arXiv: hep-ph/0404258.
- [49] A. V. Smirnov. “Algorithm FIRE – Feynman Integral REduction”. In: *JHEP* 10 (2008), p. 107. DOI: 10.1088/1126-6708/2008/10/107. arXiv: 0807.3243 [hep-ph].

- 
- [50] A. V. Smirnov and V. A. Smirnov. “FIRE4, LiteRed and accompanying tools to solve integration by parts relations”. In: *Comput. Phys. Commun.* 184 (2013), pp. 2820–2827. DOI: 10.1016/j.cpc.2013.06.016. arXiv: 1302.5885 [hep-ph].
- [51] Alexander V. Smirnov. “FIRE5: A C++ implementation of Feynman Integral REduction”. In: *Comput. Phys. Commun.* 189 (2015), pp. 182–191. DOI: 10.1016/j.cpc.2014.11.024. arXiv: 1408.2372 [hep-ph].
- [52] C. Studerus. “Reduze-Feynman Integral Reduction in C++”. In: *Comput. Phys. Commun.* 181 (2010), pp. 1293–1300. DOI: 10.1016/j.cpc.2010.03.012. arXiv: 0912.2546 [physics.comp-ph].
- [53] A. von Manteuffel and C. Studerus. “Reduze 2 - Distributed Feynman Integral Reduction”. In: (Jan. 2012). arXiv: 1201.4330 [hep-ph].
- [54] Philipp Maierhöfer, Johann Usovitsch, and Peter Uwer. “Kira—A Feynman integral reduction program”. In: *Comput. Phys. Commun.* 230 (2018), pp. 99–112. DOI: 10.1016/j.cpc.2018.04.012. arXiv: 1705.05610 [hep-ph].
- [55] Jonas Klappert et al. “Integral reduction with Kira 2.0 and finite field methods”. In: *Comput. Phys. Commun.* 266 (2021), p. 108024. DOI: 10.1016/j.cpc.2021.108024. arXiv: 2008.06494 [hep-ph].
- [56] Jiaqi Chen, Chichuan Ma, and Li Lin Yang. “Alphabet of one-loop Feynman integrals\*”. In: *Chin. Phys. C* 46.9 (2022), p. 093104. DOI: 10.1088/1674-1137/ac6e37. arXiv: 2201.12998 [hep-th].
- [57] M. Beneke and Vladimir A. Smirnov. “Asymptotic expansion of Feynman integrals near threshold”. In: *Nucl. Phys. B* 522 (1998), pp. 321–344. DOI: 10.1016/S0550-3213(98)00138-2. arXiv: hep-ph/9711391.
- [58] Alexander B. Goncharov. “Multiple polylogarithms, cyclotomy and modular complexes”. In: *Math. Res. Lett.* 5 (1998), pp. 497–516. DOI: 10.4310/MRL.1998.v5.n4.a7. arXiv: 1105.2076 [math.AG].
- [59] Christian W. Bauer, Alexander Frink, and Richard Kreckel. “Introduction to the GiNaC framework for symbolic computation within the C++ programming language”. In: *J. Symb. Comput.* 33 (2002), pp. 1–12. DOI: 10.1006/jsc.2001.0494. arXiv: cs/0004015.
- [60] Jonathan M. Borwein et al. “Special values of multiple polylogarithms”. In: *Trans. Am. Math. Soc.* 353 (2001), pp. 907–941. DOI: 10.1090/S0002-9947-00-02616-7. arXiv: math/9910045.
- [61] Marco Besier, Duco Van Straten, and Stefan Weinzierl. “Rationalizing roots: an algorithmic approach”. In: *Commun. Num. Theor. Phys.* 13 (2019), pp. 253–297. DOI: 10.4310/CNTP.2019.v13.n2.a1. arXiv: 1809.10983 [hep-th].
- [62] T. Gehrmann and E. Remiddi. “Analytic continuation of massless two loop four point functions”. In: *Nucl. Phys. B* 640 (2002), pp. 379–411. DOI: 10.1016/S0550-3213(02)00569-2. arXiv: hep-ph/0207020.
- [63] Paulo Nogueira. “Automatic Feynman Graph Generation”. In: *J. Comput. Phys.* 105 (1993), pp. 279–289. DOI: 10.1006/jcph.1993.1074.

- [64] Nicolas Deutschmann. *QGRAF Diagram Drawer*. DOI: 10.5281/zenodo.164393.
- [65] J. A. M. Vermaseren. “New features of FORM”. In: (Oct. 2000). arXiv: math-ph/0010025.
- [66] J. Kuipers et al. “FORM version 4.0”. In: *Comput. Phys. Commun.* 184 (2013), pp. 1453–1467. DOI: 10.1016/j.cpc.2012.12.028. arXiv: 1203.6543 [cs.SC].
- [67] Jorge C. Romao and Joao P. Silva. “A resource for signs and Feynman diagrams of the Standard Model”. In: *Int. J. Mod. Phys. A* 27 (2012), p. 1230025. DOI: 10.1142/S0217751X12300256. arXiv: 1209.6213 [hep-ph].
- [68] Michael S. Chanowitz, M. Furman, and I. Hinchliffe. “The Axial Current in Dimensional Regularization”. In: *Nucl. Phys. B* 159 (1979), pp. 225–243. DOI: 10.1016/0550-3213(79)90333-X.
- [69] Wolfram Research Inc. *Mathematica, Version 13.2*. Champaign, IL, 2022.

# Acknowledgments

I would like to extend my heartfelt gratitude to my advisor Dr. Marco Bonetti for his remarkable patience in giving me feedback and his dedication in sharing his knowledge with me over countless hours. His enthusiasm for the subject inspired and motivated me when I needed it most.

I am also very grateful to my office mates, Maurice Schüßler and Pavao Brica, for their fruitful discussions and for fostering a positive atmosphere. A special thanks goes to Emil Overduin who was always willing to help me and saved me from hours of troubleshooting.

Lastly, I want to express my deepest appreciation to my family, especially to my parents, for their unwavering support throughout my studies and to my partner, Lilly. During stressful times, she provided me with invaluable support, allowing me to focus entirely on my thesis.